

RIPRAP DESIGN FOR SAF
STILLING BASINS

By

RICHARD C. PERALTA

Bachelor of Science
University of South Carolina
Columbia, South Carolina
1971

Master of Science
Utah State University
Logan, Utah
1977

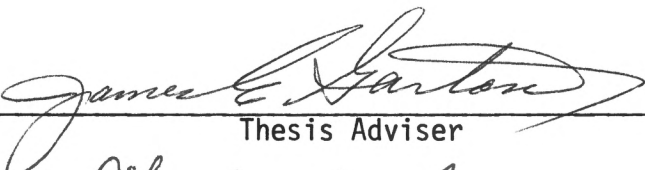
Submitted to the Faculty of the Graduate College
of the Oklahoma State University
in partial fulfillment of the requirements
for the Degree of
Doctor of Philosophy
December, 1979

Thesis
1979D
P426r
cop. 2

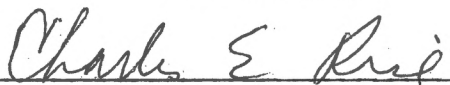


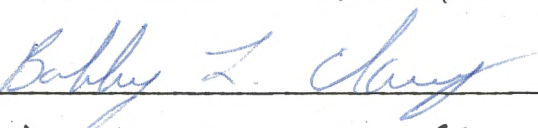
RIPRAP DESIGN FOR SAF
STILLING BASINS

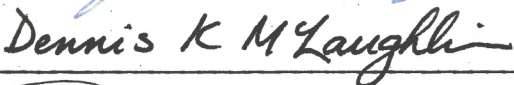
Thesis Approved:

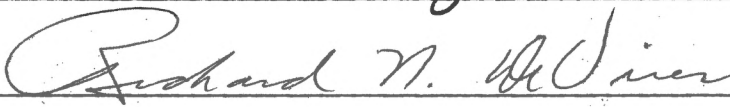



Thesis Adviser











Dean of the Graduate College

PREFACE

Saint Anthony Falls (SAF) stilling basins are hydraulic jump type energy dissipators. Riprap is a desirable means of preventing erosion downstream of SAF basins. This study uses Froude modeling to provide guidance for riprap placement in the downstream channel.

Dr. James E. Garton, my major adviser, has my sincere thanks for the guidance he rendered in the professional development of this work. Dr. Wendell R. Gwinn has my heartfelt appreciation for the many ways he supported and guided my efforts. Appreciation is also expressed to my committee members: Dr. Bobby L. Clary, Dr. Richard N. DeVries, Dr. Dennis K. McLaughlin and Dr. Charles E. Rice for their assistance in the preparation of the final manuscript.

A note of thanks is given to Ruth K. Wright for her assistance in editing and typing and to Darlene Richardson for her preparation of the final manuscript. Thanks are also extended to the men of the Water Conservation Structures Laboratory: Ollis V. Thompson, Walter C. Crane, C. Gayle Ward and most especially Eldon W. Hills for their patient assistance. Jack Fryrear is thanked for his careful and timely preparation of the figures.

I appreciate the financial support provided by: the United States Department of Agriculture, Science and Education Administration, Southern Region, Water Conservation Structures Laboratory; the U.S. Department of Agriculture, Soil Conservation Service, Stillwater,

Oklahoma; and the Agricultural Engineering Department, Oklahoma State University, Stillwater, Oklahoma. All reported opinions, conclusions or recommendations are those of the author and not those of the funding agencies or the United States Government.

I am forever indebted to my eternal companion, Ann, and our beloved children, Lydia, Samantha and Nancy, for the support they have given me.

TABLE OF CONTENTS

Chapter	Page
I. INTRODUCTION AND LITERATURE REVIEW	1
Introduction.	1
The SAF Basin	1
Erosion Below Hydraulic Jump Type Energy Dissipators	3
Methods of Channel Protection	6
Methods of Determining the Stable Size of Riprap Below Hydraulic Jump Type Energy Dissipators.	7
II. THE RESEARCH PROBLEM AND APPROACH.	11
Problem and Objectives.	11
Research Approach	11
Pre-Testing Similitude.	12
Analysis of Flow Through a SAF Stilling Basin.	12
Analysis of Scour in the "Equilibrium" Scour Hole Below SAF Stilling Basins	17
Applicability of Results.	19
III. THE PHYSICAL SET-UP.	25
Introduction.	25
Head Tank and Entering Depth Control Devices.	25
Chute and Model SAF Basin	28
Riprap.	32
Instrumentation and XYZ Orientation	36
IV. INITIAL TESTING AND TEST PROCEDURE	40
Initial Testing	40
Determination of Test Duration	40
Determination of Channel Initial Condition	42
Test Procedure.	49
Pre-Test Settings to Achieve Correct Water Surface.	49
Preparation of Downstream Channel.	50
Measurements of Flow and Scour	50
V. MAJOR TEST RESULTS	52
Observations of the Water Surface.	52

Chapter	Page
Scour Holes	52
VI. ANALYSIS	63
Analysis of Scour on the Channel Bottom	63
Analysis of Scour on the Channel Sides.	73
Comparison of Results with Two State of the Art Methods	85
VII. APPLICATION.	89
Pertinent Procedures and Assumptions.	89
Design Guidance	91
Introduction	91
Guidelines for Erosion on the Channel Bottom	92
Guidelines for Erosion on Channel Sides.	93
Example.	95
VIII. SUMMARY AND CONCLUSIONS.	102
A SELECTED BIBLIOGRAPHY	105
APPENDICES.	108
APPENDIX A - LETTER FROM SCS HEADQUARTERS SHOWING THE NUMBER OF COMPUTER DESIGNS PREPARED FOR SAF BASINS, MARCH 1974 THROUGH JUNE 1978.	109
APPENDIX B - AVERAGE CENTERLINE WATER SURFACE PROFILES AND CENTERLINE DEPOSITION PROFILE	111
APPENDIX C - MAXIMUM SCOUR CONTOUR MAPS.	116
APPENDIX D - NONDIMENSIONAL LENGTH OR DEPTH OF SCOUR AS A FUNCTION OF ROCK SIZE FOR SPECIFIED POSITIONS IN THE DOWNSTREAM CHANNEL	127

LIST OF TABLES

Table	Page
I. Nondimensional Characteristics of SAF Stilling Basins Showing That Π_1 , Π_2 , and Π_3 Are Constant at Constant Π_4 Regardless of Variation in D_1 and V_1	15
II. Comparison of Experimental Rock with Spheres of Same D_{50} (D_{50_m}), Same Mass ($Mass_m$) and Specific Gravities of 2.65 and 2.81.	35
III. Pre-Test Variation in Channel Floor Elevations.	50
IV. Nondimensional Characteristics of SAF Stilling Basins for Design Froude Numbers (Π_{4_D}) of 1 Through 17	66

LIST OF FIGURES

Figure	Page
1. Proportions of the SAF Stilling Basin	2
2. Design Formulas and Symbol Definition for SAF Stilling Basins Used by the Soil Conservation Service	4
3. Modified Formulas for SAF Stilling Basins Used by the Corps of Engineers.	4
4. Erosion Around the Wingwalls of a SAF Basin	5
5. Graph to Determine the D40 to Be Used Below Hydraulic Jump Type Energy Dissipators.	10
6. Side View of SAF Basin and Downstream Channel Showing Variables Used in Similitude.	14
7. Range of Entrance Froude Numbers (Fl_D) for Which SAF Stilling Basins May Be Designed	16
8. Location of Significant Positions Shown in a Side View of the Downstream Scour Beds Which Occur Below Basins of $PI4_D = 4$ and $PI4_D = 8$	18
9. Critical Boundary Shear at Incipient Movement of Riprap in Terms of D50.	20
10. Shield's Diagram Showing Relation Between Shear Froude Number and Shear Reynolds Number at Initiation of Motion.	24
11. Side View of Laboratory Showing Supply Pipe, Head Tank, and Model in the Flume.	26
12. Photograph Showing Supply Pipe, Head Tank, and Model with False Walls in Place	27
13. Side View of Head Tank Exit Showing How Opening Could Be Adjusted	29
14. Set-Up to Achieve Short Tube Control in the Chute	30

Figure	Page
15. Top and Side Views of Model SAF Basin Showing How Pieces Were Varied to Obtain Basins of Different $F1_D$'s	31
16. Rock Screens, Carriage, and Willing Worker.	33
17. Grain Size Distributions of Rock Used in the Model Tests	34
18. Pointed End of Probe Used for Measuring Water Surface Elevations for $F1_D = 4.0$	38
19. Electronic System for Estimating the Average Water Surface Elevation	39
20. Side View Showing the Development with Time of Scour Downstream of the End Sill.	41
21. Maximum Scour Contour Map After Testing at $F1_D = 8.0$, $W = 24.75 \times D1_D$, $D50 = 3.45 \text{ mm} (.0113 \text{ ft})$	43
22. Initial Conditions and Maximum Scour Contour Map for Test 29	45
23. Maximum Scour Contour Map Resulting from Test 30.	46
24. Contour Map After Tests 31, 32, and 33 Showing That Relative "Stability" Was Reached in First 24 Hours of Flow	47
25. Contour Map After Tests 34 and 35	48
26. Side View of Jump in Basin of $F1_D = 4$, Width = $24.75 \times D1_D$	53
27. Downstream View of Jump in Basin of $F1_D = 4$, Width = $24.75 \times D1_D$	54
28. Side View of Jump in Basin of $F1_D = 4$, Width = $9.75 \times D1_D$	55
29. Downstream View of Jump in Basin of $F1_D = 4$, Width = $9.75 \times D1_D$	56
30. Side View of Jump in Basin of $F1_D = 8$, Width = $24.75 \times D1_D$	57
31. Top View of Jump in Basin of $F1_D = 8$, Width = $24.75 \times D1_D$	58

Figure	Page
32. Side View of Jump in Basin of $Fl_D = 8$, Width = $9.75 \times D1_D$	59
33. Downstream View of Jump in Basin of $Fl_D = 8$, Width = $9.75 \times D1_D$	60
34. Contoured Scour Bed After Test 44 ($Fl_D = 4.0$, $W = 24.75 \times D1_D$, Elevation of Basin Floor = 0.659, Elevation of Top of End Sill = 0.692)	61
35. Calculated Values of $\Pi5A$ and $\Pi5B$ Versus $\Pi4$	64
36. Design Values of $\Pi1$, $\Pi2$, and $\Pi3$ Versus $\Pi4$	65
37. Composite Maximum Scour Profiles for $Fl_D = 4.0$, Width = $9.75 \times D1_D$	68
38. Composite Maximum Scour Profiles for $Fl_D = 4.0$, Width = $9.75 \times D1_D$	69
39. Composite Maximum Scour Profiles for $Fl_D = 8.0$, Width = $24.75 \times D1_D$	70
40. Composite Maximum Scour Profiles for $Fl_D = 8.0$, Width = $9.75 \times D1_D$	71
41. $\Pi DS2$ Versus $\Pi13$ at Position 2	72
42. Nondimensional Location of Positions 2 and 3 as a Function of $D50/D1_D$ Applicable for Basins of $3 \leq Fl_D \leq 4$, Width = $9.75 \times D1_D$ Through $24.75 \times D1_D$	74
43. Nondimensional Depth of Scour as a Function of $D50/D1_D$ at Positions 1 and 2 Applicable for Basins of $3 \leq Fl_D \leq 4$, Width = $9.75 \times D1_D$ Through $24.75 \times D1_D$	75
44. Nondimensional Location of Positions 2, 3, 4, and 5 as a Function of $D50/D1_D$ Applicable for Basins of $4 \leq Fl_D \leq 8$, Width = $9.75 \times D1_D$ Through $24.75 \times D1_D$	76
45. Nondimensional Depth of Scour as a Function of $D50/D1_D$ at Positions 1, 2, and 4 Applicable for Basins of $4 \leq Fl_D \leq 8$, Width = $9.75 \times D1_D$ Through $24.75 \times D1_D$	77
46. Nondimensional Cross Section of Channel Side Showing Maximum Latitudinal Scour After Testing of Models of $Fl_D = 8$, Width = $9.75 \times D1_D$ and $24.75 \times D1_D$, $D50 = 7.85$ mm (0.0258 ft)	78

Figure	Page
47. Nondimensional Cross Section of Channel Side Showing Maximum Latitudinal Scour After Testing of Models of $F_{1D} = 8$, Width = $9.75 \times D_{1D}$ and $24.75 \times D_{1D}$, $D_{50} = 3.45 \text{ mm (0.0113 ft)}$	79
48. Nondimensional Cross Section of Channel Side Showing Maximum Latitudinal Scour After Testing of Models of $F_{1D} = 4$, Width = $9.75 \times D_{1D}$ and $24.75 \times D_{1D}$, $D_{50} = 7.85 \text{ mm (0.0258 ft)}$	81
49. Nondimensional Cross Section of Channel Side Showing Maximum Latitudinal Scour After Testing of Models of $F_{1D} = 4$, Width = $9.75 \times D_{1D}$ and $24.75 \times D_{1D}$, $D_{50} = 3.45 \text{ mm (0.0113 ft)}$	81
50. Nondimensional Cross Section of Channel Side Showing Maximum Latitudinal Scour After Testing of Models of $F_{1D} = 4$ and 8 a) $D_{50} = 7.85 \text{ mm (0.0258 ft)}$ b) $D_{50} = 3.45 \text{ mm (0.0113 ft)}$	82
51. Nondimensional Maximum Scour Contour Map of Channel Side Resulting from Tests at $F_{1D} = 4$, Width = $9.75 \times D_{1D}$ and $24.75 \times D_{1D}$ for Three Different Rock Sizes.	83
52. Nondimensional Maximum Scour Contour Map of Channel Side Resulting from Tests at $F_{1D} = 8$, Width = $9.75 \times D_{1D}$ and $24.75 \times D_{1D}$ for Three Different Rock Sizes.	84
53. Comparison Between Rock Used in the Tests and Suitable Rock Sizes Calculated by State of the Art Methods as Related to Maximum Vertical Scour on the Channel Side Slopes.	86
54. Estimation of the Nondimensional Scour Which Would Occur at Position 2 for Rock Sizes Calculated by Methods 1 and 2	88
55. Side View of Channel Bottom Showing the Excavation Profile (Without Safety Factor), the Maximum Scour Profile, and the Finished Channel Bottom Level with the End Sill	97
56. Contour Map of the Channel Side Slope Showing Contours Which Must Be Excavated Around.	98
57. Cross Section of the Channel Side Slope Taken at $\Delta X = 74$ Feet Showing the Intended Finished Surface, the Maximum Expected Scour and the Excavation Slope (Without Safety Factor)	101

Figure	Page
58. Correspondence from SCS Indicating Number of Computer Designs Prepared for SAF Basins of Different $(Fl_D)^2$, Where Fl_D^2 Equals the F in the Correspondence	110
59. Centerline Water Surface Profile and Deposition Profile for $Fl_D = 4.0$, $W = 24.75 \times D1_D$	112
60. Centerline Water Surface Profile and Deposition Profile for $Fl_D = 4.0$, $W = 9.75 \times D1_D$	113
61. Centerline Water Surface Profile and Deposition Profile for $Fl_D = 8.0$, $W = 24.75 \times D1_D$	114
62. Centerline Water Surface Profile and Deposition Profile for $Fl_D = 8.0$, $W = 9.75 \times D1_D$	115
63. Maximum Scour Contour Map After Testing at $Fl_D = 4.0$, $W = 24.75 \times D1_D$, $D50 = 7.85 \text{ mm (0.0258 ft)}$	117
64. Maximum Scour Contour Map After Testing at $Fl_D = 4.0$, $W = 24.75 \times D1_D$, $D50 = 5.65 \text{ mm (0.0185 ft)}$	118
65. Maximum Scour Contour Map After Testing at $Fl_D = 4.0$, $W = 24.75 \times D1_D$, $D50 = 3.45 \text{ mm (0.0113 ft)}$	119
66. Maximum Scour Contour Map After Testing at $Fl_D = 4.0$, $W = 9.75 \times D1_D$, $D50 = 7.85 \text{ mm (0.0258 ft)}$	120
67. Maximum Scour Contour Map After Testing at $Fl_D = 4.0$, $W = 9.75 \times D1_D$, $D50 = 5.65 \text{ mm (0.0185 ft)}$	121
68. Maximum Scour Contour Map After Testing at $Fl_D = 4.0$, $W = 9.75 \times D1_D$, $D50 = 3.45 \text{ mm (0.0113 ft)}$	122
69. Maximum Scour Contour Map After Testing at $Fl_D = 8.0$, $W = 24.75 \times D1_D$, $D50 = 7.85 \text{ mm (0.0258 ft)}$	123
70. Maximum Scour Contour Map After Testing at $Fl_D = 8.0$, $W = 9.75 \times D1_D$, $D50 = 7.85 \text{ mm (0.0258 ft)}$	124
71. Maximum Scour Contour Map After Testing at $Fl_D = 8.0$, $W = 9.75 \times D1_D$, $D50 = 5.65 \text{ mm (0.0185 ft)}$	125
72. Maximum Scour Contour Map After Testing at $Fl_D = 8.0$, $W = 9.75 \times D1_D$, $D50 = 3.45 \text{ mm (0.0113 ft)}$	126
73. Nondimensional Depth of Scour at Position 1 as a Function of $D50/D1_D$	128
74. Nondimensional Depth of Scour at Position 2 as a Function of $D50/D1_D$	129

Figure	Page
75. Nondimensional Depth of Scour at Position 4 as a Function of D_{50}/D_1	130
76. Nondimensional Length to Positions 2, 3, 4, and 5 as Functions of D_{50}/D_1	131

NOMENCLATURE

b	Horizontal distance		ft
c	Subscript denoting calculated as opposed to design value		
C	End sill height		ft
C_I	Isbash coefficient		
CA	Cauchy number = $\frac{\rho_w V^2}{e_w}$		
CMSP	Composite maximum scour profile		
D_w	Depth of water		ft
D	Stone diameter		ft
D	Subscript denoting design value as opposed to calculated value		
DF	Drag force on the channel bottom		lb
DS#	Depth of scour at some position #		ft
D0	Smallest diameter of rock in a population	mm	ft
D1	Entrance depth		ft
D2	Sequent depth		ft
D3	Depth of water over the end sill		ft
D2P	Minimum acceptable tailwater for SAF basins		ft
D40	The diameter of the rock which is greater than 40 percent of the rocks in a population	mm	ft
D50	The diameter of the rock which is greater than 50 percent of the rocks in a population	mm	ft
D100	The diameter of the largest rock in a rock population	mm	ft

e_w	Bulk modulus of water	1b/ft ²
EX	Subscript denoting excavation	
f	Function, as in f(x)	
F	Froude number = $\frac{V}{\sqrt{g(D_w)}}$	
F1	Entrance Froude number = $\frac{V1}{\sqrt{g(D1)}}$	
F1 _D	Design entrance Froude, i.e. Froude number for which the basin was designed	
F*	Shear Froude number (Shield's Parameter) = $\frac{\tau_{c50}}{(\gamma_s - \gamma_w)D50}$	
G	An unknown function of Π terms	
g	Acceleration of gravity	ft/s ²
j	Horizontal position on S2 profile	ft
K	Shape factor for the rock	
LB	Basin length	ft
LS#	Length of scour to some position #	ft
m	Subscript denoting model	
MSCM	Maximum scour contour map	
p	Subscript denoting prototype	
P2	An unknown function of Π terms	
R	Reynolds number = $\frac{\rho_w V(D_w)}{\mu}$	
R _h	Hydraulic radius	ft
R*	Shear Reynolds number = $\frac{V_{*c} D50}{\nu}$	
S _b	Bed slope	ft/ft
SG	Specific gravity of rock	

V	Velocity of water		ft/s
V _b	Velocity of water at the rock		ft/s
V1	Average velocity of water at entrance to the stilling basin		ft/s
V3	Average velocity of the water over the end sill		ft/s
V*	Boundary shear velocity = $\sqrt{T_0/\rho_w}$		ft/s
V* _C	Critical shear velocity = boundary shear velocity at impending motion		ft/s
w	Subscript denoting water		
W	Basin width		ft
WE	Weber number = $\frac{\rho_w V^2 D_w}{\sigma}$		
Z1	Distance above basin floor		ft
γ	Submerged unit weight of rock under water		1b/ft ³
γ _S	Specific weight of rock		1b/ft ³
γ _W	Specific weight of water		1b/ft ³
δ	Thickness of the laminar sublayer		ft
θ	Angle of repose of the rock		degrees
λ	Ratio of length scales of prototype to model (=length _p /length _m)		1b _m /ft(s)
μ	Viscosity of water		
ν	Kinematic viscosity of water		ft ² /s
Π#	A nondimensional term where # denotes the specific term referred to (= Π#)		
σ	Surface tension of water		1b _f /ft
ρ _w	Density of water	kg/m ³	1b/ft ³
τ _{C50}	Critical shear stress required to move a particle of diameter D50		1b/ft ²
T ₀	Shear stress on the wetted area of the channel acting in the direction of flow = γ _w (R _h)(S _b)		1b/ft ²
ω	Weight of stone		1b

CHAPTER I

INTRODUCTION AND LITERATURE REVIEW

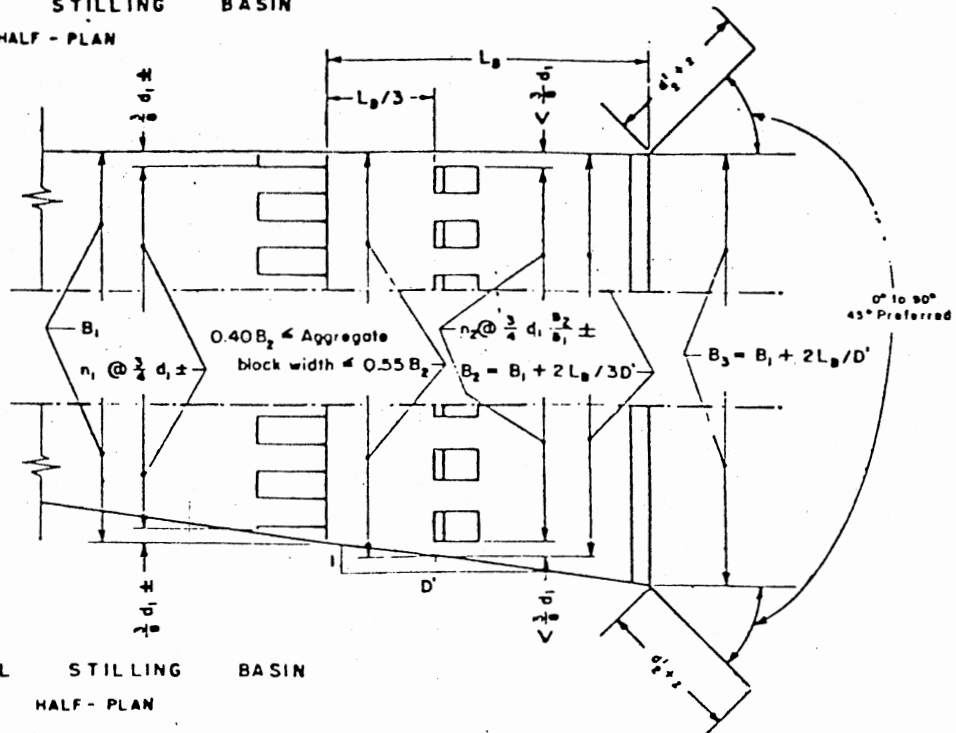
Introduction

The Saint Anthony Falls (SAF) stilling basin is widely used as an energy dissipator for dam releases as well as storm drain outlets. An unprotected channel downstream of a SAF basin may erode. Recent emphasis on sedimentation has encouraged the author to seek information on erosion protection below SAF basins. The model study presented herein is a result of that interest.

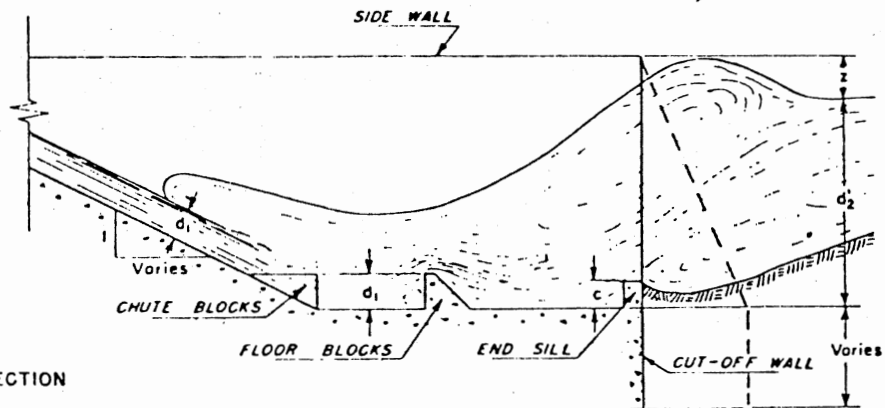
The SAF Basin

SAF stilling basins have been used since the late 1940's for the dissipation of energy found in the high velocity flow exiting from dam chutes or other conveyance structures (3, 6, 11, 14, 21, 22). They cause a hydraulic jump and associated turbulence to occur at a controlled location. The SAF design has been extensively tested and is effective for flow velocities of 2.8 through 70 fps (although cavitation may damage the structure at velocities above 65 fps). Entrance flow depths of up to 6 feet have been tested (6, 10, 21, 25). The design has been used for prototype flow volumes ranging from 110 cfs (as the dissipator for a storm drain outlet) to 24,000 cfs (as a dam outlet structure) although neither of these figures represent absolute limits (14, 21). Top and centerline sections of a SAF basin may be seen in Figure 1.

RECTANGULAR STILLING BASIN
HALF - PLAN



TRAPEZOIDAL STILLING BASIN
HALF - PLAN



CENTERLINE SECTION

SOURCE: Blaisdell, F. W. The SAF Stilling Basin. Washington, D. C.: U.S. Department of Agriculture, Agricultural Handbook No. 156, 1956.

Figure 1. Proportions of the SAF Stilling Basin

Design formulas used by the Soil Conservation Service are found in Figure 2. The Corps of Engineers has modified the third equation from Figure 2 to compensate for Froude number differences. This is shown in Figure 3.

Erosion Below Hydraulic Jump Type Energy Dissipators

Concern about erosion below SAF basins is twofold. First, unremedied erosional processes may eventually cause structural failure. Second, a great deal of emphasis has recently been placed on the maintenance of high water quality standards. Erosion and subsequent sedimentation receive more social, political, and legal attention now than they did several decades ago. Accordingly, there is increasing economic support for soil protection below new and existing structures.

Pictures of existing SAF basins show downstream scour holes (25). Apparently, some basins have been constructed without any outlet channel protection, although riprap installation along the wingwalls is a common practice. Field experience and model studies show this to be a region of relatively high erosion (21). Figure 4 shows erosion which occurred in a model study. Note the scour around the wingwalls. The downstream channel was composed of sand.

Large scale turbulence associated with the hydraulic jump causes severe pressure pulses inside the basin. The magnitude of the pulses has been measured to be about 1.5 times the entering velocity head above or below the static pressure head (26). Bowers and Tsai (7) cited pressure fluctuations on the order of ± 40 percent of the incoming velocity head and indicated that similar pulses must exist downstream.

$$(1) F = \frac{v_1^2}{gd_1} \quad (2) d_2 = \frac{d_1}{2} (-1 + \sqrt{6F+1})$$

$$(3) d_2' = 1.4d_1 F^{0.45} \quad (4) L_B = \frac{4.5d_2}{F^{0.38}}$$

$$(5) z = d_2/3 \quad (6) c = 0.07 d_2$$

B_1 - width of stilling basin at upstream end, in feet
 B_2 - width of stilling basin at floor blocks, in feet
 B_3 - width of stilling basin at downstream end, in feet
 c - height of end sill, in feet
 d_1 - depth of flow at entrance to stilling basin, in feet
 d_2 - downstream depth computed by momentum equation for the hydraulic jump, in feet
 d_2' - water surface elevation in downstream channel

above stilling basin floor, in feet
 D' - side wall divergence, D' longitudinal to l transverse
 F - the Froude number
 g - acceleration due to gravity, in feet per second per second
 L_B - length of stilling basin, in feet
 v_1 - velocity at entrance to stilling basin, in feet per second
 z - height of stilling basin side walls above maximum tailwater level, in feet

SOURCE: Blaisdell, F. W. The SAF Stilling Basin. Washington, D. C.: U. S. Department of Agriculture, Agricultural Handbook No. 156, 1959.

Figure 2. Design Formulas and Symbol Definition for SAF Stilling Basins Used by the Soil Conservation Service

$$F = \frac{v_1^2}{gd_1} \quad (1)$$

$$d_2 = \frac{d_1}{2} (-1 + \sqrt{6F+1}) \quad (2)$$

$$F = 3 \text{ TO } 30 \quad d_2' = (1.10 - F/120) d_2 \quad (3a)$$

$$F = 30 \text{ TO } 120 \quad d_2' = 0.85 d_2 \quad (3b)$$

$$F = 120 \text{ TO } 300 \quad d_2' = (1.00 - F/800) d_2 \quad (3c)$$

$$L_B = \frac{4.5 d_2}{F^{0.38}} \quad (4)$$

$$z = \frac{d_2}{3} \quad (5)$$

$$c = 0.07 d_2 \quad (6)$$

SOURCE: Grace, John L. and Glenn A. Pickering. Evaluation of Three Energy Dissipators for Storm Drain Outlets. Vicksburg, Mississippi: U.S. Army Engineers Waterways Experiment Station, Research Report H-71-1, April 1971.

Figure 3. Modified Formulas for SAF Stilling Basins Used by the Corps of Engineers

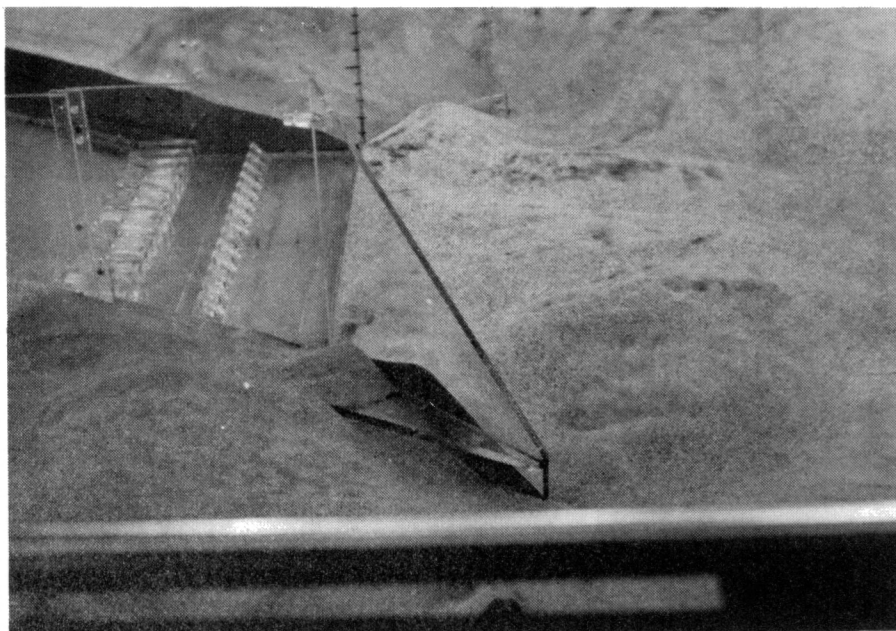


Figure 4. Erosion Around the Wingwalls of a SAF Basin

Campbell (14) stated that vertical pulses affect the stability of rip-rap on the channel floor.

Side rollers are also present in the flow leaving the basin. They are only partially suppressed by the use of wing walls (26). Particles dislodged by wave action are often transported laterally by the side rollers, resulting in semicircular erosion patterns on each channel bank (9).

Equation 1 is commonly used to predict sequent depth after a hydraulic jump (8).

$$D2 = \frac{D1}{2} (-1 + \sqrt{8(F1)^2 + 1}) \quad (1)$$

where,

D2 = Sequent depth (ft).

D1 = Entrance depth (ft).

F1 = Entrance Froude number $\frac{V1}{\sqrt{g(D1)}}$.

V1 = Entrance velocity (ft/s).

g = Acceleration of gravity (ft/s²).

Actual sequent depth is usually 10 to 15 percent less than the theoretical value. This however, does not help one to know how high the waves will be on the channel bank. No means of predicting wave height below SAF basins has been found although research has been performed with other basin types (1).

Methods of Channel Protection

When SAF basins are used with storm drains or other intermittent flow systems (11, 14, 25), it might be assumed that turf would provide suitable channel protection. However, vegetal linings are effective only at relatively low flow velocities and require regular maintenance.

Asphaltic or concrete paving of a section of downstream channel is costly and may also require extensive maintenance. Undissipated pore water pressures beneath the sealed surface can cause fracturing of the surface (4). The ensuing discontinuity results in flow concentration and subsequent undercutting and channel lining failure.

A third soil conservation method is the emplacement of prefabricated blocks of various types. Although effective, this is an expensive alternative.

Another means of erosion protection is the use of stone large enough to remain immobile despite the forces exerted on it by flowing water. Rock is generally available as an economical alternative to the previously mentioned methods. The use of rock riprap is thus suitable as a channel lining for both intermittent and continuous flow conditions (14, 20, 21, 25).

Methods of Determining the Stable Size of Riprap Below Hydraulic Jump Type Energy Dissipators

Different equations have been developed to determine appropriate riprap size below stilling basins. Several of these are based on the Airy Law, which states that the weight of a rock necessary to retain immobility in a flow of water varies as the sixth power of the impinging velocity (2, 15, 23). Isbash developed coefficients to be used with the Airy Law in situations of essentially no boundary layer (16). This equation is shown below.

$$V_b = C_I \left[2g \left(\frac{\gamma_s - \gamma_w}{\gamma_w} \right) \right]^{1/2} \left(\frac{6\omega}{\pi\gamma_s} \right)^{1/6} \quad (2)$$

where, V_b = The velocity of water at the rock \approx the average water velocity (ft/s).

C_I = The Isbash coefficient.

γ_g = Acceleration of gravity (ft/s²).

γ_s = Specific weight of stone (lb/ft³).

γ_w = Specific weight of water (lb/ft³).

ω = The weight of the stone (lb).

Equation 2 may be rewritten by substitution of D for $(6\omega/\pi\gamma_s)^{1/3}$ where D is the diameter of the stone in feet. The coefficients are 0.86 when erosion is by sliding or 1.20 when movement results from rolling or overturning. Tests at the Bonneville Hydraulic Laboratory have confirmed these coefficients and Airy's Law (27). Tests at the U.S. Army Engineers Waterways Experiment Station indicated that the average velocity over the end sill and the C value of 0.86 should be used to determine riprap size below stilling basins (23). The lower coefficient value is selected because of the extreme turbulence in that flow regime.

The Bureau of Reclamation has a design curve for rock of 165 lb/ft³ unit weight. It is very similar to the Isbash curve for a coefficient of 0.86 (20). This curve allows determination of the minimum size of rock necessary to withstand a specific bottom velocity. Initial work by Berry (5) and Mavis and Laushey (18) was combined with lab tests and field observations in preparing the curve. Berry's equation is used for rock of 165 lb/ft³ unit weight. Conversion to units compatible with the rest of the text yields:

$$V_b = 2.57 (0.0833D)^{1/2} \quad (3)$$

where, V_b = Bottom velocity in the channel (ft/s) and is usually estimated to be the same as the average flow velocity.

D = Rock diameter (ft).

Similarly Mavis and Laushey's equation is:

$$V_b = (1/2) (0.00328D)^{1/2} (SG-1)^{1/2} \quad (4)$$

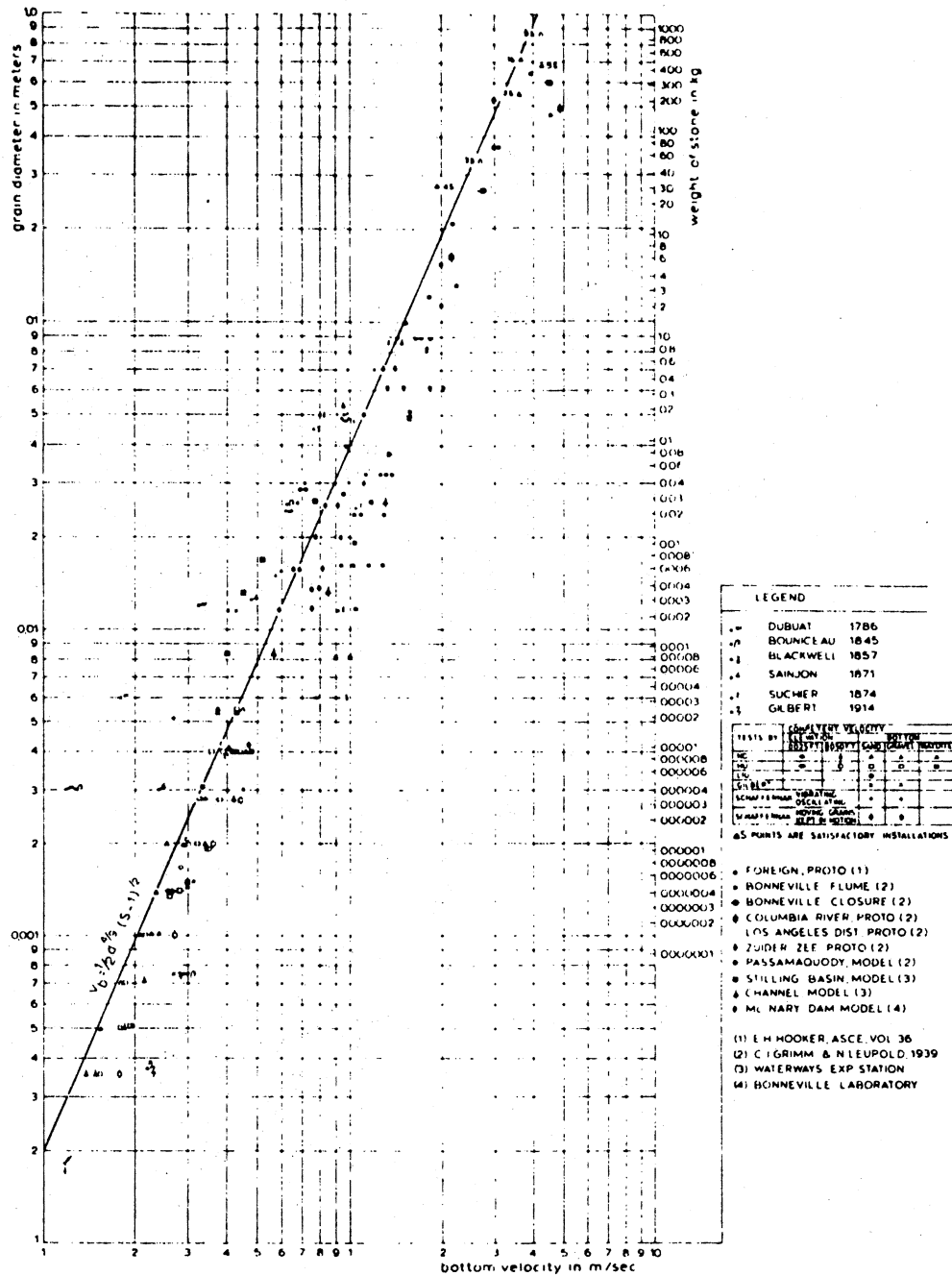
where, SG = The specific gravity.

A slightly more conservative version of Mavis and Laushey's equation has recently been prepared for international use (17). After conversion to units consistent with those of this report, the formula is:

$$V_b = (1/2) (0.00328(D40))^{4/9} (SG-1)^{1/2} \quad (5)$$

where D40 is the diameter of rock in feet of which 40 percent of the material is smaller and V_b is estimated to be the average velocity over the end sill (See Figure 5).

The preceding methods for selecting rock size apply mainly for riprap that is dumped without tamping. They do not reflect the effect of particle interlocking on size requirement.



SOURCE: International Institute for Land Reclamation and Improvement/ILRI. Discharge Measurement Structures. Wageningen, The Netherlands: Publication 20, 1976.

Figure 5. Graph to Determine the D40 to Be Used Below Hydraulic Jump Type Energy Dissipators

CHAPTER II

THE RESEARCH PROBLEM AND APPROACH

Problem and Objectives

SAF basins are used internationally. Engineers have not known if the design equations shown in the Literature Review are applicable for SAF structures, especially since SAF basins are now being built larger and wider than ever before. There has been an associated question which also needed to be answered: "Might smaller rock be used if the desired rock size calculated by formula is locally unobtainable?"

Accordingly, there were two main objectives to this study:

- 1) determine the relative applicability of state of the art techniques for calculating rock size suitable for use below SAF basins,
- 2) determine whether smaller rock may be used.

Research Approach

SAF basins were analyzed by the laws of similitude (See subsequent section entitled Pre-Test Similitude). It was shown that at minimum acceptable tailwater ($D2P_D$), all basins of a particular design entrance Froude number ($F1_D$) could be modeled two-dimensionally by a single model of the same $F1_D$. (The $_D$ subscript denotes design as opposed to calculated values.) Most SAF structures are designed for $F1_D$ values of 2 to 8.4 (See Figure 58 in Appendix A). Making the reasonable assumption

that downstream erosion increases as $F1_D$ increases, it was decided that basins of $F1_D = 4$ and $F1_D = 8$ should be tested. The effect of width was to be studied by using two widths for each $F1_D$. These widths were $9.75 \times D1_D$ and $24.75 \times D1_D$, narrow and wide, respectively. $D1_D$ was .0299 meter (.098 ft). Three rock sizes were to be tested, ranging from a small size near the lower limit of modeling dependability (See section entitled Applicability of Results) to a large size near that considered desirable by a state of the art technique. After each test the scour was to be recorded and subsequently analyzed. Froude modeling criteria could then be used to apply the results of the study to prototypes. There is an upper limit on the size of prototype to which the results should be applied. Since error is magnified when scaling up, the upper limit is determined primarily by the degree of error which is acceptable in a particular situation.

Pre-Testing Similitude

Analysis of Flow Through a SAF Stilling Basin

"Design flow" was used to designate the conditions of design depth and velocity entering the basin ($D1_D, V1_D$) and the minimum tailwater described in Figures 1 and 2. Water will be the fluid in both model and prototype. In a subsequent section entitled Applicability of Results, it is shown that the viscosity, density, compressibility and surface tension of water flowing through a SAF basin need not be considered when analyzing flow through the basin. Hence, Froude modeling criteria are applicable and only the following variables need to be considered when modeling flow through the basin:

$$D1_D, g, LB_D, C_D, D2P_D, V1_D, V3, W_D \quad (6)$$

where W_D is the basin width and the other new terms, except for gravity, are shown in Figure 6.

Use of the Buckingham Π theorem with length and time as basic units and $D1_D$ and g as repeating variables results in Π terms 1-6.

$$\Pi 1 = LB_D/D1_D \quad \Pi 2 = C_D/D1_D \quad (7,8)$$

$$\Pi 3 = D2P_D/D1_D \quad \Pi 4 = V1_D/\sqrt{gD1_D} \quad (9,10)$$

$$\Pi 5A = V3/\sqrt{gD1_D} \quad \Pi 6 = W_D/D1_D \quad (11,12)$$

$\Pi 1$, $\Pi 2$, and $\Pi 3$, etc. are used in the Figures and Tables and are equivalent to $\Pi 1$, $\Pi 2$, $\Pi 3$, etc. If $D3$ is used instead of $V3$:

$$\Pi 5B = D3/D1_D \quad (13)$$

LB_D , C_D , and $D2P_D$ are functions of the design entrance Froude number ($F1_D$ or $\Pi 4$). In Table I we see that $\Pi 1$, $\Pi 2$, and $\Pi 3$ are constants for any particular $\Pi 4$, regardless of how $D1_D$ and $V1_D$ are varied. In other words, SAF basins designed for the same Froude number are geometrically similar as long as their $W_D/D1_D$ ratios ($\Pi 6$) are similar. At the minimum acceptable tailwater depth ($D2P_D$) dynamic similarity is also maintained. Figure 7 shows the range of $D1_D$, $V1_D$, and $F1_D$ for which SAF basins may be designed. It appeared that testing of basins of $F1_D$ values of 4 and 8 would encompass most of the combinations of $V1$ and $D1$ for which basins might be designed. Correspondence with the Soil Conservation Service confirmed this (See Appendix A).

If $f(G)$ represents unknown functions of $\Pi 1$, $\Pi 2$, $\Pi 3$, $\Pi 4$, and $\Pi 6$, it is seen that

$$\Pi 5A = f(G) \quad (14)$$

$$V3 = \sqrt{gD1_D} \times f(G) \quad (15)$$

$$\Pi 5B = f(G) \quad (16)$$

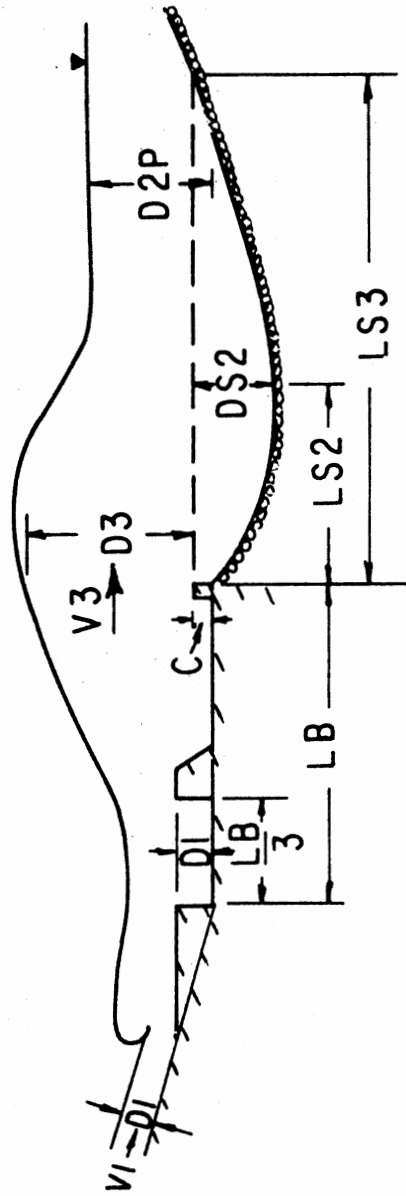


Figure 6. Side View of SAF Basin and Downstream Channel Showing Variables Used in Similitude

TABLE I

NONDIMENSIONAL CHARACTERISTICS OF SAF STILLING
BASINS SHOWING THAT π_1 , π_2 , AND π_3 ARE
CONSTANT AT CONSTANT π_4 REGARDLESS
OF VARIATION IN D_1 AND V_1

D_1	V_1	F_1^2	D_2 WIDTH π_{11}	D_2P CUFF π_{12}	L_2 D π_{13}	C H π_{14}	D_2/D_1 R # π_{15A}	D_3 HWHL π_{15B}	V_3 π_{11}	π_{12}	π_{14}
1.0981	5.9426	1.0000	1.0981 2.4354 4.5000	1.5373 1.0000 0.0700	4.9414 15.8924 1.4000	0.0769 0.5490 1.0000	1.0000 536204 0.5051	2.1742 1.9034 1.9800	3.0013 0.3589	0.7071	0.0354
2.0981	8.2143	1.0000	2.0981 2.4354 4.5000	2.9373 1.0000 0.0700	9.4414 41.9727 1.4000	0.1469 1.0480 1.0000	1.0000 1416141 0.5051	4.1542 3.8367 1.9800	4.1486 0.3589	0.7071	0.0354
3.0981	9.9817	1.0000	3.0981 2.4354 4.5000	4.3373 1.0000 0.0700	13.9414 75.3132 1.4000	0.2169 1.5490 1.0000	1.0000 2541033 0.5051	6.1342 5.3700 1.9800	5.0413 0.3589	0.7071	0.0354
4.0981	11.4802	1.0000	4.0981 2.4354 4.5000	5.7373 1.0000 0.0700	18.4414 114.5782 1.4000	0.2869 2.0490 1.0000	1.0000 3865818 0.5051	8.1142 7.1034 1.9800	5.7981 0.3589	0.7071	0.0354
1.0981	11.8853	4.0000	2.6050 2.4354 6.3037	2.8688 1.0000 0.1661	6.9221 31.7849 2.6125	0.1823 2.1962 2.0000	2.3723 1072408 0.7194	3.0527 3.7371 2.7800	4.2753 0.4315	0.9397	0.0597
2.0981	16.4286	4.0000	4.9773 2.4354 6.3037	5.4813 1.0000 0.1661	13.2258 83.9454 2.6125	0.3484 4.1962 2.0000	2.3723 2832279 0.7194	5.8327 7.1408 2.7800	5.9096 0.4315	0.9397	0.0597
3.0981	19.9635	4.0000	7.3496 2.4354 6.3037	8.0938 1.0000 0.1661	19.5295 150.6265 2.6125	0.5145 6.1962 2.0000	2.3723 5082068 0.7194	8.6127 10.5436 2.7800	7.1811 0.4315	0.9397	0.0597
4.0981	22.9604	4.0000	9.7218 2.4354 6.3037	10.7062 1.0000 0.1661	25.8332 229.1564 2.6125	0.6805 8.1962 2.0000	2.3723 7731631 0.7194	11.3927 13.9469 2.7800	8.2591 0.4315	0.9397	0.0597
1.0981	17.8279	9.0000	4.1420 2.4354 7.3650	4.1322 1.0000 0.2640	8.0875 47.6773 3.7630	0.2899 4.9414 3.0000	3.7720 1608609 0.8380	3.9312 5.5128 3.5800	4.9799 0.4429	1.0511	0.0738
2.0981	24.6429	9.0000	7.9140 2.4354 7.3650	7.8952 1.0000 0.2640	15.4525 125.9182 3.7630	0.5540 9.4414 3.0000	3.7720 4248420 0.8380	7.5112 10.5332 3.5800	6.8835 0.4429	1.0511	0.0738
3.0981	29.9452	9.0000	11.6860 2.4354 7.3650	11.6582 1.0000 0.2640	22.8175 225.9397 3.7630	0.8180 13.9414 3.0000	3.7720 7623100 0.8380	11.0912 15.5536 3.5800	8.3646 0.4429	1.0511	0.0738
4.0981	34.4406	9.0000	15.4580 2.4354 7.3650	15.4212 1.0000 0.2640	30.1825 343.7344 3.7630	1.0821 18.4414 3.0000	3.7720 11597440 0.8380	14.6712 20.5739 3.5800	9.6203 0.4429	1.0511	0.0738
1.0981	23.7705	16.0000	5.6870 2.4354 8.1262	5.3533 1.0000 0.3625	8.9233 61.5698 4.8751	0.3981 8.7848 4.0000	5.1789 2144815 0.9132	4.8097 7.2490 4.3800	5.4271 0.4364	1.1130	0.0828

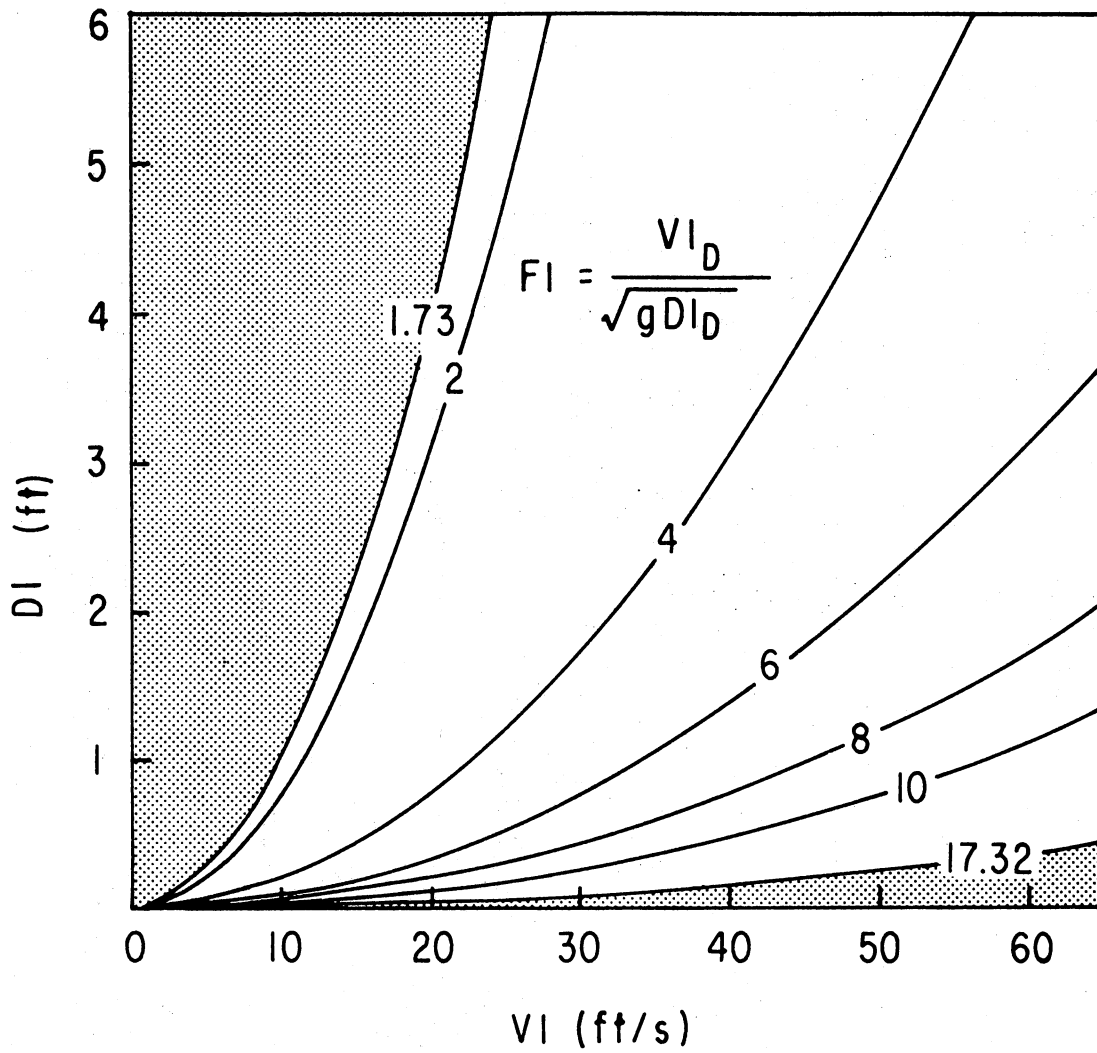


Figure 7. Range of Entrance Froude Numbers ($F1_D$) for Which SAF Stilling Basins May Be Designed

$$D3 = D1_D \times f(G) \quad (17)$$

Analysis of Scour in the "Equilibrium" Scour

Hole Below SAF Stilling Basins

Scour holes are near an "equilibrium" condition when little or no subsequent degradation occurs with time at a particular flow rate (24, 28). Under equilibrium conditions the boundary material of the scour hole is no longer susceptible to the turbulence associated with the structure (13, 24). Also, lift forces are not comparable in magnitude with drag forces (28), just as is true for uniform flow conditions (29). Since, within limits, the thickness of the end sill has little effect on flow patterns (19), this parameter was not considered. It was assumed that the downstream channel would be the same at the beginning of all tests. Thus the following variables were initially used to describe the scour hole. (The # symbol refers to the position numbers seen in Figure 8.)

$$\gamma, g, D3, V3, D2P_D, \tau_{C50}, LS\#, C_D, W_D \quad (18)$$

where, $\gamma = (\gamma_S - \gamma_W)$, the submerged particle specific weight (lb/ft³).

γ_S = Unit weight of the rock material (lb/ft³).

γ_W = Unit weight of water (lb/ft³).

τ_{C50} = The critical shear stress required to remove a particle of diameter D50 (lb/ft²).

D50 = Diameter of rock which is greater than 50% of the rocks in a population (ft).

LS# = Length to a particular position number (#) in the scour hole.

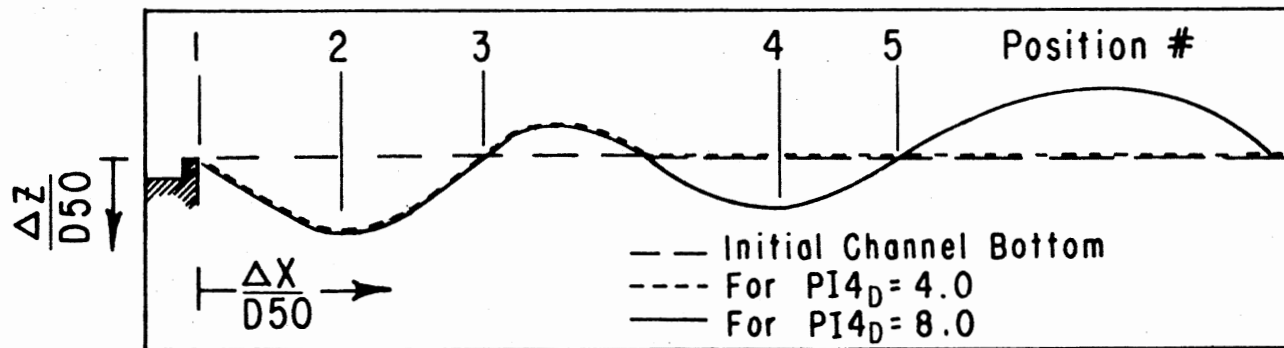


Figure 8. Location of Significant Positions Shown on a Sideview of the Downstream Scour Beds Which Occur Below Basins of $PI4_D = 4$ and $PI4_D = 8$

When mass, length, and time are the basic units and γ , g , and D_3 are repeating variables, the Buckingham Π theorem yields:

$$\Pi_{11} = V_3/\sqrt{g(D_3)} = \Pi_{5A}/\sqrt{\Pi_{5B}} \quad (19)$$

$$\Pi_{12} = D_2 P_D / D_3 = \Pi_3 / \Pi_{5B} \quad (20)$$

$$\Pi_{13} = \tau_{C50} / \gamma D_3 = \tau_{C50} / (\gamma) (D_{1D}) (\Pi_{5B}) \quad (21)$$

$$\Pi_{14} = C_D / D_3 = \Pi_2 / \Pi_{5B} \quad (22)$$

$$\Pi_{LS\#} = LS\# / D_3 = LS\# / (D_{1D}) (\Pi_{5B}) \quad (23)$$

$$\Pi_{16} = W_D / D_3 = \Pi_6 / \Pi_{5B} \quad (24)$$

Let $f(P_2)$ be unknown functions of Π_{11} , Π_{12} , Π_{13} , Π_{14} , and Π_{16}

$$LS\# = D_{1D} \times \Pi_{5B} \times f(P_2) \quad (25)$$

Depth of scour at a location # ($DS\#$) was described by substitution for $LS\#$ in the above equations.

$$DS\# = D_{1D} \times \Pi_{5B} \times f(P_2) \quad (26)$$

It should be noted that there is a linear relation between D_{50} and τ_{C50} at impending motion (See Figure 9).

$$D_{50} = \tau_{C50} / 5 \quad (27)$$

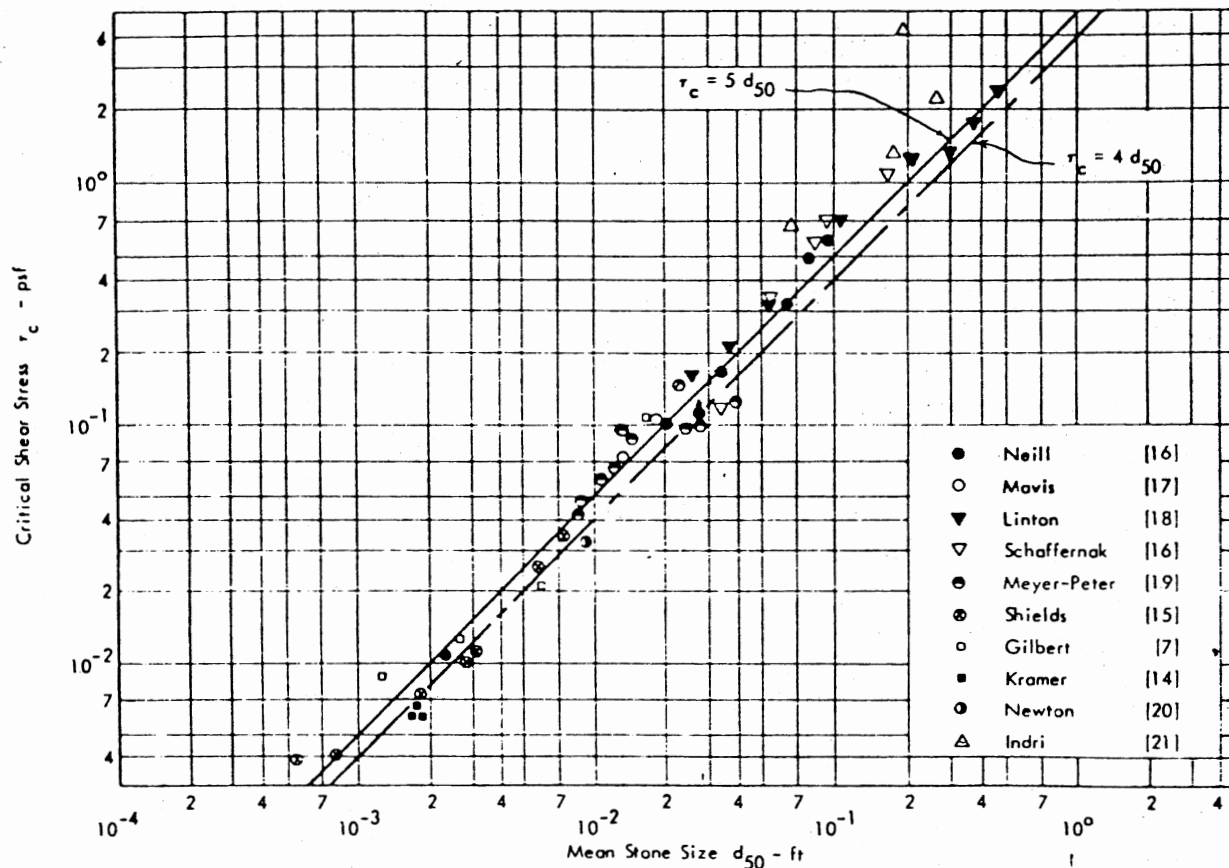
A more conservative estimate has been widely used in riprap design in open channels (4).

$$D_{50} = \tau_{C50} / 4 \quad (28)$$

Applicability of Results

This research depended upon correct modeling of the stability of riprap particles in different locations in a scour bed. Assumptions of uniform open channel flow are generally used with success in this situation and were used in the following analysis.

The specific gravity and particle size distribution in the model was similar to that expected in a prototype. Since a particle's



SOURCE: Anderson, A. G. and A. S. Paintal. Tentative Design Procedure for Riprap-Lined Channels. Washington, D. C.: Highway Research Board, National Cooperative Highway Research Program Report No. 108, 1970.

Figure 9. Critical Boundary Shear at Incipient Movement of Riprap in Terms of D_{50}

stability depends on the interaction of its weight and the drag exerted on it by the flowfield, the following system analysis was made.

$$\frac{DF}{\rho_w V^2 D_w^2} = f(\lambda, F, R, WE, CA) \quad (29)$$

where DR is the drag force on the channel bottom (lb) and ρ_w , V and D_w are the density (lb/ft³), velocity (ft/s) and depth (ft) of the fluid (19). The ratio of prototype to model length is equal to λ and the other Π terms are the Froude, Reynolds, Weber and Cauchy numbers, respectively.

Water was used as the fluid in both model and prototype. Since it is incompressible, CA could be disregarded. As long as the flow depth in the model exceeded 0.25 inches, surface tension was negligible and WE could be discarded. It was necessary to show that viscous effects would be similar in both model and prototype. The following paragraphs show how this was determined for the initiation of motion of particles on the channel bottom.

Begin by assuming that the rock particles may be simulated by spheres. For spheres, graphing of $DF/(\rho_w V^2 D_w^2)$ versus R shows that $DF/(\rho_w V^2 D_w^2)$ ceases to be affected by variation of R in fully developed turbulent flow (19). Assume that fully turbulent flow exists in the prototype. In this flow regime the critical shear stress on a particle of diameter D50 lying on a horizontal bed is:

$$\tau_{C50} = k (\gamma_s - \gamma_w) D50 \tan \theta \quad (30)$$

where k adjusts for the irregularities in particle shape and θ is the angle of repose (24). Rearranging this equation, the left term is the ratio of drag to gravitational force and is called the shear Froude number F_* (Shield's Parameter).

$$\frac{\tau_{C50}}{(\gamma_S - \gamma_W) D50} = k \tan \theta \quad (31)$$

Simons and Senturk (24) showed that dimensional analysis of a particle at incipient motion may yield:

$$\frac{\tau_c}{(\gamma_S - \gamma_W) D50} = \frac{\rho V_{*c}^2}{(\gamma_S - \gamma_W) D50} = f\left(\frac{V_{*c} D50}{\nu}\right) \quad (32)$$

where ν is the kinematic viscosity (ft²/s), V_{*c} is the critical shear velocity (ft/s) and the term on the right represents the shear Reynolds number R_{*} . This relation between F_{*} and R_{*} has often been plotted on "Shields diagrams". Yalin (30) indicates completely rough turbulent flow will exist when $R_{*} > 70$ to 150. $(V_{*c} D50)$ will always be larger for the prototype than for the model. Therefore, as long as fully developed turbulent flow exists in the model, it will exist in the prototype, and viscous effects will be similar in each. The following procedure has been used by Yalin (30). It determines the size of the smallest particles which can be used to simulate initiation of motion.

$$70 < R_{*m} < R_{*p} \quad (33)$$

$$70 < \left(\frac{V_{*c} D50}{\nu}\right)_m \quad (34)$$

$$\left(\frac{70}{\left(\frac{V_{*c} D50}{\nu}\right)_p}\right) < \frac{(V_{*c})_m}{(V_{*c})_p} \left(\frac{D50_m}{D50_p}\right) \quad (35)$$

From the Froude modeling criteria

$$\lambda = \frac{L_p}{L_m} \quad \text{and} \quad \lambda^{1/2} = \frac{V_p}{V_m} \quad (36,37)$$

$$\left(\frac{70}{\left(\frac{V_{*c} D50}{\nu}\right)_p}\right)^{2/3} < \frac{1}{\lambda} \quad (38)$$

The "Shield's Diagram" in Figure 10 shows that $F_* = 0.047$ when $R_* = 70$. From Equation 32:

$$V_{*c} = \sqrt{0.047(\gamma_s - \gamma_w) D50/\rho} \quad (39)$$

$$\frac{1}{\lambda} = \frac{1}{D50} \frac{70}{(0.047 (\gamma_s - \gamma_w)/\rho)^{1/2}} \quad (40)$$

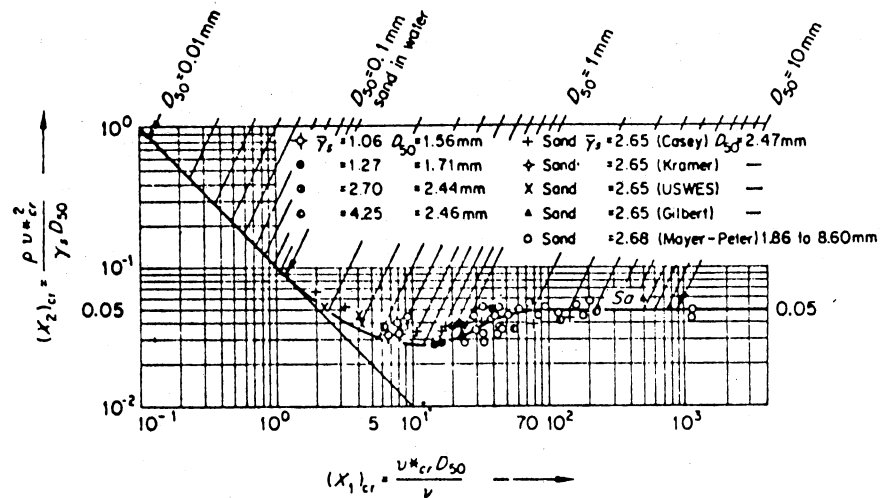
Using $\gamma_s = 2.81 \gamma_w$ and ρ and ν at 70° F, one obtains

$$D50 > 0.0059\lambda \text{ feet}$$

Therefore, to have relative confidence in simulating initiation of motion, the smallest D50 which may be used in the model is 1.798 mm (0.0059 ft). Rock this size or larger, should guarantee that completely rough turbulent flow exists in both model and prototype. It also sets a lower limit on the size of prototype rock which may be modeled, i.e. if λ is 50, the smallest prototype rock which may be modeled is .295 feet.

Thus, as long as the rock used in the model study was greater than or equal to 1.798 mm (0.0059 ft), fully rough turbulent flow would exist in the model and prototype and similarity would be achieved by Froude modeling

$$\frac{DF}{\rho_w V_w^2 D_w^2} = f(\lambda, F) \quad (41)$$



SOURCE: Yalin, M. Selim. Theory of Hydraulic Models.
New York: The MacMillan Press Ltd., 1971.

Figure 10. Shield's Diagram Showing Relation Between
Shear Froude Number and Shear Reynolds
Number at Initiation of Motion

CHAPTER III

THE PHYSICAL SET-UP

Introduction

Experimentation was conducted at the USDA-SEA-AR Water Conservation Structures Laboratory at Lake Carl Blackwell, west of Stillwater, Oklahoma. An 11.28 x 3.05 meter (37 x 10 ft) level flume was used in the study (See Figure 11). Water was obtained from the lake by 0.508 m (20 inch) siphon. The lake water surface elevation was relatively unaffected by the water withdrawn during the tests. The flowrate obtainable at the flume depended on the lake water level. The flowrate of 0.095 cms (3.4 cfs) which was required for the full width, $F1_D = 8$ model, was not available throughout the year. The experimental system was composed of an entering .3048 m (12 inch) line, head tank, chute and model riprap scour bed, and appropriate instrumentation. The supply line, tank, narrow width chute and basin are shown in Figure 12.

Head Tank and Entering Depth Control Devices

A head tank was built to reduce turbulence and to straighten flow streamlines prior to their entering the chute. It was assembled using structural steel angles and aluminum sheet, and contained a vertical wire and baffle with 6.35 mm (0.25 in) screen mesh, both of which were perpendicular to the flow direction. There were also false walls parallel to the flow which served as extensions of the chute side walls

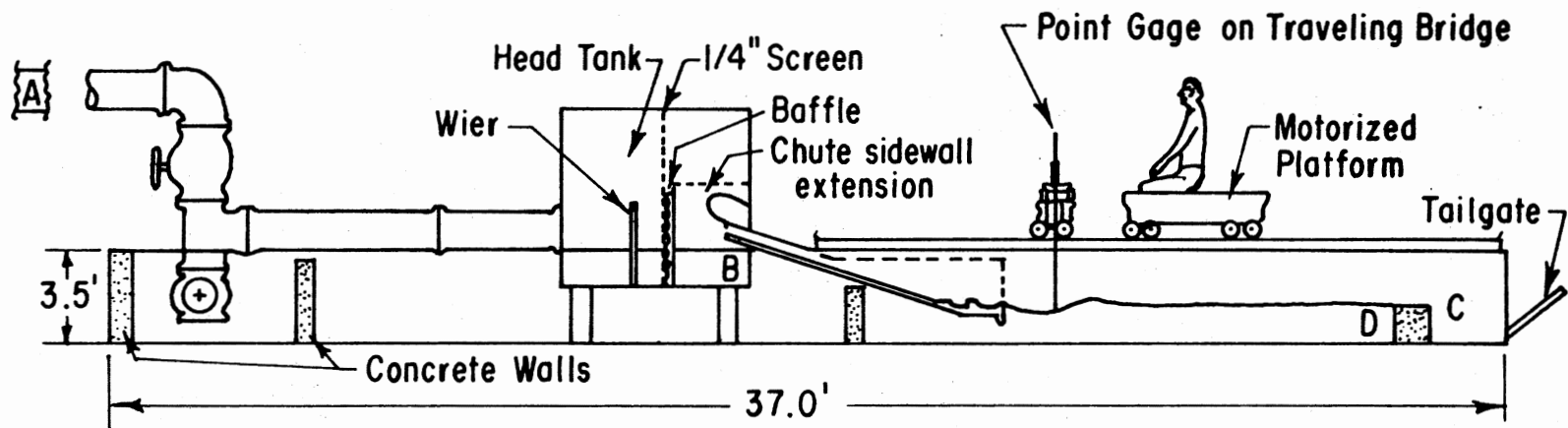


Figure 11. Side View of Laboratory Showing Supply Pipe, Head Tank, and Model in the Flume

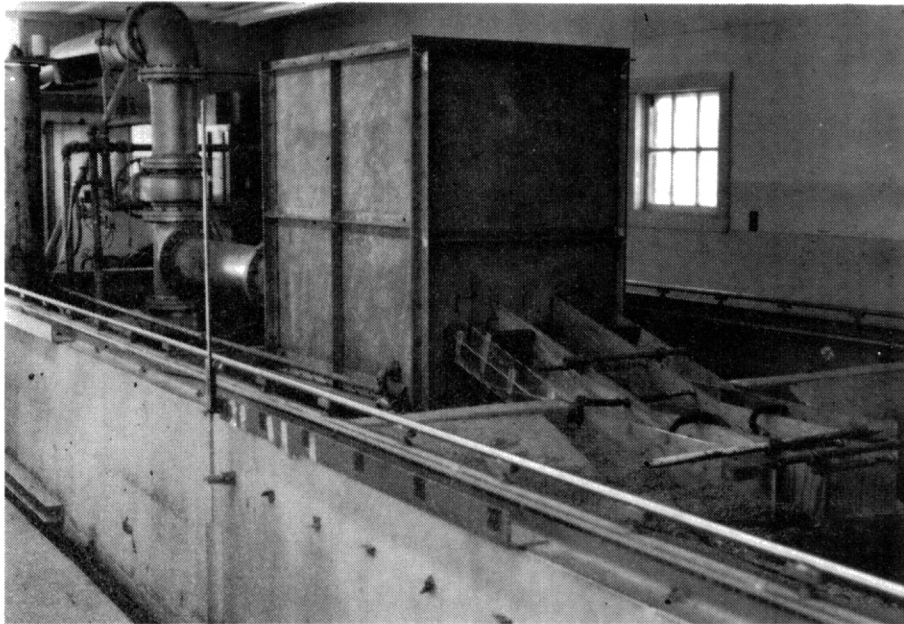


Figure 12. Photograph Showing Supply Pipe, Head Tank, and Model with False Walls in Place

(See Figure 11). The height of the opening through which flow left the tank was controlled as shown in Figure 13. The exit lip was parabolic in shape to encourage the development of parallel streamlines. This exit lip was used to control the depth of flow entering the basin (D_1) for $F1_D$ equal to 8. When $F1_D$ was 4, however, "short tube control" was used to slow and deepen the flow to achieve the proper depth (See Figure 14). Two banks of 1.27 cm (0.05 in) O.D., 7.62 cm (3 in) long PVC tubes were placed parallel to the flow in the chute. Each bank was 5 tubes high and reached from sidewall to sidewall. The banks were covered by a piece of plywood parallel to the chute floor, which served to anchor them in place and prevented their overtopping. The disturbance to the water surface caused by the tubes smoothed out a short distance downstream.

Chute and Model SAF Basin

SCS design equations (Figure 2) were used for the model stilling basin. Except for the false side and wingwalls used in the narrow basin experiments, the chute and model were machined from plexiglas to tolerance less than 0.0015 m (0.005 ft). The slope of the chute was 1:3.48 ($\cos \theta = 0.961$). The chute was supported at the head tank, at the basin and at two locations in between. One center support was bolted to each side of the concrete cutoff wall seen in Figure 11. Five screws were used in each support to level the chute across its width.

Figure 15 shows a cross section and top view of the model and chute. To minimize labor and material costs, the model was designed for a constant chute block and floor block height ($D1_D$). The following

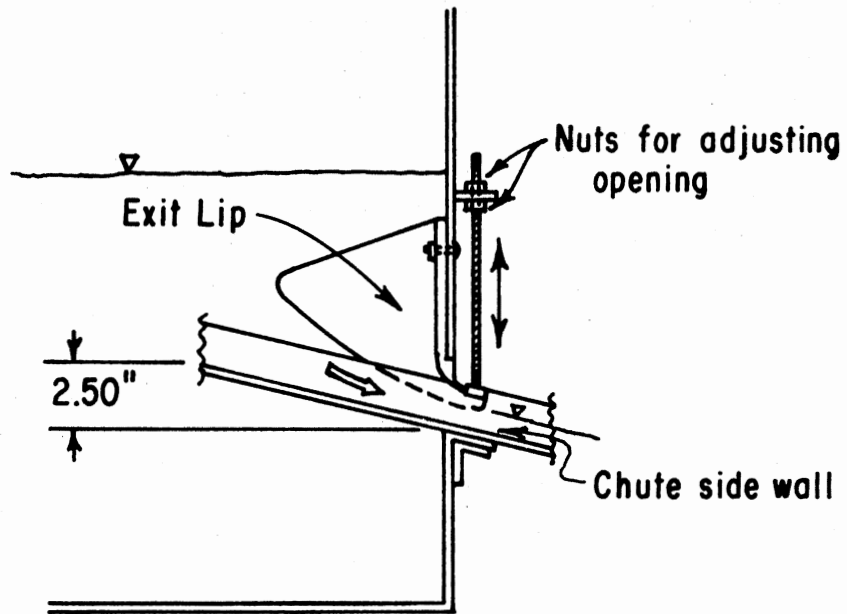


Figure 13. Side View of Head Tank Exit Showing How Opening Could Be Adjusted

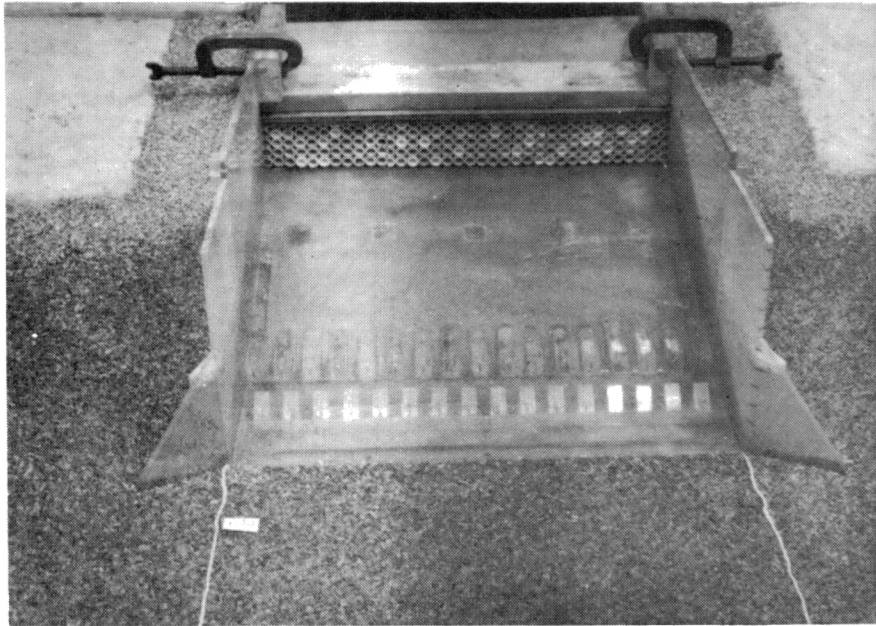


Figure 14. Set-Up to Achieve Short Tube Control
in the Chute

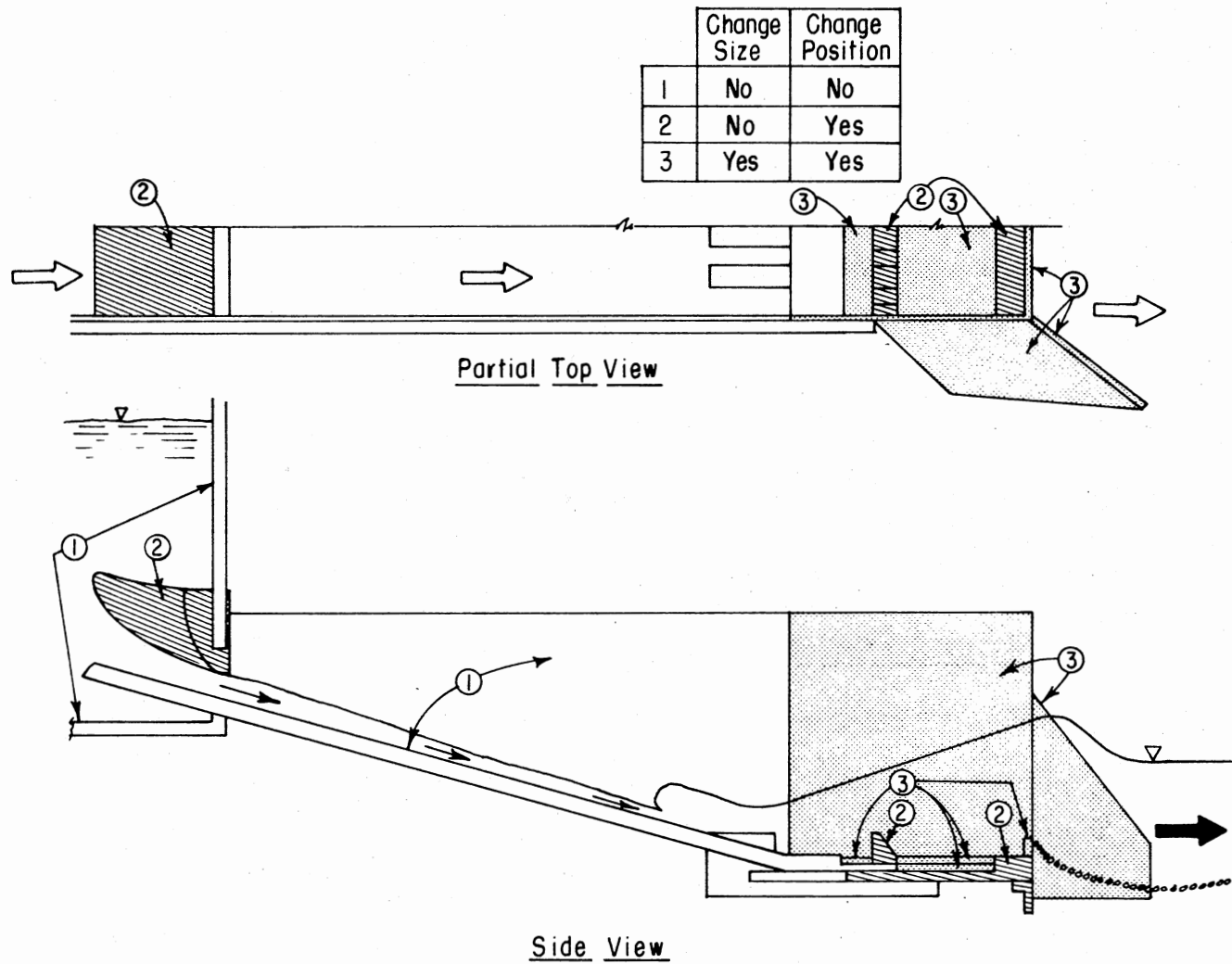


Figure 15. Top and Side Views of Model SAF Basin Showing How Pieces Were Varied to Obtain Basins of Different Fl_D 's

dimensions, however, varied depending on the design entrance Froude number (Fl_D): basin length, end sill height, wingwall length and height and the distance between the basin entrance and the floor blocks. To handle the variation in dimensions, the model was designed with certain pieces fixed, some moveable, and some variable in size and location. The basin was attached to the floor of the flume using threaded bolts and was leveled prior to testing.

Riprap

Crushed stone ($SG = 2.81$) was obtained from local quarries. This angular stone was sorted into distinct groups, each with a narrow range of sizes. The Soil Conservation Service uses this criterion for riprap layers: the largest rock diameter (D_{100}) divided by the D_{50} diameter should equal 1.3. Therefore, the ratio between D_{100} and D_0 (the smallest size) could be estimated by $(1.3)^2 = 1.69$. Bearing in mind that 1.8 mm (.0059 ft) is the smallest size that can be used with relative confidence in modeling rock of this SG , screens with the following opening sizes were purchased: 2.588, 4.351, 7.272, and 12.446 mm (0.0085, 0.0143, 0.0239, and 0.0408 ft). These were mounted in frames and a carriage was devised to facilitate hand screening of the rock (See Figure 16). The grain size distributions and D_{50} values of the three resultant groups are shown in Figure 17.

Table II shows a comparison between the experimental rock and spheres of the same D_{50} (D_{50_m}) and average particle mass ($MASS_m$) for $SG = 2.81$ (columns C, D, G, and H). Because of their shape, the particles generally had less mass than spheres of the same specific gravity and of diameter equaling D_{50} (See Column D).



Figure 16. Rock Screens, Carriage, and Willing Worker

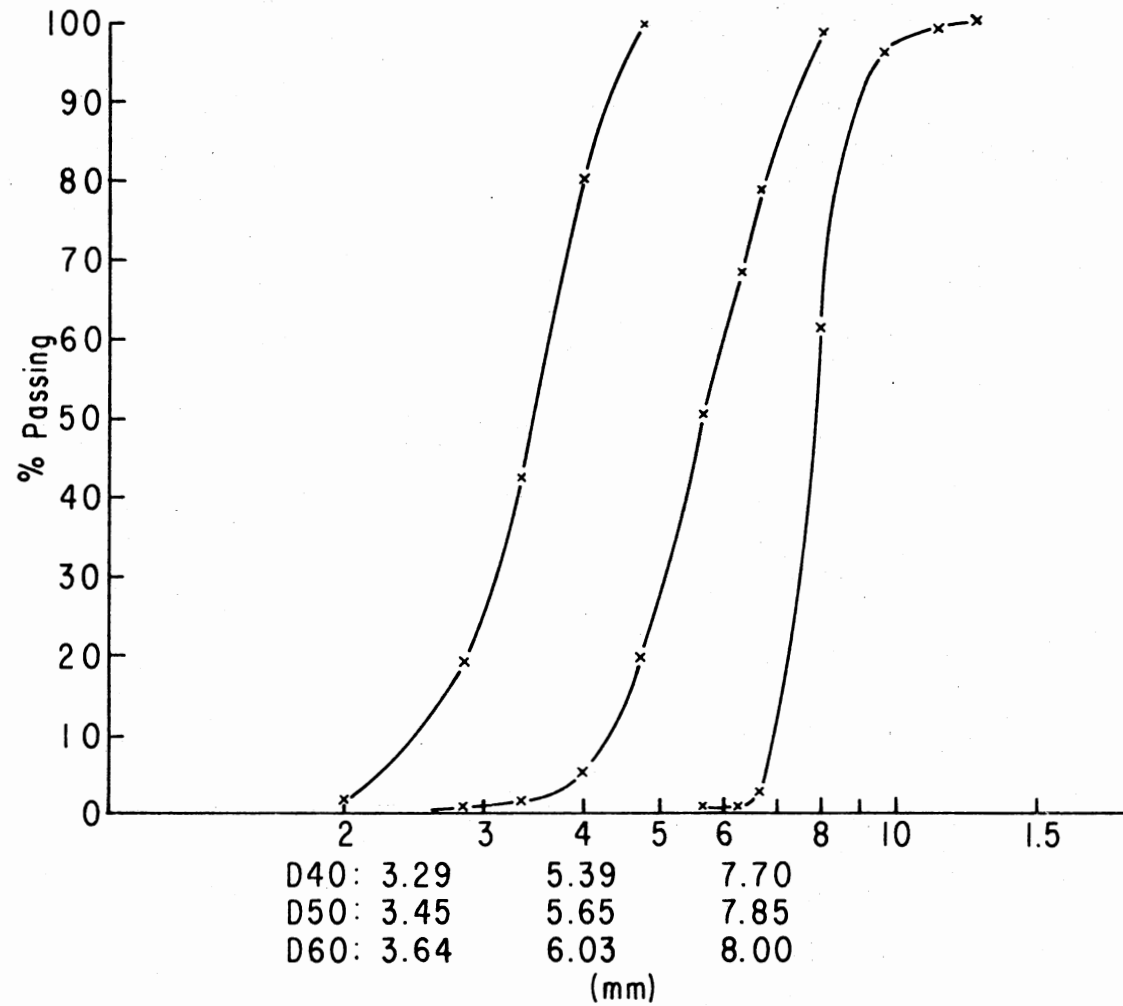


Figure 17. Grain Size Distributions of Rock Used in the Model Tests

TABLE II

COMPARISON OF EXPERIMENTAL ROCK WITH SPHERES OF
 SAME D50 ($D50_m$), SAME MASS ($MASS_m$) AND
 SPECIFIC GRAVITIES OF 2.65 AND 2.81

Experimental			Calculated						
A*	B*	C	D	E	F	G	H	I	J
$D50_m$	$MASS_m$	Mass of sphere of $D50=D50_m$ (SG=2.81)	$\frac{B - C}{C}$	Mass of sphere of $D50=D50_m$ (SG=2.65)	$\frac{B - E}{E}$	D50 of sphere of mass= $MASS_m$ (SG=2.81)	$\frac{A - G}{G}$	D50 of sphere of mass= $MASS_m$ (SG=2.65)	$\frac{A - I}{I}$
(cm)	(g)	(g)		(g)		(cm)		(cm)	
0.345	0.055	0.060	-0.083	0.057	-0.028	0.335	0.03	0.342	0.009
.565	.255	.265	- .040	.250	.018	.557	.014	.568	- .005
.785	.547	.712	- .231	.671	- .185	.719	.092	.733	.071

* Experimental Data.

Since the weight of a particle is generally considered to be more important than the shape as far as resistance to erosion is concerned and the specific gravity of riprap is often simply estimated to be 2.65, the experimental rock was also compared with appropriate spheres of $SG = 2.65$ (See columns E, F, I and J). Once again, the particles were lighter than comparable spheres. The conclusion is the same in both cases. If the prototype rock is more rounded than the model rock, prototype scour will be less than that predicted by the model tests.

Instrumentation and XYZ Orientation

Flowrate through the system was determined by use of a manometer and calibrated orifice plates (Position A in Figure 11). The water surface in the head tank and at the downstream end of the flume were monitored in gage wells connected to positions B and C. (Position B is outside of the false walls in a relatively placid region.) Twenty-four hour monitoring was achieved through the use of recorders. A sand filter was buried beneath the channel bottom at position D. This was connected to a gage well whose water surface could be determined by point gage. In the extreme left of Figure 12 is the gage well connected to position B. The point gage and gage well used to monitor position D are seen in the left foreground.

The X and Y axes were coincident with and perpendicular to the basin centerline, respectively. X increased downstream from XZERO which was located at the downstream edge of the basin end sill. YZERO existed at the basin centerline. Y increased in both directions away from YZERO. The Z axis was perpendicular to the XY plane. ZZERO was located at the elevation of the basin floor.

A point gage on a traveling bridge was used to determine locations of solid and fluid boundaries. The blunt end of a 0.635 cm (0.25 in) probe was used in examining the scour bed. The pointed end of the probe was used to determine water surface elevations for the $F1 = 4$ flow (Figure 18).

The water surface near the hydraulic jump was very irregular for the flow of $F1 = 8$. For these tests an electronic system was devised to locate the average water surface. The system used is shown in Figure 19. A 10-volt P-P, 100 kHz sine wave signal was generated and sent through the upstream probe. When that probe touched the water surface, the downstream probe picked up the signal. The counter counted the pulses and averaged their frequency over 10 second intervals. The averages of 6 intervals were generally used to determine location average in XYZ space. To determine the water surface elevation at a specific location in the XY plane, 60 second averages were made at two elevations, one with an average count greater than 50 kHz, the other with an average less than 50 kHz. Linear interpolation was used to determine the elevation which would have a count of 50 kHz. This was assumed to represent the average water surface.

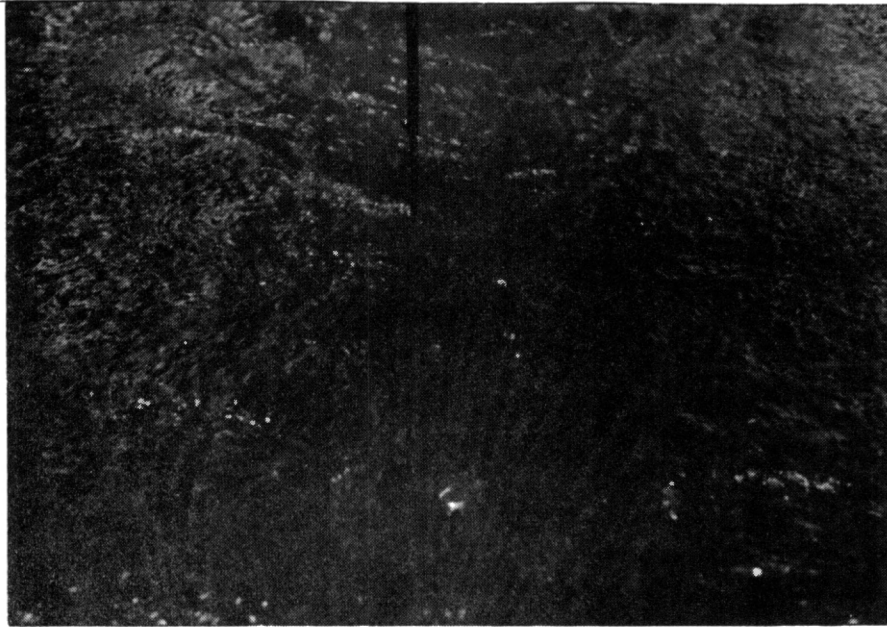


Figure 18. Pointed End of Probe Used for Measuring
Water Surface Elevations for $Fl_D = 4.0$

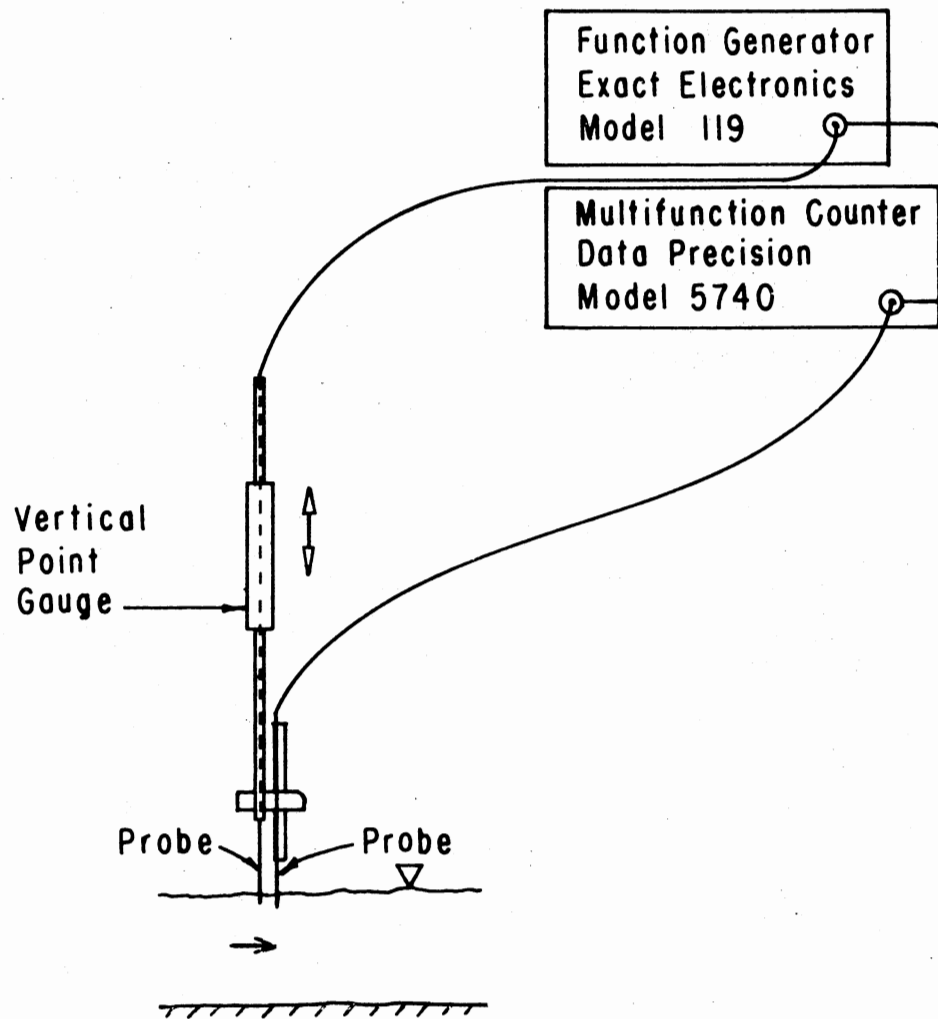


Figure 19. Electronic System for Estimating the Average Water Surface Elevation

CHAPTER IV

INITIAL TESTING AND TEST PROCEDURE

Initial Testing

Determination of Test Duration

One of the first decisions to be made was how long tests should run. The Corps of Engineers Waterways Experiment Station often has tests of 20 to 60 minutes in duration, during which time a relatively "stable" scour hole develops. Some personnel at other laboratories feel that longer tests are desirable. A 60-minute test is adequate to determine relative stability of a given riprap size under a given flow. Whether or not it is adequate to determine eventual scour hole size had to be determined. Six tests of various time durations were run using a model basin for $F1_D = 4$, width of $24.75 \times D1$ and riprap of 3.45 mm (0.0113 ft) D50 diameter. As in all other tests in this dissertation, the Froude number of the flow was as close as possible to the $F1_D$ of the model. Three of these tests are compared in Figure 20 by the use of composite scour profiles (CMSP). These profiles were formed by finding the maximum depths, and lengths to specified elevations, across the entire width of the channel floor, and combining them into a single CMSP. This artifice was necessary because the scour hole shape varied with location from the channel centerline. One notes that the 24-hour test scoured about 2 x D50 deeper than the 4-hour test. Since riprap

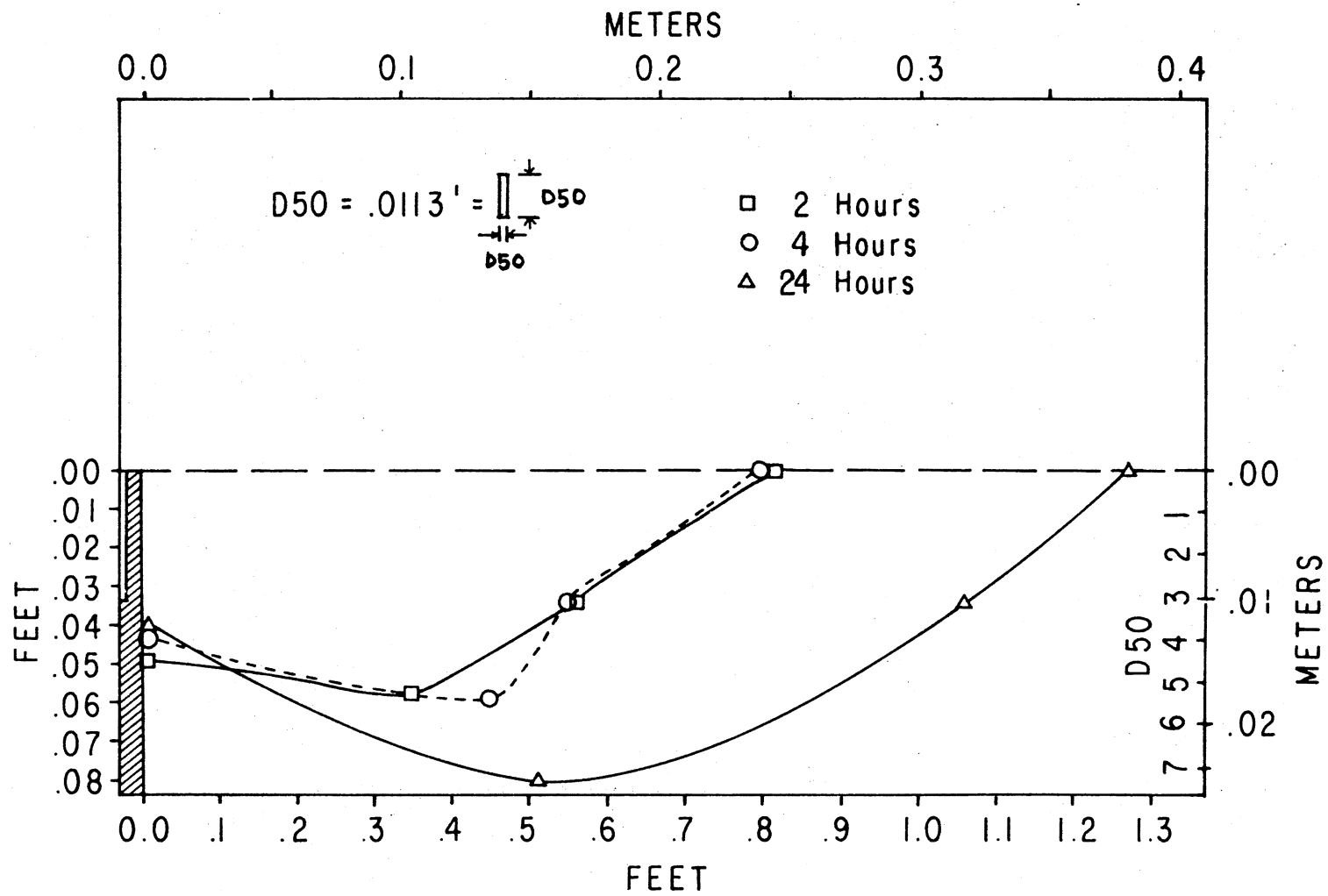


Figure 20. Side View Showing the Development with Time of Scour Downstream of the End Sill

layers are often made 2 x D50 thick, it seemed appropriate to use a test of duration exceeding 4 hours.

The SCS builds SAF basins with widths as small as 1.22 m (4 feet). This would correspond to a length scale of $n = 1.639$ or a time scale of $\sqrt{1.639}$. In order to model at least one day of prototype flow in each test, 24 hours was chosen to be the length of all subsequent tests, unless stated otherwise.

Determination of Channel Initial Condition

It was felt that the information obtained by this research program could be utilized in the field in the following manner:

Given certain initial conditions, a 24-hour test would be run, and the resultant scour hole mapped. Appropriately scaled up, a prototype preformed scour hole could be designed using easy-to-construct geometric shapes. As long as the preformed "hole" encompassed the entire volume of expected scour, it could be expected to be a stable design.

This hypothesis was tested.

A test was run with $Fl_D = 8$, width = $24.75 \times D1$, and $D50 = 3.45$ mm (0.0113 ft). The downstream trapezoidal channel was initially of the same width with 3:1 side slopes and zero bottom slope. Its bottom was at the same elevation as the top of the end sill. The resultant scour hole was contoured and the halves on each side of the X axis were compared point by point. Points indicating the most scour were combined into a maximum scour contour map (MSCM). This is shown in Figure 21. A preformed scour hole using easy to construct straight gradients was designed around the scour hole. Another test was run and the scour

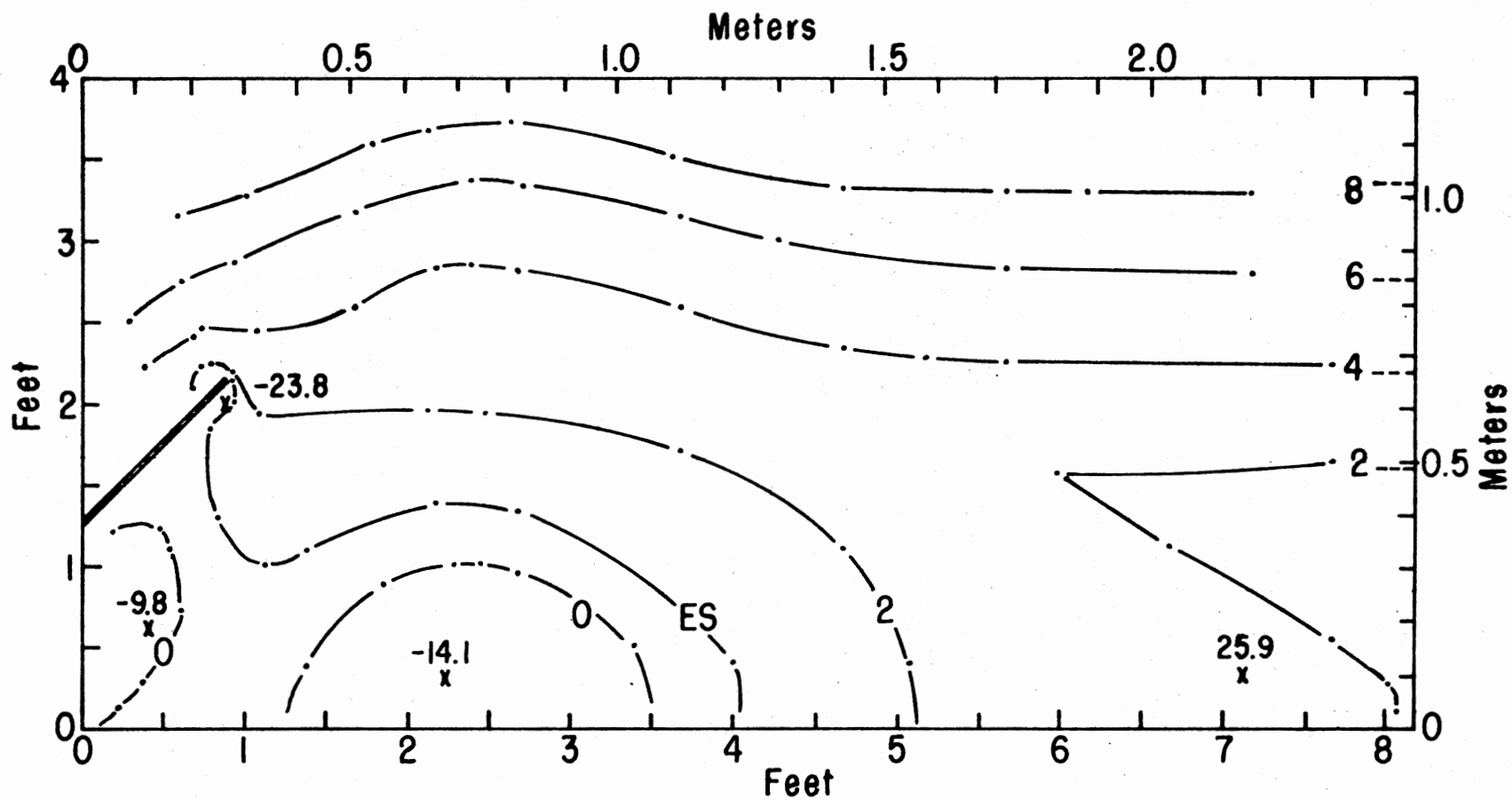


Figure 21. Maximum Scour Contour Map After Testing at $F1_D = 8.0$, $W = 24.75 \times D1_D$, $D50 = 3.45 \text{ mm}$ (.0113 ft)

hole mapped (See Figure 22). The preformed scour hole was not satisfactory. In some places the side slopes were flattened to slopes of 4-6:1. It was concluded that the stone was too light for the flow, so the stone was replaced with the next larger size, 5.65 mm (0.0185 ft).

The downstream channel was formed to a trapezoidal shape, with slope of 3:1, and a bottom elevation the same as that of the basin floor. This design was tested (Test 30) and the resultant mapped in Figure 23. After this test all material deposited above the design elevations was removed. Scoured areas were left untouched. Another test (Test 31) was run and scour recorded (Figure 24). Removal of the deposition mound permitted increased erosion of the channel bottom to occur. The effect on the channel sides was slight. Another 20 hours of flow was run through the existing channel and significant details of the resulting scour noted (Test 32 and Figure 24). Sixty-eight more hours were run (Test 33 and Figure 24). The changes after the first 24 hours of testing (Test 31) were minimal. A relatively "stable" scour hole was formed within that length of time. Tests 31-33 indicate that the bottom of the channel alternately fills and scours about an "equilibrium shape".

After Test 33 the downstream channel was shaped into a preformed hole encompassing all the scoured volume. This was then tested and contoured, (Test 34 and Figure 25). Flow was resumed (Test 35), and subsequent scour changes noted (See Figure 25). The lesson was inescapable: the initial conditions determined the final conditions. Therefore, the hypothesis could not be used. In order to minimize the size of the "equilibrium" scour hole for a given size of rock, the flow should initially be restricted as much as is practical. All subsequent

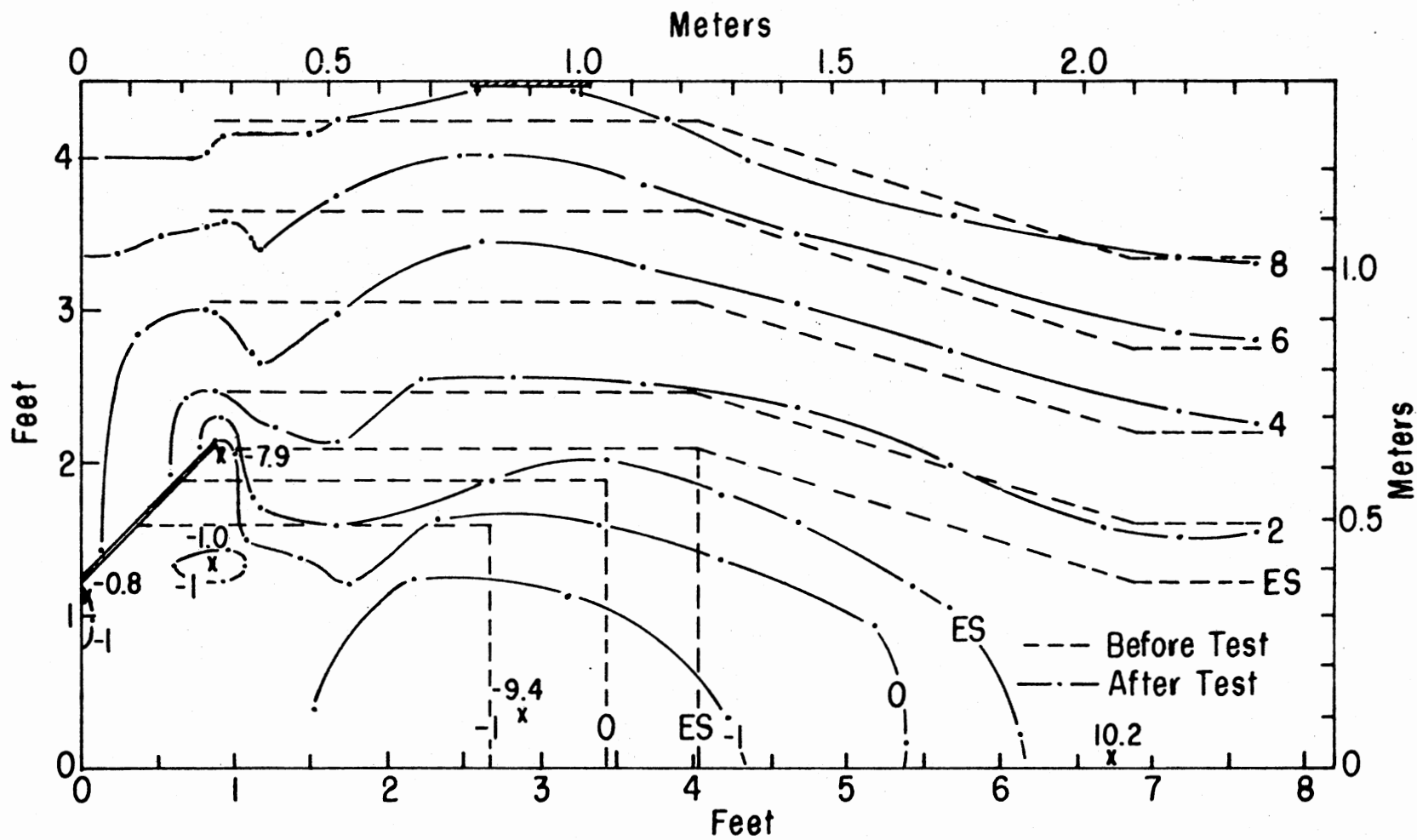


Figure 22. Initial Conditions and Maximum Scour Contour Map for Test 29

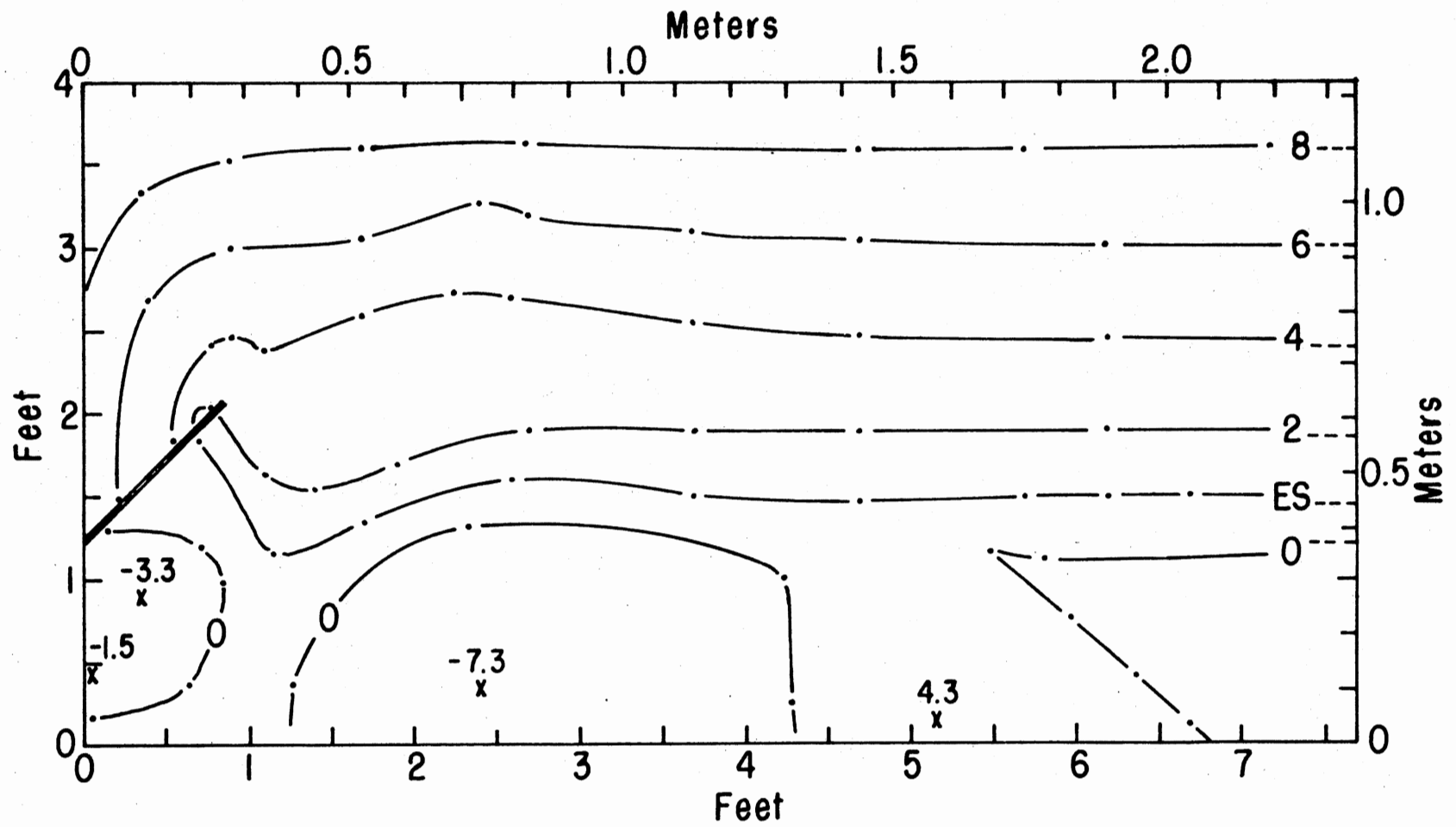


Figure 23. Maximum Scour Contour Map Resulting from Test 30

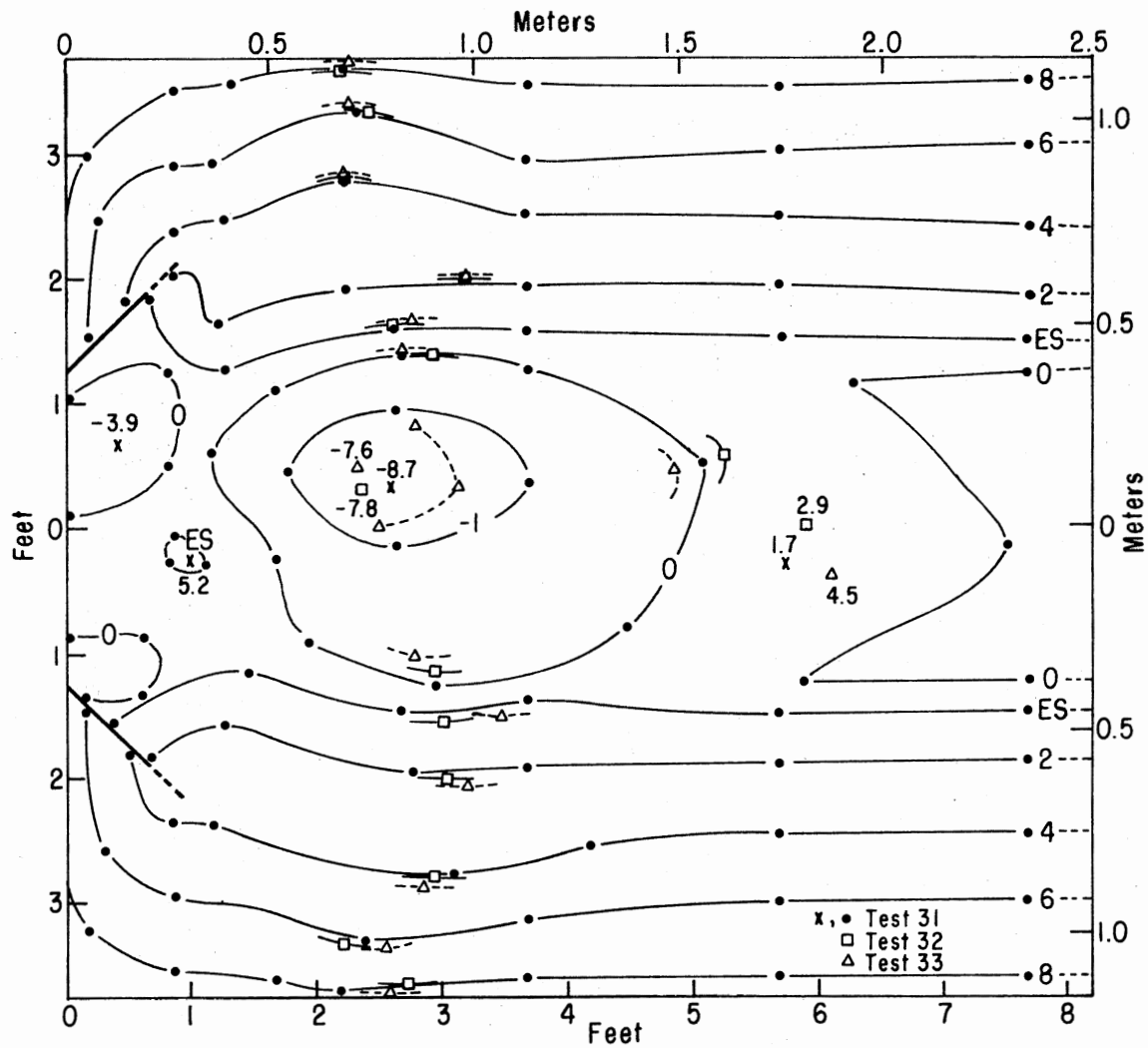


Figure 24. Contour Map After Tests 31, 32, and 33 Showing That Relative "Stability" Was Reached in First 24 Hours of Flow

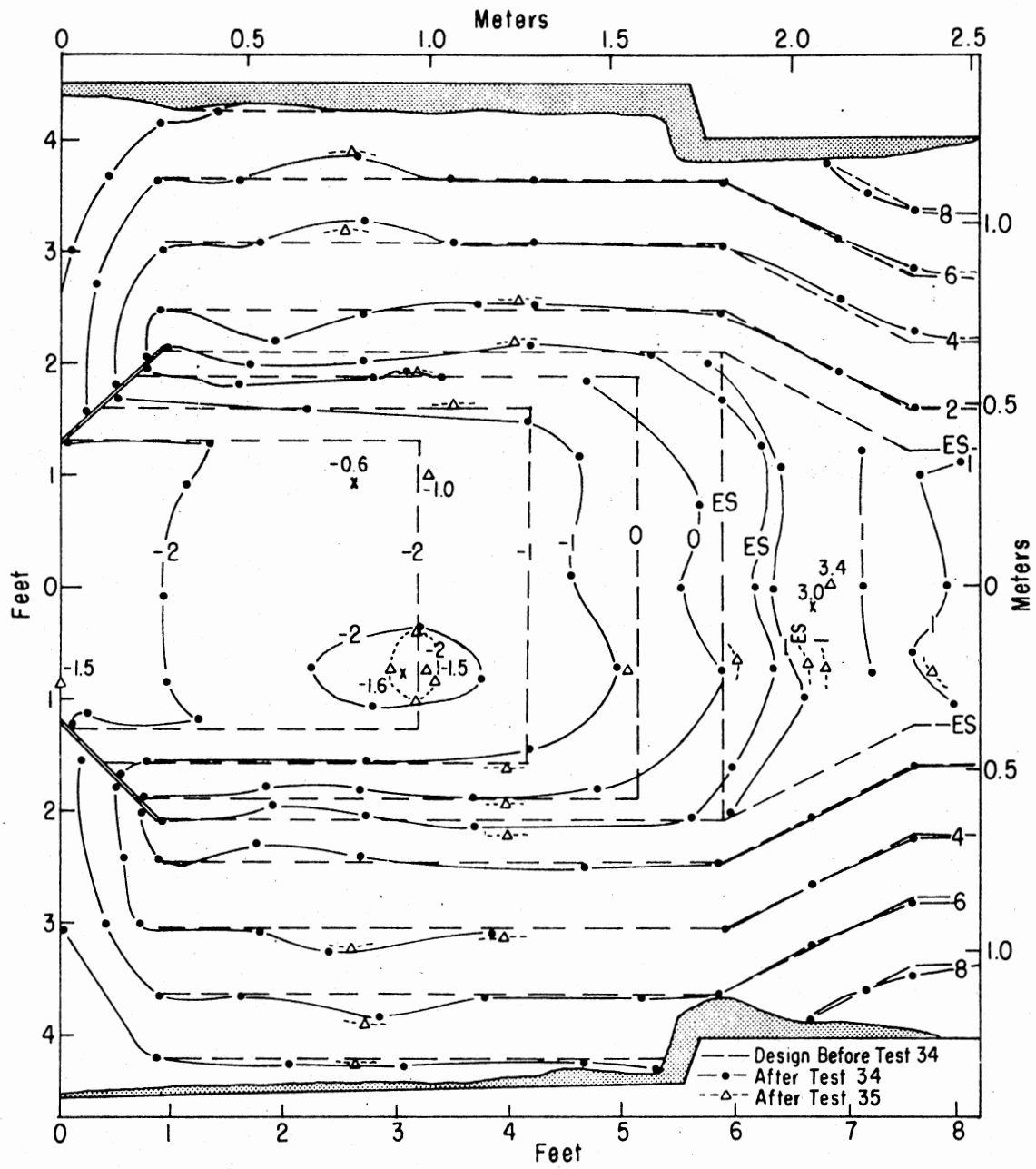


Figure 25. Contour Map After Tests 34 and 35

tests were run with the channel bottom level with the top of the end sill and as wide as the inside width of the basin.

Test Procedure

Pre-Test Settings to Achieve Correct

Water Surface

Prior to each test the design flowrate was released through the basin. The tailgate was adjusted to achieve the correct tailwater depth. The theoretical depth of flow entering the basin (D_1) could not be determined directly since the jet was submerged at that point. Accordingly, it was estimated by the following procedure:

Preliminary trials were run with minimal tailwater. These indicated that calculated water profiles using the standard step method (kinetic energy correction factor = 1; Manning $n = 0.008$) agreed well with the observed profiles. Thus before the actual testing, S2 flow profiles were computed beginning at critical depth for a range of flowrates incrementally larger and smaller than the design rate. During the pre-test experimentation, the depth of flow (D) was measured as far downstream on the chute as possible. The horizontal distance (b) between that point and the basin entrance was calculated.

The S2 curve for the appropriate flowrate was then referred to. The location j on the S2 profile which had the depth D was noted. An estimate of D_1 is the depth at position $j + b$ on the S2 profile. Either the location of the tube banks on the chute, or the height of the opening of the head tank exit, were adjusted until the correct D_1 was obtained. The average D_1 obtained for the tests used to present information on scour designs was always within 4.7% of D_{1D} .

Preparation of Downstream Channel

Before each test the appropriate riprap was shaped into a trapezoidal channel by the use of an aluminum form. Figure 11 shows the platform to which the form was mounted. The channel was shaped and reshaped until the vertical setting of the form was such that the average elevation of the channel floor without tamping was within a couple of thousandths of a foot of the desired elevation. The rock was not tamped because most commonly the riprap in the field is dumped and bulldozed into position and not hand placed. Profiles and cross sections were taken prior to each test. Recorded values indicated some variation in elevation. Sample deviation may be seen in Table III.

Measurements of Flow and Scour

During the 24 hour tests the water surface elevation at positions B and C (Figure 11) were continuously monitored. The flowrate and water surface at D were recorded several times during each test. As a minimum

TABLE III
PRE-TEST VARIATION IN CHANNEL FLOOR ELEVATIONS

Test No.	D50 (mm)	D50 (ft)	Design Elevation (ft)	Max. Elev. (ft)	Min. Elev. (ft)	Range (ft)	Range/D50
41	3.45	0.0113	0.692	0.699	0.682	0.017	1.504
42	5.65	.0185	.692	.702	.681	.021	1.135
46	7.85	.0258	.692	.711	.684	.027	1.047

standard, D1 and D3 were usually determined at the beginning and end of each test. The centerline water surface profile and the maximum wave height found on the channel edge were both recorded as often as practical. After each test was completed the flume was drained and the scour bed was contoured.

CHAPTER V

MAJOR TEST RESULTS

Observations of the Water Surface

In review, four different models were tested, reflecting the possible combinations of $F1_D = 4$ and 8 and $W = 24.75 \times D1_D$ and $W = 9.75 \times D1_D$. Eight photographs are presented for inspection. Views of the hydraulic jump from the side and from above or downstream for the four models are found in Figures 26 - 33. There was little difference in centerline flow profiles made at the beginning and end of a test. Rock size also had minimal effect on the flow profiles. Figures 59 - 62 in Appendix B show centerline water surface profiles and deposition.

Scour Holes

The scour holes were contoured and photographed after each important test. The channel centerline (X axis) divided the scour bed into two halves, which were never perfectly symmetrical (See Figure 34). Since knowledge of maximum scour was sought, a maximum scour contour map (MSCM) was prepared for each test (See Figures 63 - 72, Appendix C). In these figures, all integer valued contours (n) lie $n \times D1_D$ above the basin floor ($D1_D = 0.0984 \text{ ft} \approx 0.1 \text{ ft}$). Contours labeled ES are at the same elevation as the end sill. A point in the XY plane marked with a

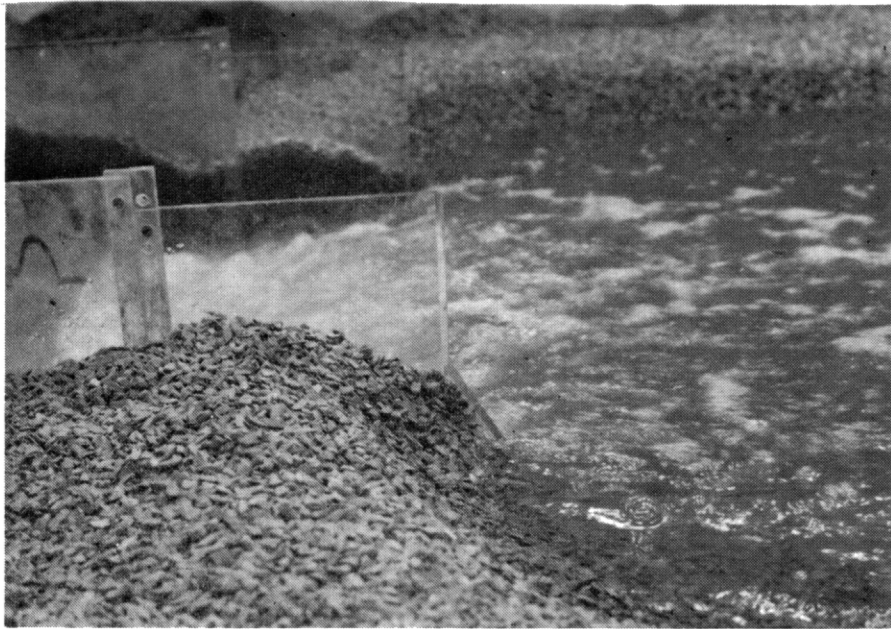


Figure 26. Side View of Jump in Basin of $Fl_D = 4$,
Width = $24.75 \times D_I$

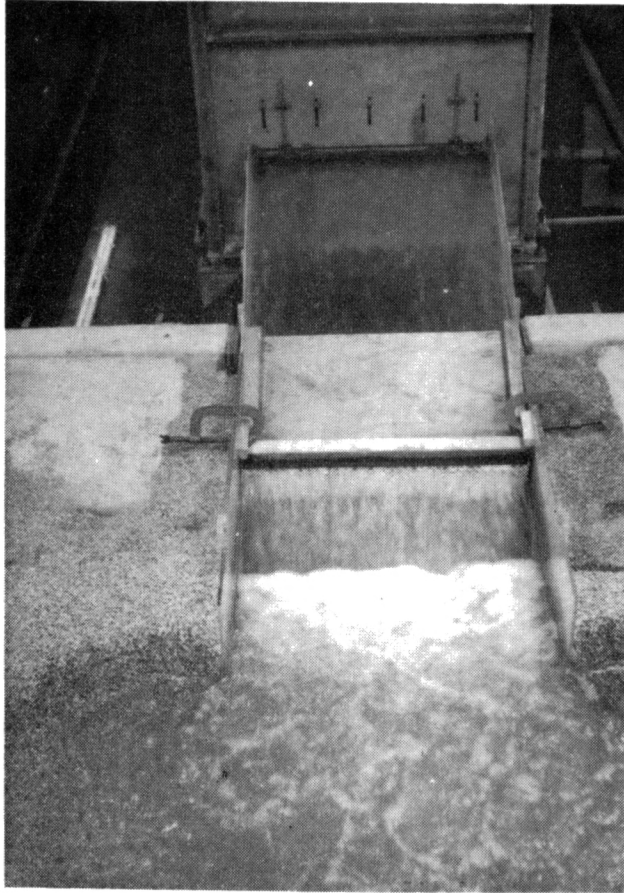


Figure 27. Downstream View of Jump in Basin of $F1_D = 4$, Width = $24.75 \times D1_D$

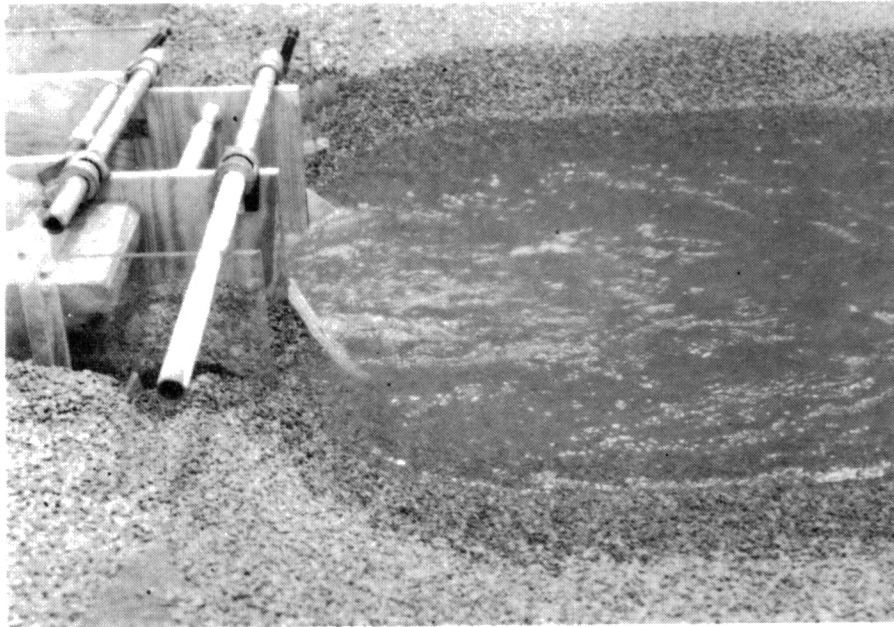


Figure 28. Side View of Jump in Basin of $F1_D = 4$,
Width = $9.75 \times D1_D$

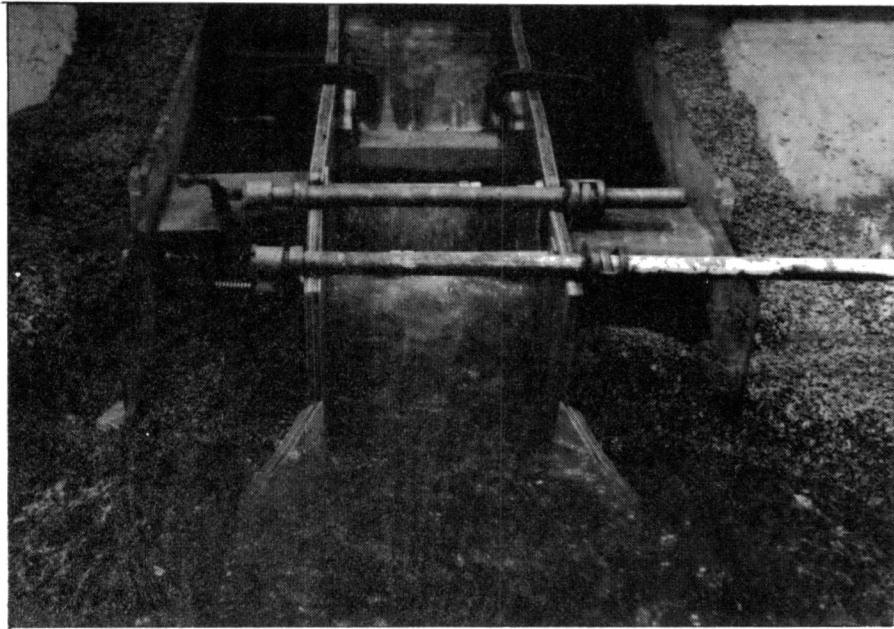


Figure 29. Downstream View of Jump in Basin of $Fl_D = 4$,
Width = $9.75 \times D1_D$

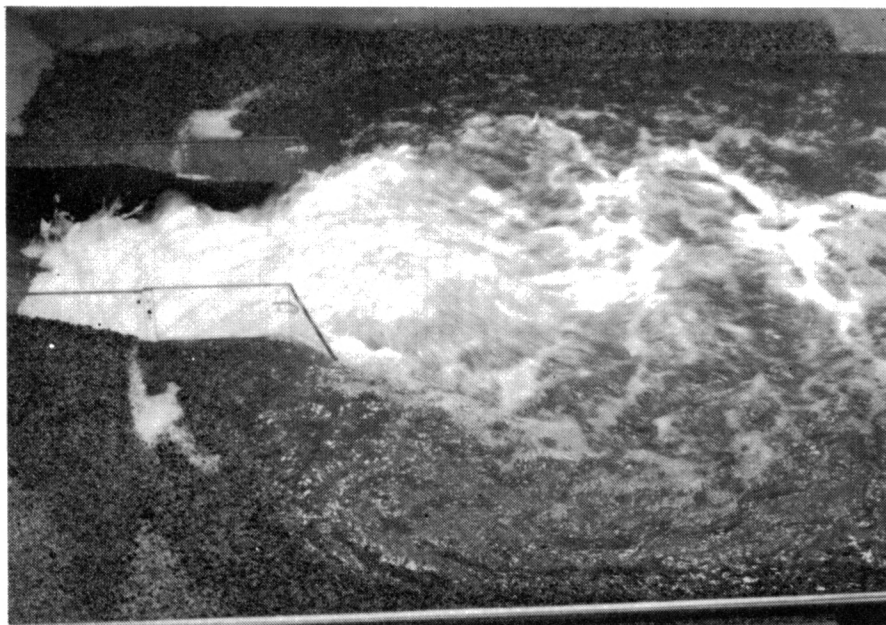


Figure 30. Side View of Jump in Basin of $Fl_D = 8$,
Width = $24.75 \times D1_D$



Figure 31. Top View of Jump in Basin of
 $F1_D = 8$, Width = $24.75 \times$
 $D1_D$

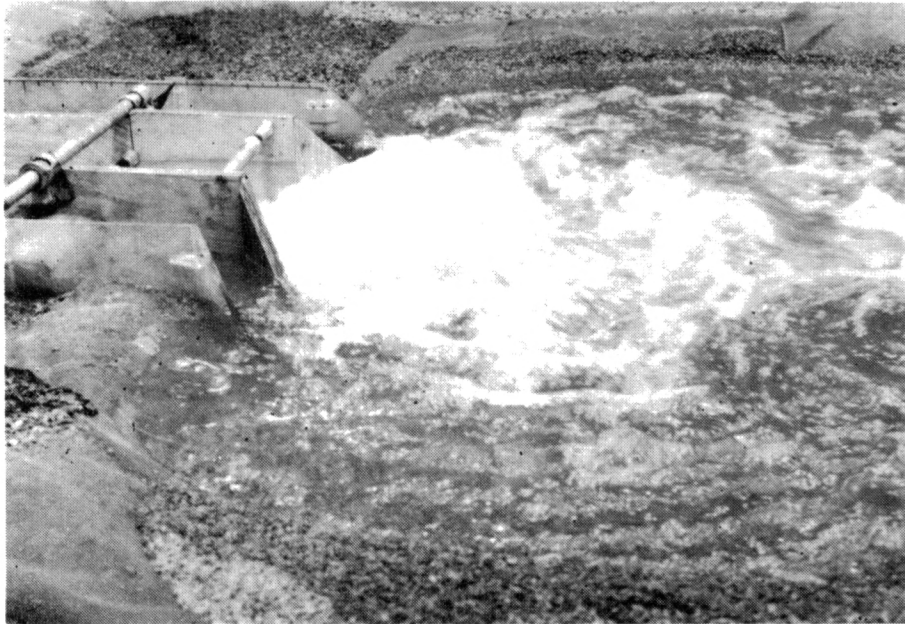


Figure 32. Side View of Jump in Basin of $F1_D = 8$,
Width = $9.75 \times D1_D$



Figure 33. Downstream View of Jump in Basin of $F1_D = 8$, Width = $9.75 \times D1_D$



Figure 34. Contoured Scour Bed After Test 44 ($F1_D = 4.0$, $W = 24.75 \times D1_D$, Elevation of Basin Floor = 0.659 , Elevation of Top of End Sill = 0.692)

cross is attended by a number (r) where:

$$r = \frac{(\text{scoured elevation})_{\text{point}} - (\text{design elevation})_{\text{point}}}{D50} \quad (42)$$

CHAPTER VI

ANALYSIS

Analysis of Scour on the Channel Bottom

Following the procedure outlined in the section on pre-test similitude, an initial concern was to identify a means of predicting π_{5A} and π_{5B} . Depth over the end sill (D_3) was measured during testing and π_{5B} was calculated. This was plotted against calculated values of π_4 yielding the points shown on Figure 35. π_6 , which includes the basin width, had no apparent effect. Calculated values of variables were indicated with a subscript. π_1 , π_2 , and π_3 may all be estimated by a linear relationship with π_4 (See Figure 36). It was reasonable to use a straight line fit for π_4 versus π_{5B} :

$$D_3 = D_1 \times (0.8 \pi_4 + 1.18) \quad (43)$$

Use of this function and the relationship $\pi_{5A} = \pi_4/\pi_{5B}$ yielded the curve on Figure 36. These equations were used in the determination of the subsequent terms shown in Tables I and IV. Table I shows that for constant π_4 at design conditions, π_{5A} , π_{5B} , π_{11} , π_{12} , and π_{14} were all constant regardless of initial depth. The result was that given the same initial channel conditions for all tests, the parameters describing the scour ($\pi_{LS\#}$ and $\pi_{DS\#}$) could be described in terms of π_4 , π_{13} , and π_{16} alone. Table IV gives design values for π terms for Froude numbers 1 through 17.

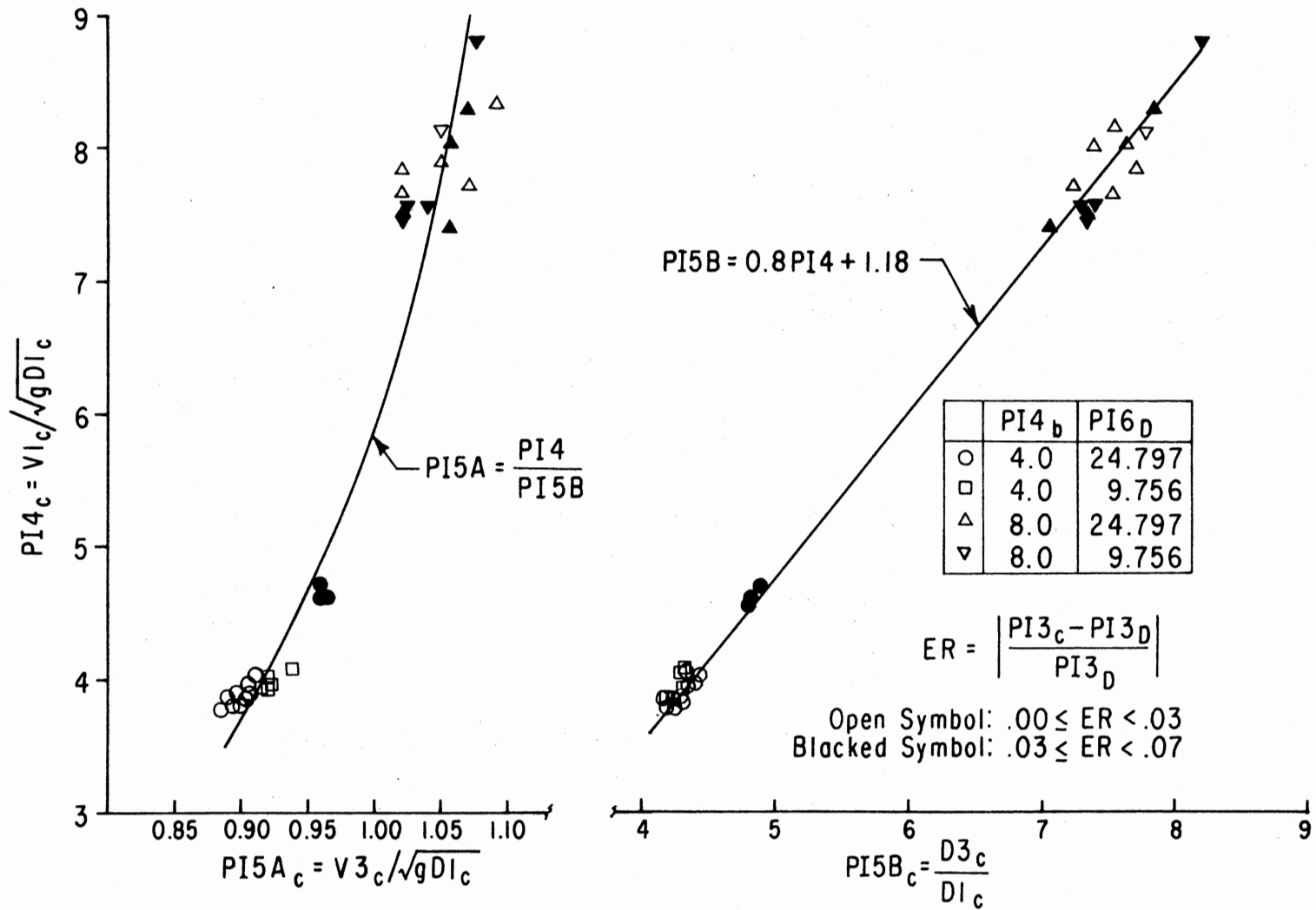


Figure 35. Calculated Values of $\pi 5A$ and $\pi 5B$ Versus $\pi 4$

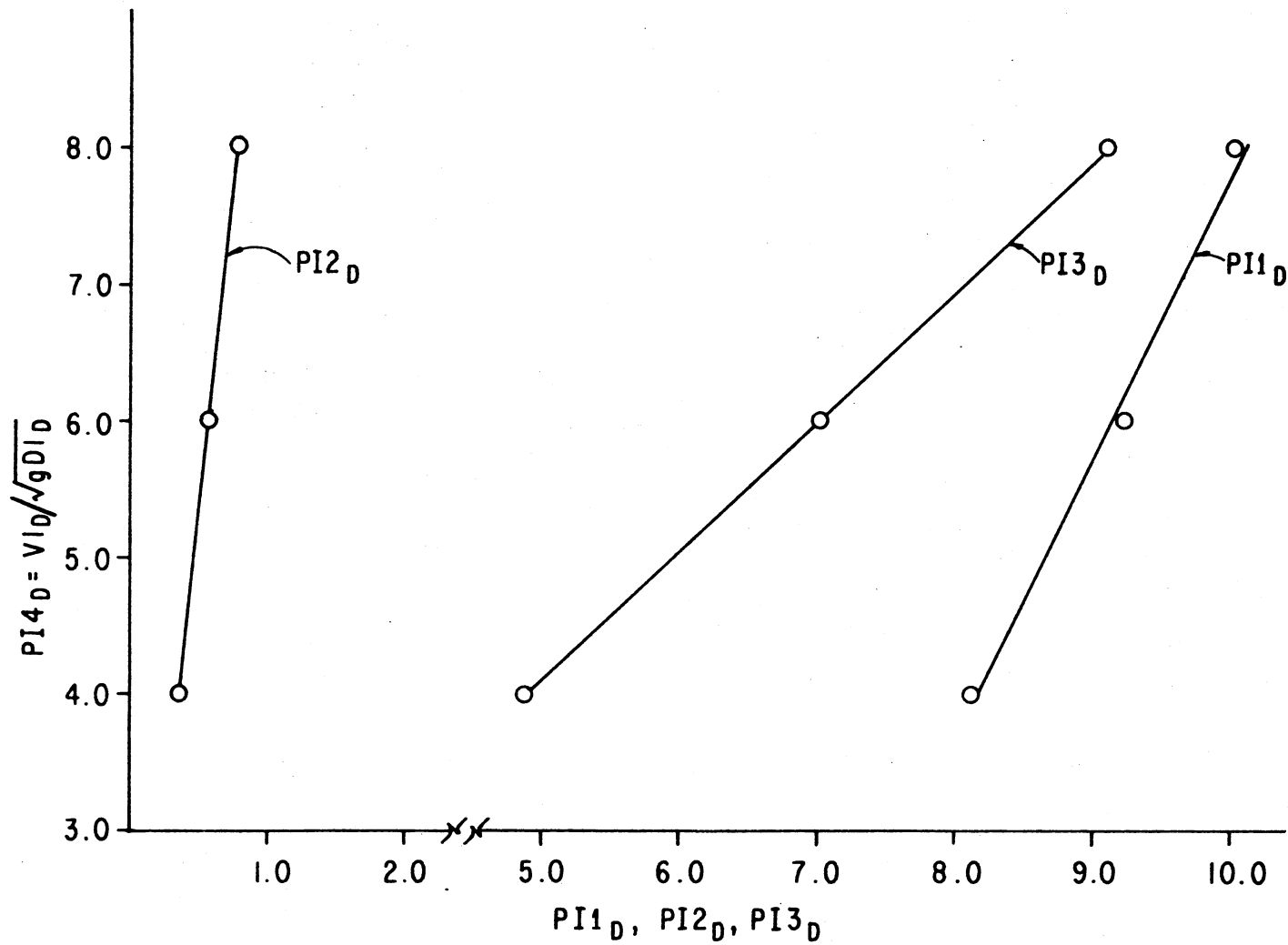


Figure 36. Design Values of π_1 , π_2 , and π_3 Versus π_4

TABLE IV

NONDIMENSIONAL CHARACTERISTICS OF SAF STILLING
BASINS FOR DESIGN FROUDE NUMBERS (F_{rD}) OF
1 THROUGH 17

D1	V1	F_{rD}	D2/D1 PI1	D2P COEF PI2	θ PI3	C PI4	D2/D1 R PI5A	D3 MH PI5B	V3 PI11	PI12	PI14
0.0984	1.7789	1.0000	0.0524 0.0700	0.1376 0.0700	0.3428 1.1600	0.0000 1.0000	1.0000 0.3551	0.1984 1.0000	0.0984 0.3569	0.7071	0.0354
0.0984	3.5578	4.0000	0.2314 0.3037	0.2571 0.1801	0.6203 2.0123	0.0163 2.0000	2.3723 2.7154	0.2176 2.7800	1.2798 0.3115	0.9397	0.0597
0.0984	5.3367	9.0000	0.3712 0.5350	0.3703 0.2880	0.7247 3.7630	0.0260 3.0000	3.7220 4.8360	0.3523 3.5800	1.4907 0.4429	1.0511	0.0738
0.0984	7.1157	16.0000	0.5096 0.7182	0.4797 0.3009	0.7999 4.0751	0.0357 3.0000	5.1569 6.5732	0.4310 4.5000	1.6246 0.3364	1.1130	0.0828
0.0984	8.8946	25.0000	0.6483 0.9354	0.5804 0.3000	0.8589 5.0512	0.0454 3.0000	6.5807 7.9974	0.5097 5.0000	1.7171 0.4241	1.1505	0.0890
0.0984	10.6735	36.0000	0.7872 1.1237	0.6910 0.3000	0.9076 6.0000	0.0551 3.0000	8.0000 9.4000	0.5804 5.0000	1.7849 0.4103	1.1743	0.0936
0.0984	12.4524	49.0000	0.9262 1.3159	0.7918 0.3000	0.9498 7.0000	0.0648 3.0000	9.4121 10.8124	0.6623 6.0000	1.8366 0.3965	1.1988	0.0972
0.0984	14.2313	64.0000	1.0653 1.5095	0.8923 0.3000	0.9849 8.0000	0.0746 3.0000	10.8247 12.2277	0.7459 7.5000	1.8775 0.3833	1.2202	0.1000
0.0984	16.0102	81.0000	1.2043 1.6579	0.9871 0.3000	1.0193 9.0000	0.0843 3.0000	12.2377 13.6370	0.8284 8.0000	1.9105 0.3710	1.2470	0.1022
0.0984	17.7892	100.0000	1.3433 1.8122	1.0823 0.3000	1.0534 10.0000	0.0940 3.0000	13.6470 15.0474	0.9113 9.0000	1.9378 0.3595	1.2718	0.1041
0.0984	19.5681	121.0000	1.4823 1.9673	1.1762 0.3000	1.0875 11.0000	0.0936 3.0000	15.0574 16.4578	0.9940 9.0000	1.9607 0.3489	1.2961	0.1057
0.0984	21.3470	144.0000	1.6213 2.1224	1.2702 0.3000	1.1216 12.0000	0.0932 3.0000	16.4678 17.8682	1.0768 10.0000	1.9802 0.3380	1.3205	0.1070
0.0984	23.1259	169.0000	1.7603 2.2775	1.3642 0.3000	1.1557 13.0000	0.0928 3.0000	17.8777 19.2781	1.1596 11.0000	1.9971 0.3280	1.3441	0.1082
0.0984	24.9048	196.0000	1.9000 2.4326	1.4581 0.3000	1.1898 14.0000	0.0924 3.0000	19.2877 20.6881	1.2424 12.0000	2.0117 0.3214	1.3680	0.1092
0.0984	26.6837	225.0000	2.0400 2.5877	1.5520 0.3000	1.2239 15.0000	0.0920 3.0000	20.6977 22.0981	1.3252 13.0000	2.0246 0.3135	1.3921	0.1100
0.0984	28.4627	256.0000	2.1799 2.7428	1.6459 0.3000	1.2580 16.0000	0.0916 3.0000	22.1077 23.5081	1.4080 14.0000	2.0364 0.3061	1.4163	0.1108
0.0984	30.2416	289.0000	2.3199 2.8977	1.7400 0.3000	1.2921 17.0000	0.0912 3.0000	23.5177 24.9181	1.4908 15.0000	2.0441 0.2992	1.4405	0.1115

Figures 37 - 40 show CMSP's and centerline water surface profiles for Froude numbers 4 and 8 at two different widths. Note that the Froude of 4 scour bed consists of a single scour hole and deposition mound and the bed for the Froude of 8 has two scour holes. The Froude of 8 water surface also has two large standing waves.

Figure 41 shows the relationship between Π_{DS2} (the ratio of depth of scour below the end sill to D_3) and Π_{I3} for different Froude numbers and widths at position 2 (Figure 8). Observe that for the Fl_D of 4 the scour was deeper for the narrow than for the wide width, while the converse was true for the Froude of 8 results. The difference in flow regimes probably causes this phenomenon. One standing wave is responsible for energy dissipation for the flow of $Fl_D = 8$. For an Fl_D of 4, most scour occurs beneath the peak of the hydraulic jump, immediately downstream of the end sill. For an Fl_D of 8, significant scour occurs beneath each of the standing waves.

An objective was to be able to provide riprap protection for basins designed with Froude numbers lying between 4 and 8. For this purpose, the two Π terms used in Figure 41 were not convenient, since D_3 varied with Froude number. When the difficulty of obtaining a meaningful relationship for Π_{DS2} , Π_{I3} , Π_4 , and Π_6 was fully appreciated, a graphical rather than equation oriented approach was used. τ_{C50} was replaced by D_{50} because of the linear relation in Equation 28. Since riprap is usually placed in layers whose thickness depends on D_{50} , D_{50} was an especially desirable factor in the Π terms. Making the reasonable assumption that all prototype riprap is going to have a specific gravity within a few percent of that of the model, γ was deleted. Dl_D was a known experimental constant. Thus, new Π terms were $\Delta Z/D_{50}$,

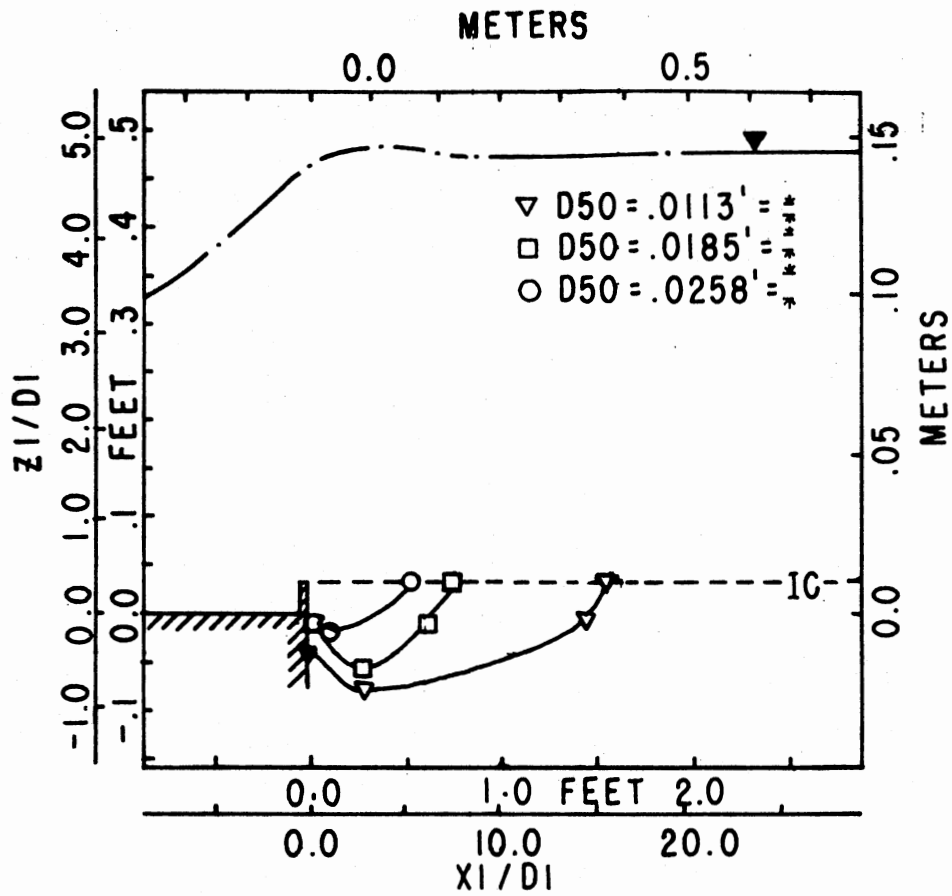


Figure 37. Composite Maximum Scour Profiles for $Fl_D = 4.0$, Width = $24.75 \times D_1$

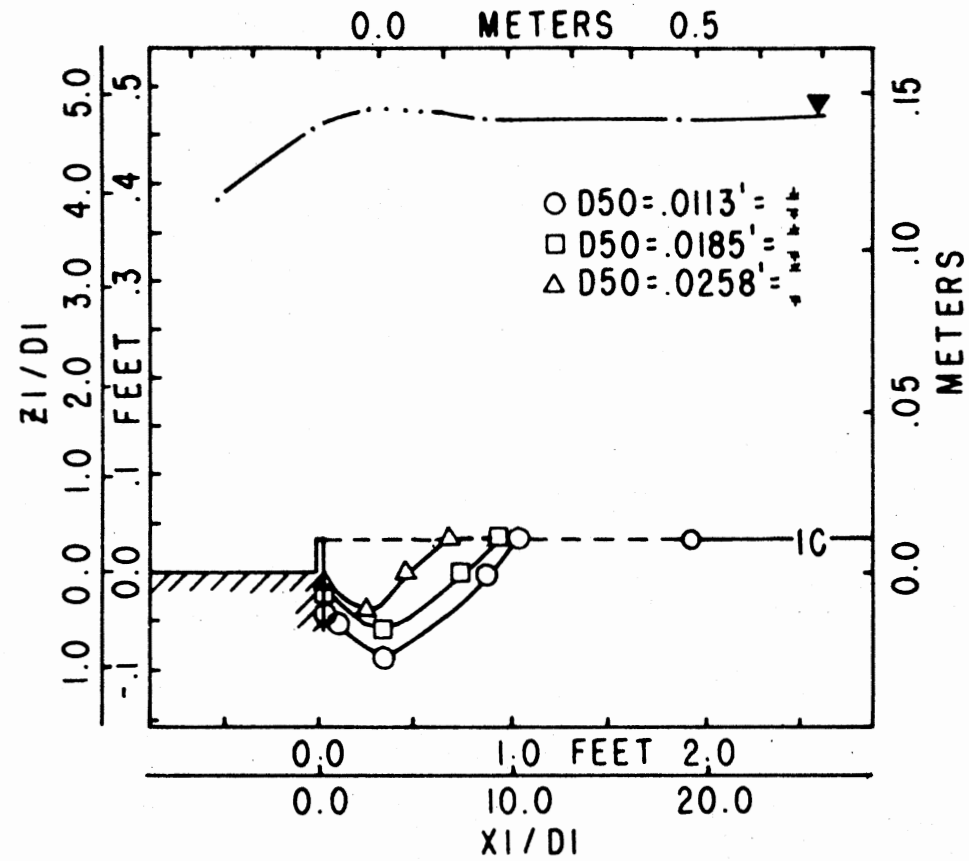


Figure 38. Composite Maximum Scour Profiles for $F1_D = 4.0$, Width = $9.75 \times D1_D$

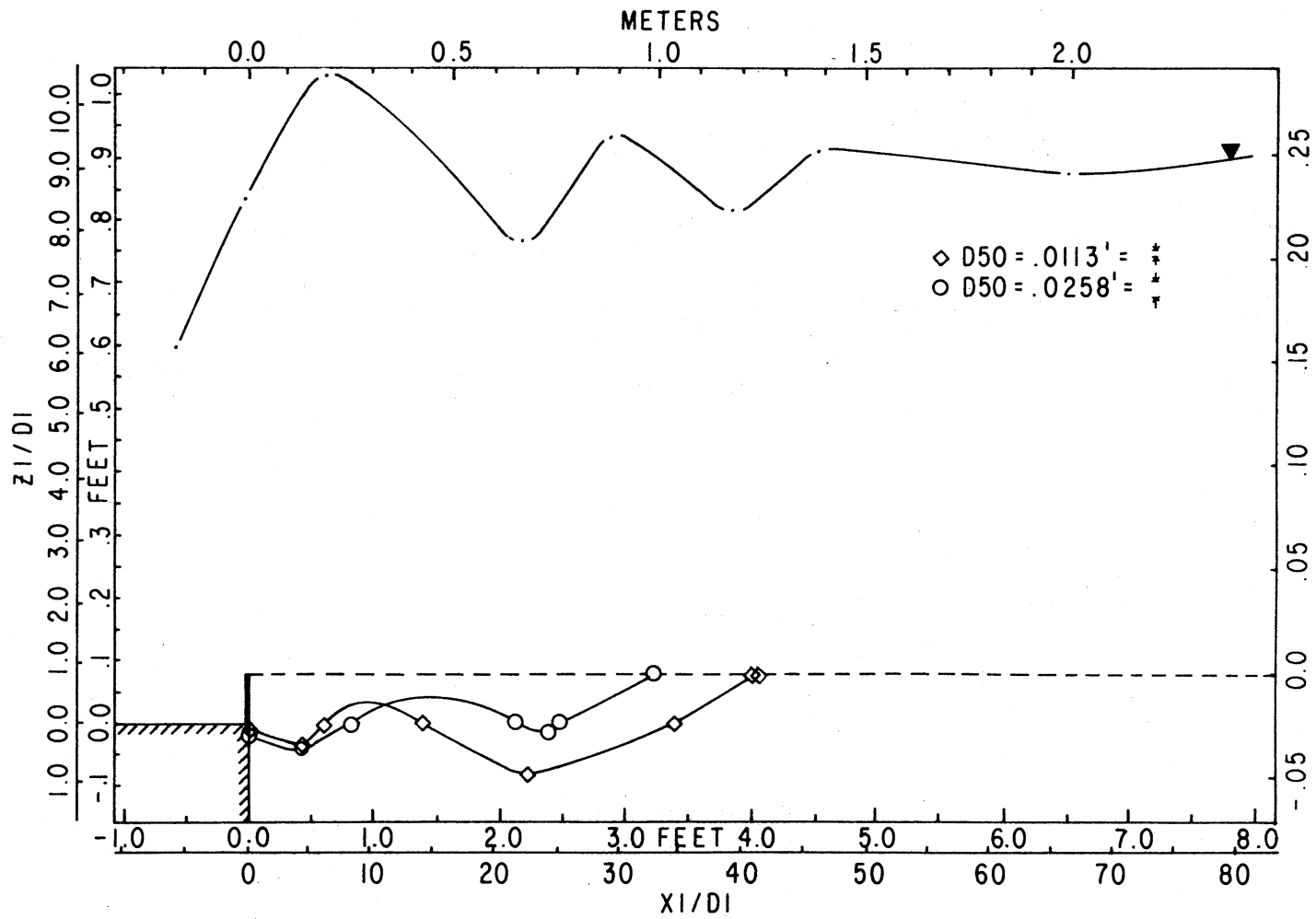


Figure 39. Composite Maximum Scour Profiles for $F1_D = 8.0$, Width = $24.75 \times D1_D$

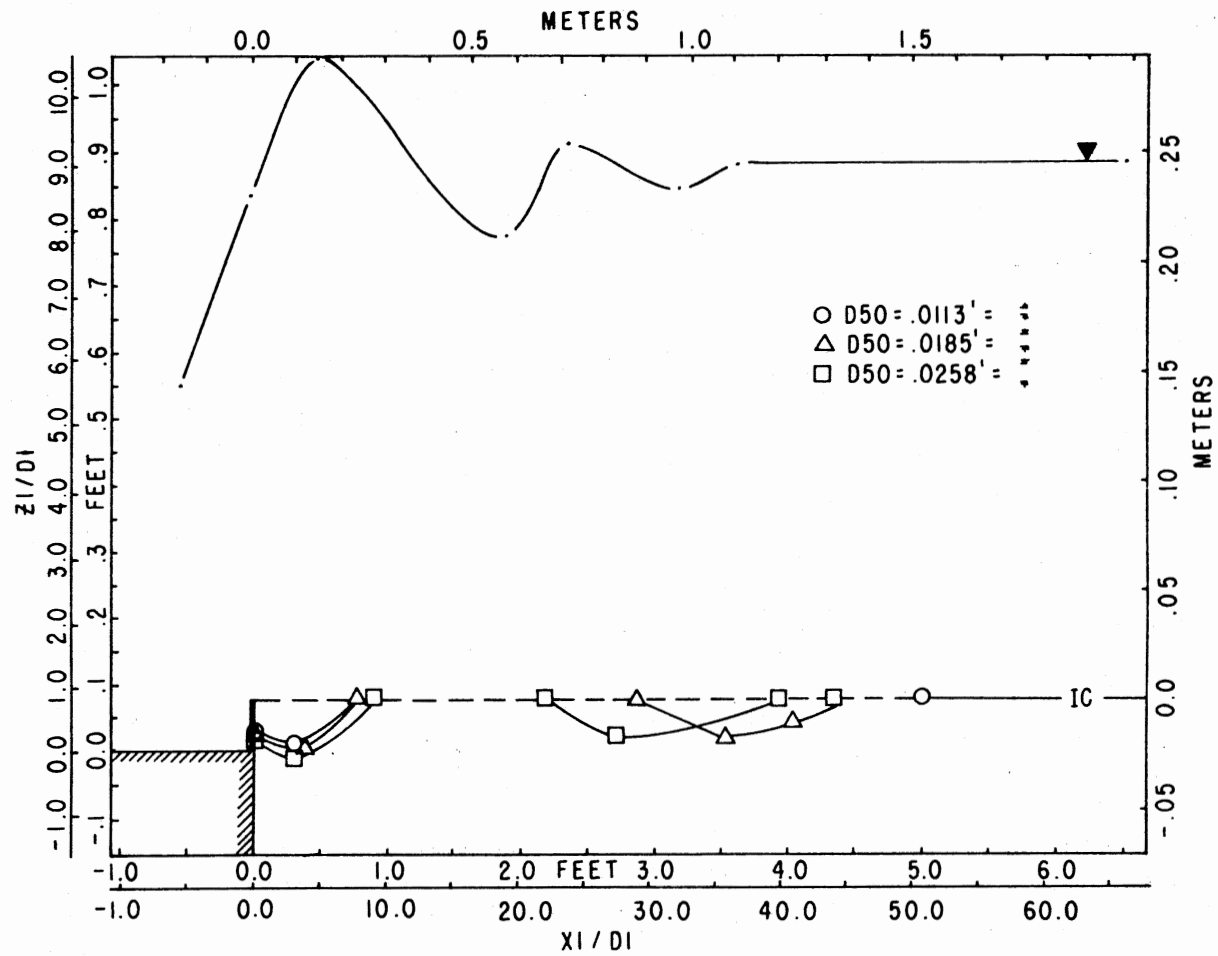


Figure 40. Composite Maximum Scour Profiles for $F1_D = 8.0$, Width = $9.75 \times D1_D$

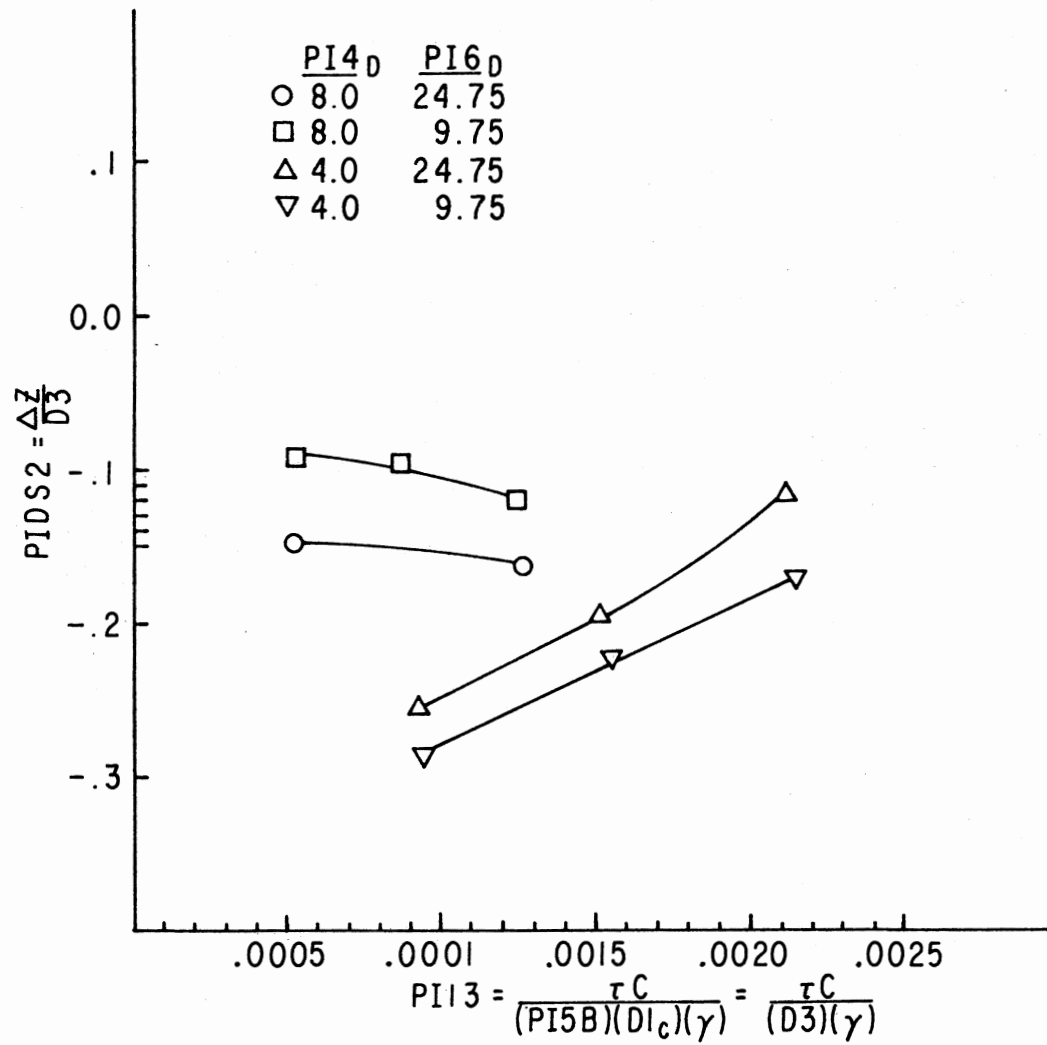


Figure 41. PIDS2 Versus PII3 at Position 2

$\Delta X/D50$, and $D50/D1_D$. The resultant nondimensional channel bottom scour is presented in Figures 73 - 76 in Appendix D for the position numbers indicated in Figure 8. For $F1_D = 4$, minimum and maximum ranges for the nondimensional location and depth of scour as a function of rock size are shown in Figures 42 and 43. These were later used in Chapter VII to design for basins of $3 \leq F1_D \leq 4$. The data from tests at $F1_D = 4$ and $F1_D = 8$ were combined to form comparable Figures 44 and 45. These figures were later used to provide design guidance for basins of $4 < F1_D \leq 8$.

It is interesting to note that after passage of the design flow, rocks in the scour bed were often aligned with their narrow edge parallel to the flow direction. This was observed on the channel sides as well as on the channel bottom.

Analysis of Scour on the Channel Sides

Figure 46 represents a cross-section of the channel side slope. The ordinate $Z1/D1$ is a nondimensional distance above the basin floor, and is coincident with the inside of the basin side wall. The design slope shows how the channel should have appeared before a test was run. It intersects the ordinate at the end sill elevation. During testing, erosion occurred, so that after the test the channel side was located some distance outward from its original location. This figure shows maximum lateral scour points in the region of Position 4 for two widths of model of $F1_D = 8.0$. The $D50$ of the rock was 7.85 mm (.0258 ft). Figure 47 was prepared in the same manner but presents data from tests where $D50$ was 3.45 mm (0.0113 ft). These figures show that maximum lateral scour was greater for the wide basin than for the narrow basin.

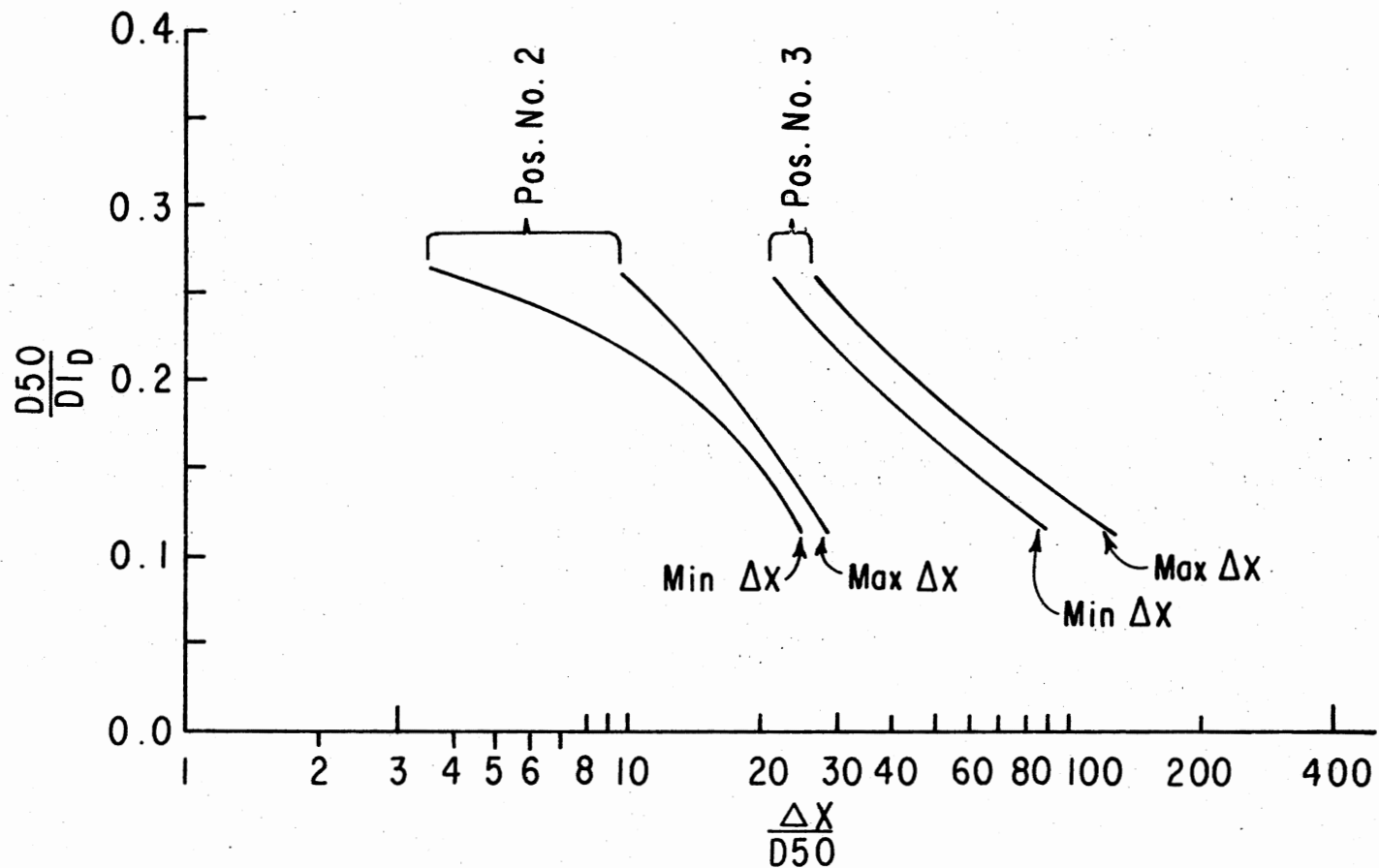


Figure 42. Nondimensional Location of Positions 2 and 3 as a Function of $D50/D1D$
 Applicable for Basins of $3 \leq F1D \leq 4$, Width = $9.75 \times D1D$ Through
 $24.75 \times D1D$

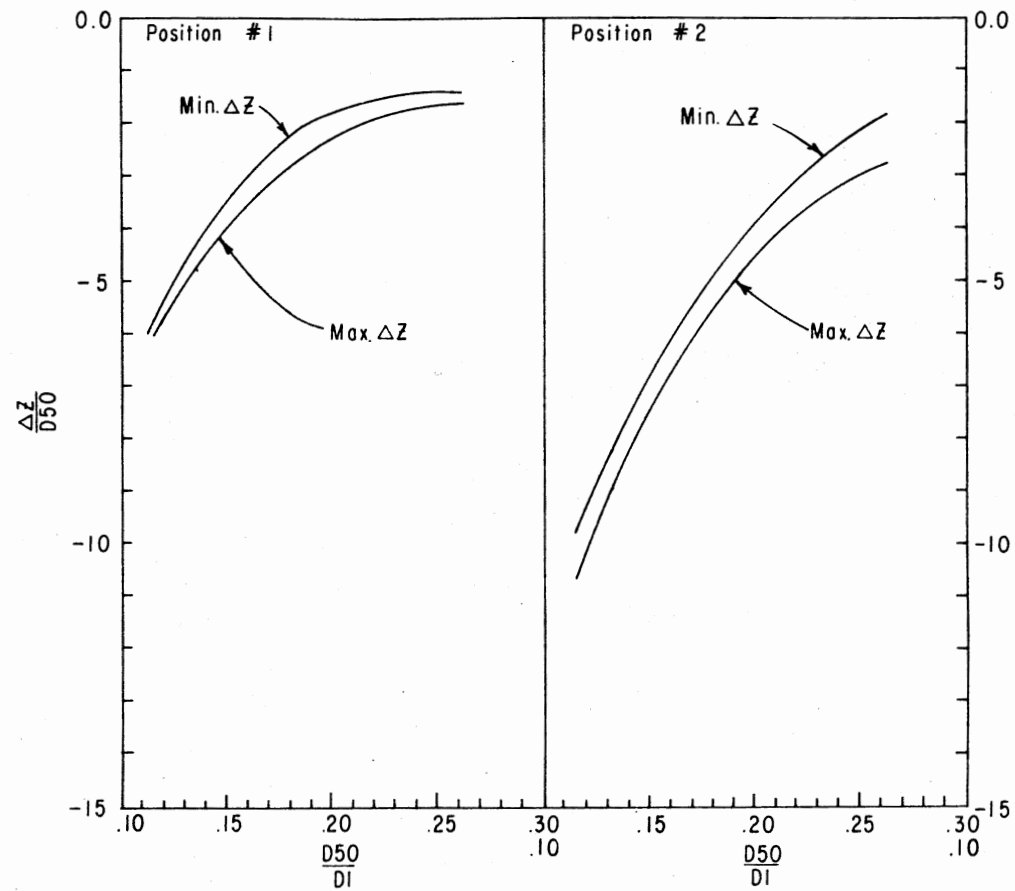


Figure 43. Nondimensional Depth of Scour as a Function of D_{50}/D_{1D} at Positions 1 and 2 Applicable for Basins of $3 \leq Fl_D \leq 4$, Width = $9.75 \times D_{1D}$ Through $24.75 \times D_{1D}$

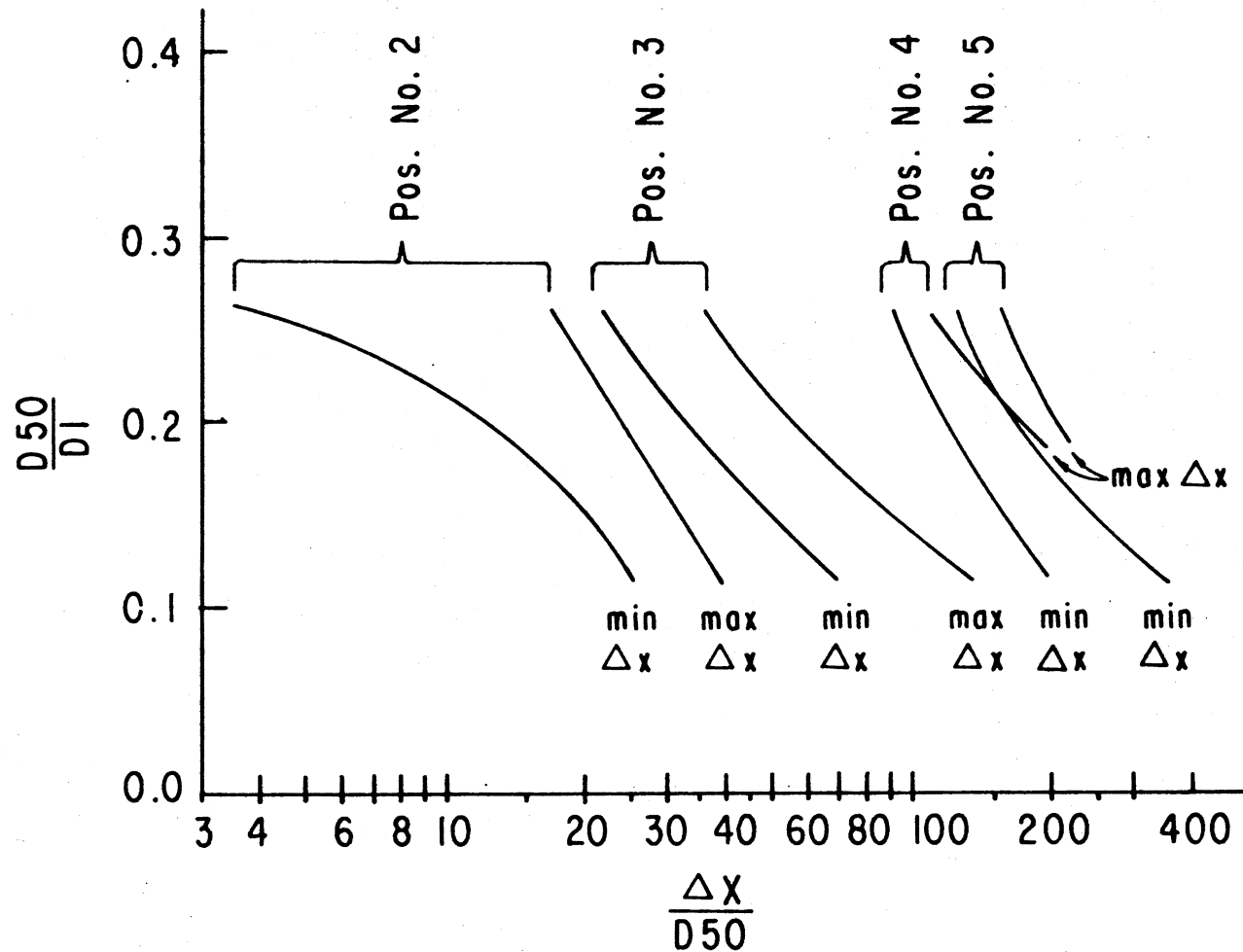


Figure 44. Nondimensional Location of Positions 2, 3, 4, and 5 as a Function of $D50/D1D$ Applicable for Basins of $4 \leq Fl_D \leq 8$, Width = $9.75 \times D1D$ Through $24.75 \times D1D$

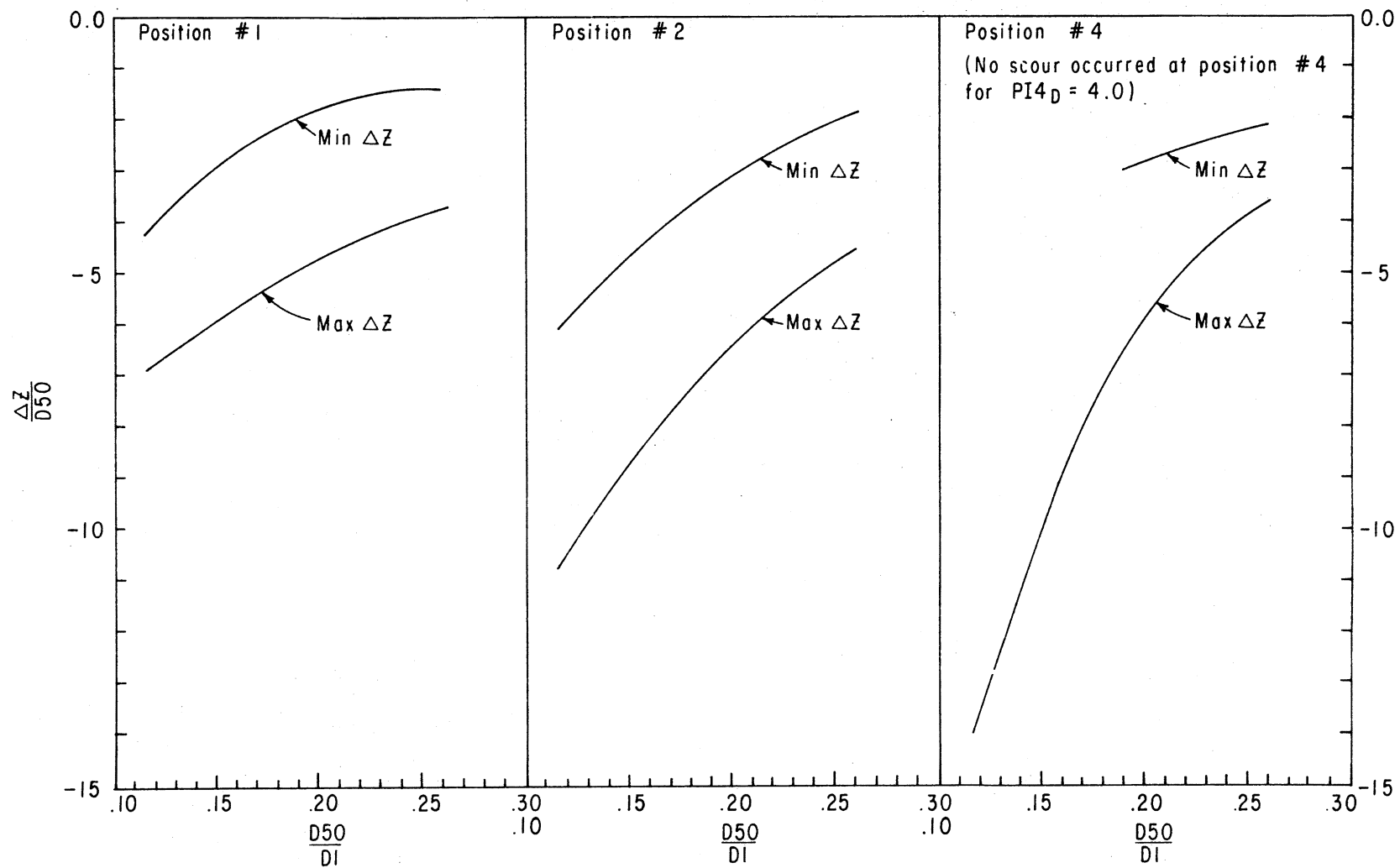


Figure 45. Nondimensional Depth of Scour as a Function of $D50/D1D$ at Positions 1, 2, and 4
 Applicable for Basins of $4 \leq F1D \leq 8$, Width = $9.75 \times D1D$ Through $24.75 \times D1D$

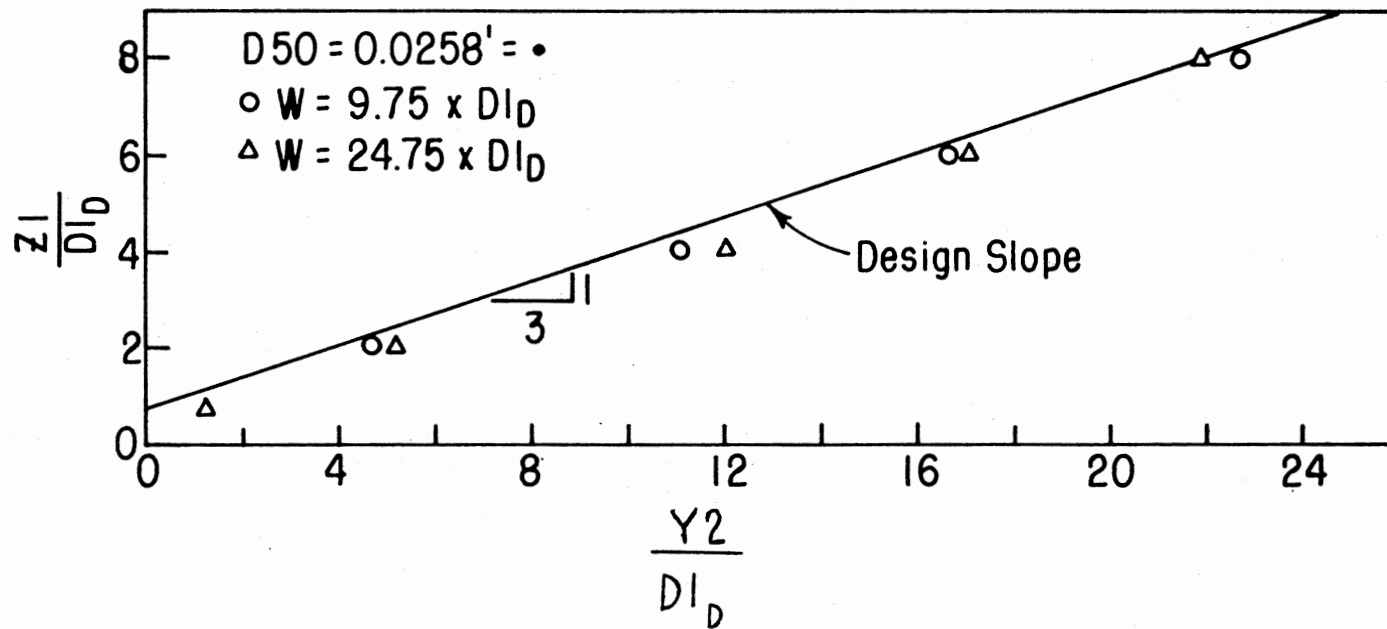


Figure 46. Nondimensional Cross Section of Channel Side Showing Maximum Latitudinal Scour After Testing of Models of $F1D = 8$, Width = $9.75 \times D1D$, $D50 = 7.85 \text{ mm}$ (0.0258 ft)

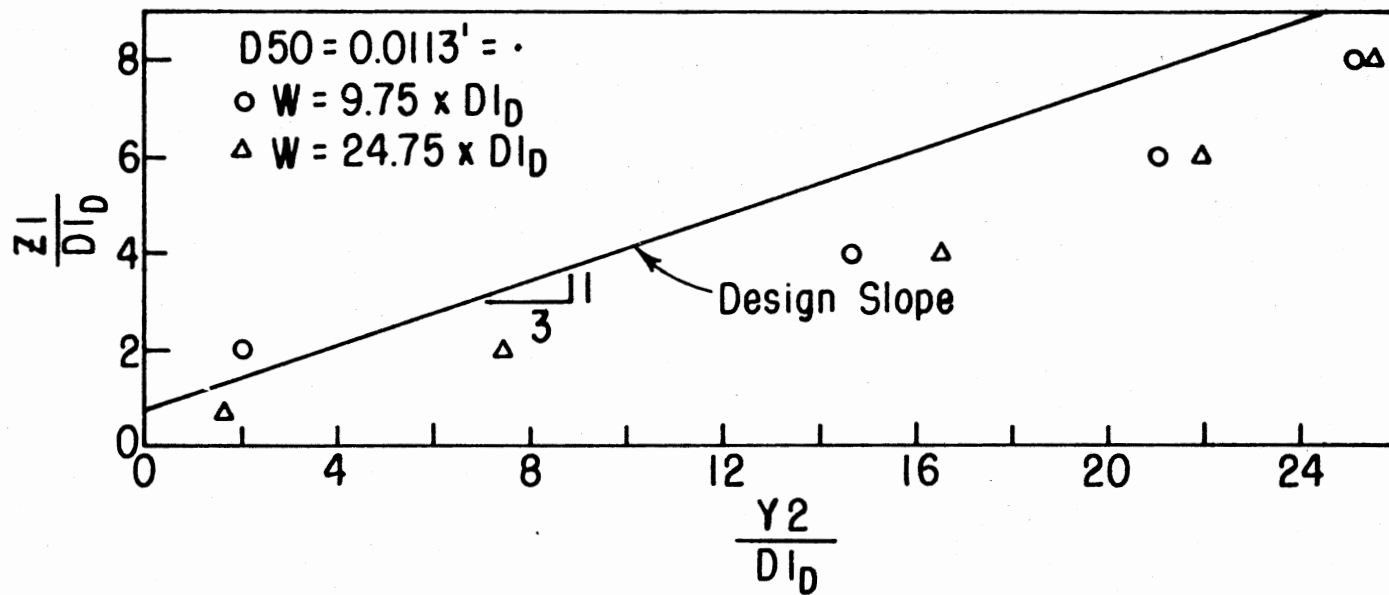


Figure 47. Nondimensional Cross Section of Channel Side Showing Maximum Latitudinal Scour After Testing of Models of $F1D = 8$, Width = $9.75 \times D1D$ and $24.75 \times D1D$, $D50 = 3.45 \text{ mm}$ (0.0113 ft)

It is obvious that the lighter particles scoured more readily from the sides than did the heavier particles and the effect of width on the scour became less important as the rock size increased.

Figures 48 and 49 are comparable to Figures 46 and 47 but contain data from tests on models of $Fl_D = 4$. Although scour could not be visibly observed on the channel sides, these figures show greater scour for narrow than for wide basins.

The depth of flow in the channel varied depending on Fl_D . Since the major scour for a $Fl_D = 4$ test may occur closer to the channel bottom than that for an $Fl_D = 8$ test, it was thought possible that the $Fl_D = 4$ scour might exceed that of the $Fl_D = 8$ at some elevation. Therefore, to compare the scour of different Froude numbers, the elevation of a particular point above the end sill was redefined as a fraction of $(D2P - C)$ and $D2P$. The nondimensional cross-sections in Figure 50 were prepared to show that nondimensional latitudinal scour increased as Fl_D increased, regardless of elevation. They also lead one to assume that the nondimensional scour of $Fl_D = 6$ will be somewhat greater than that for $Fl_D = 4$ and somewhat less than that for $Fl_D = 8$.

Figures 51 and 52 were prepared to show the effect of rock size on maximum scour for Fl_D values of 8 and 4. Each is a nondimensional top view of the channel side. A basin wing wall is seen in the lower left hand portion of each figure. The axes intersect where the downstream edge of the end sill meets the inside of the basin side wall. Nondimensional elevations of the contours are shown. In some locations in Figure 51 the larger rock appears to have scoured more than the smaller rock. This is possibly the result of local irregularities produced during pre-test leveling. Recall that side slope scour could not be

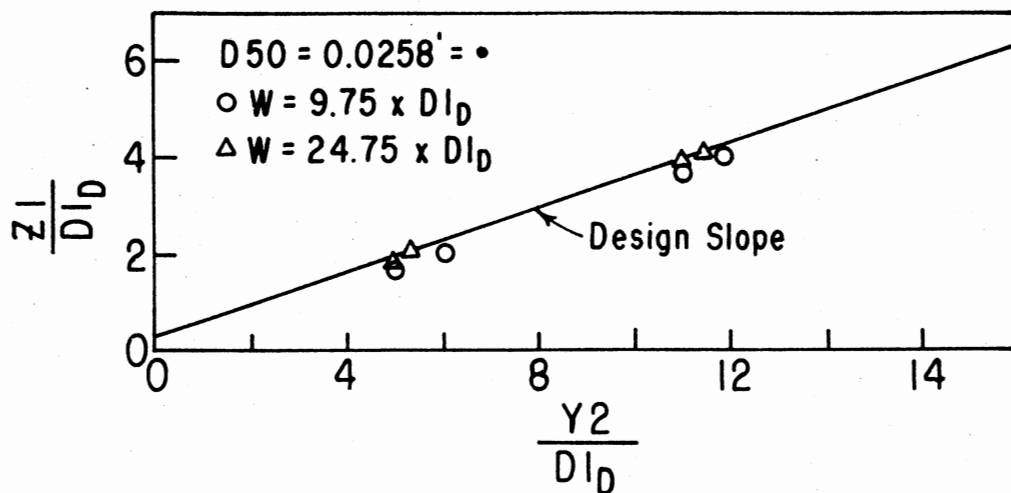


Figure 48. Nondimensional Cross Section of Channel Side Showing Maximum Latitudinal Scour After Testing of Models of $F1D = 4$, Width = $9.75 \times D1D$ and $24.75 \times D1D$, $D50 = 7.85 \text{ mm}$ (0.0258 ft)

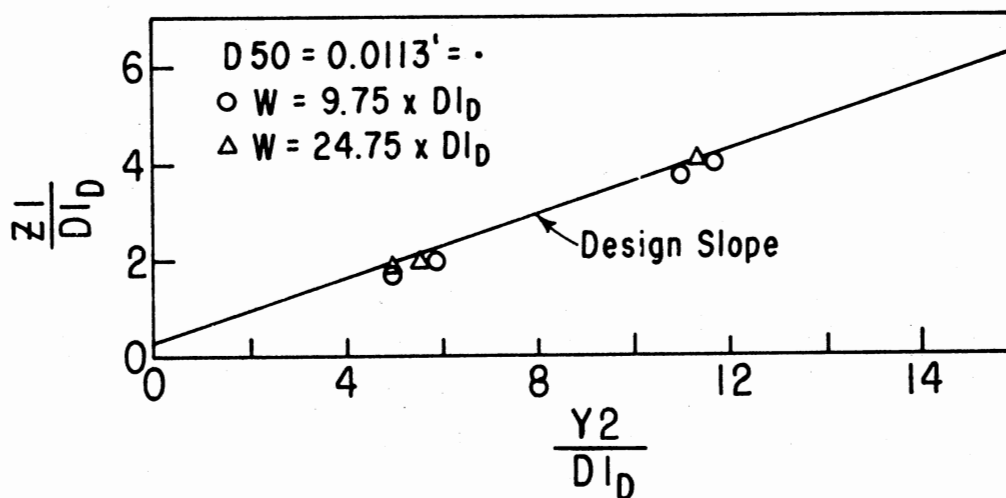


Figure 49. Nondimensional Cross Section of Channel Side Showing Maximum Latitudinal Scour After Testing of Models of $F1D = 4$, Width = $9.75 \times D1D$ and $24.75 \times D1D$, $D50 = 3.45 \text{ mm}$ (0.0113 ft)

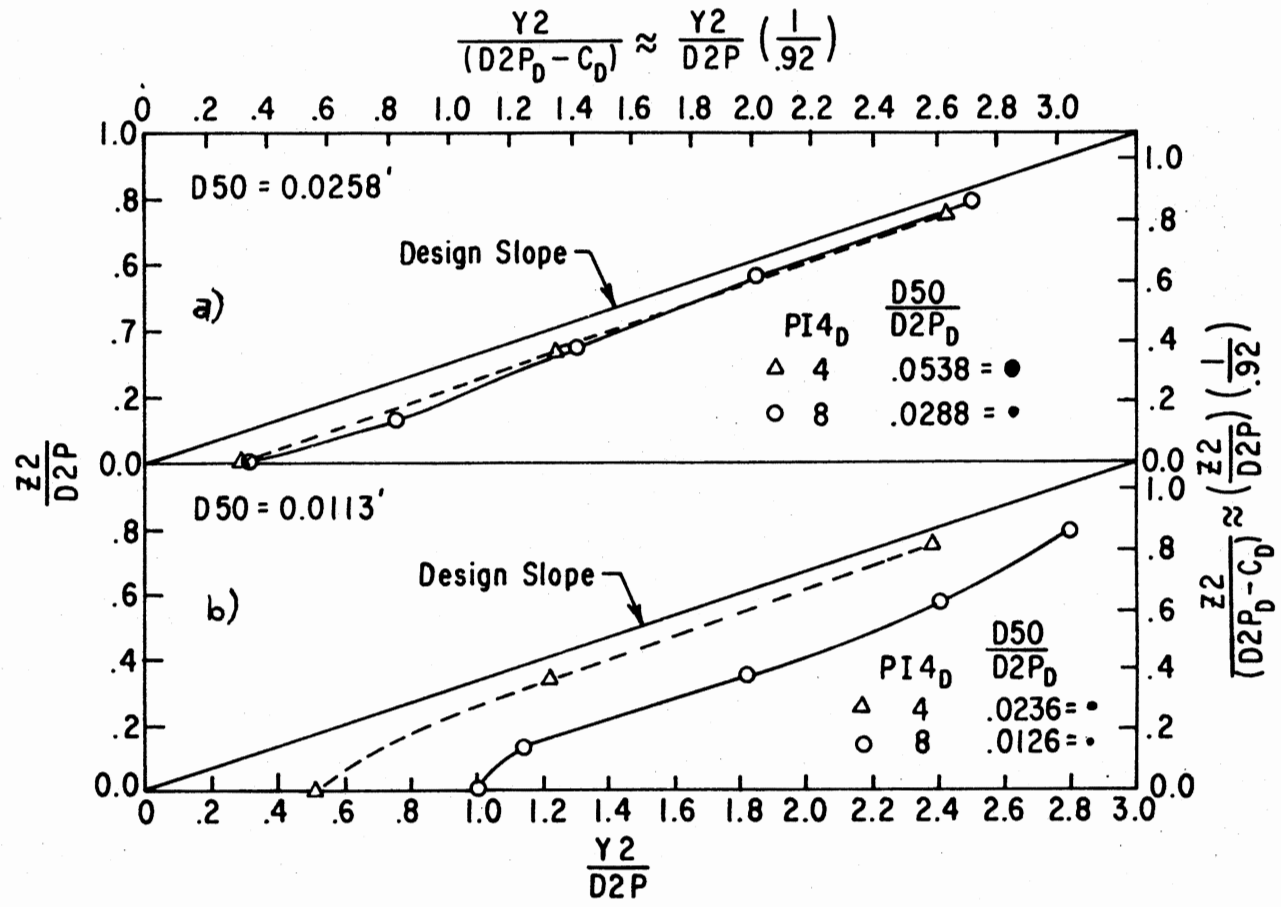


Figure 50. Nondimensional Cross Section of Channel Side Showing Maximum Latitudinal Scour After Testing of Models of $Fl_D = 4$ and 8
 a) $D_{50} = 7.85 \text{ mm}$ (0.0258 ft)
 b) $D_{50} = 3.45 \text{ mm}$ (0.0113 ft)

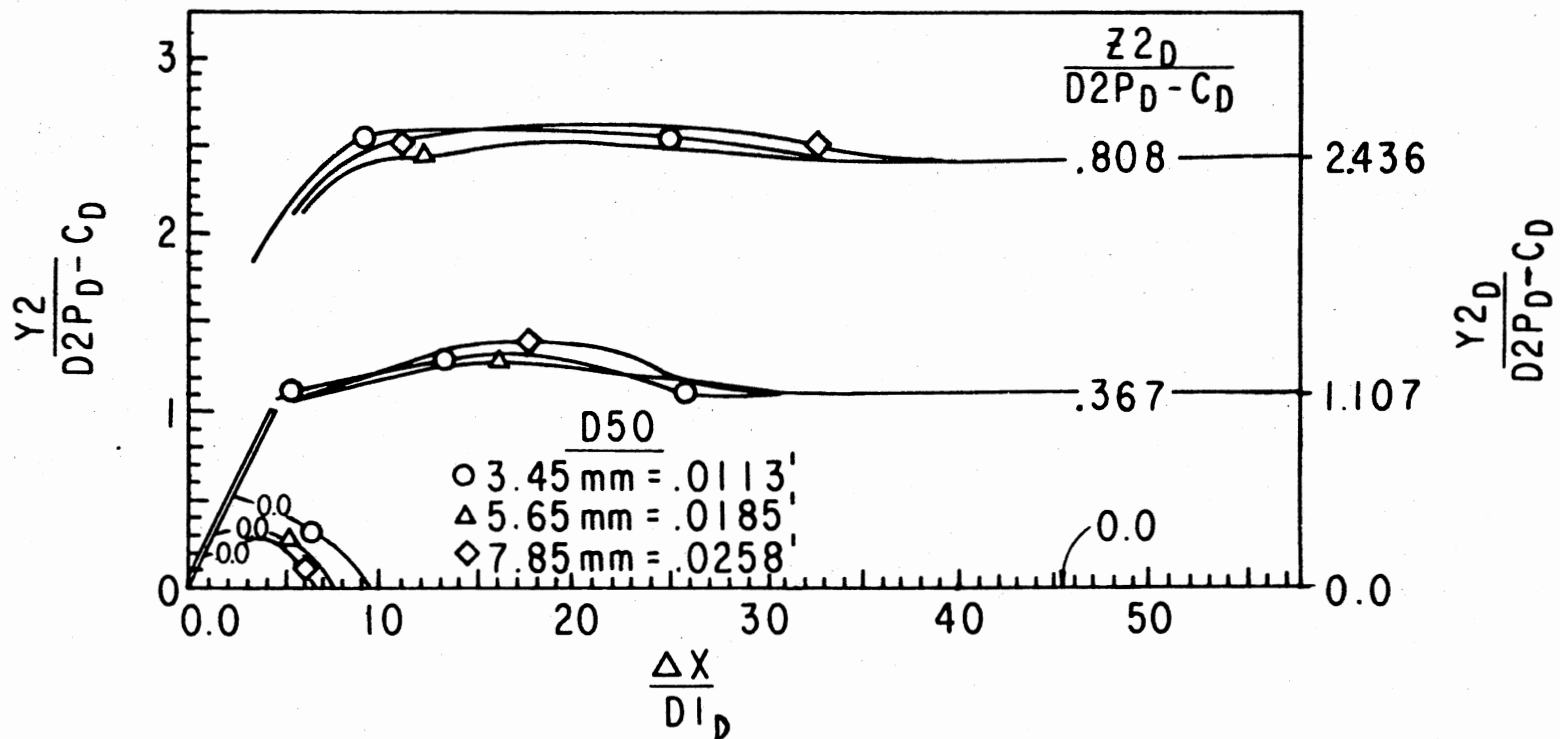


Figure 51. Nondimensional Maximum Scour Contour Map of Channel Side Resulting from Tests at $F_{1D} = 4$, Width = $9.75 \times D_{1D}$ and $24.75 \times D_{1D}$ for Three Different Rock Sizes

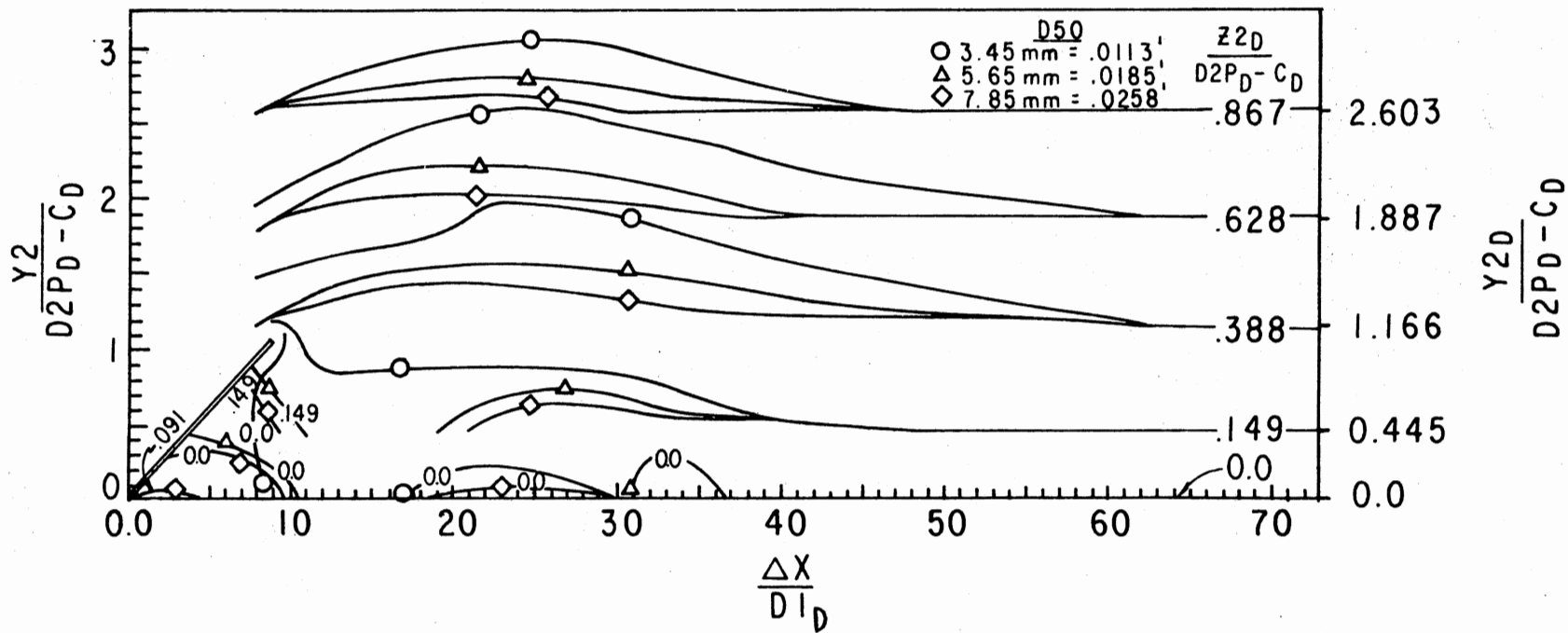


Figure 52. Nondimensional Maximum Scour Contour Map of Channel Side Resulting from Tests at $F_{1D} = 8$, Width = $9.75 \times D_{1D}$ and $24.75 \times D_{1D}$ for Three Different Rock Sizes

visibly observed for the tests at $Fl_D = 4$, although it was measured.

It is reasonable to assume that the scour shown in Figure 51 would equal or exceed that for any basin where $3 \leq Fl_D \leq 4.0$. Similarly, the scour shown in Figure 52 should be conservative for all basins where $4 \leq Fl_D \leq 8$.

Comparison of Results with Two State of the Art Methods

It was interesting to note how the tested rock sizes compared with sizes which might be recommended by state of the art methods (See Figure 53). Curves labeled 1 and 2 were obtained from Equation 5. Curves 3 and 4 came from Equation 2. For curves 1 and 3 the depth over the end sill was estimated to be $(D2P_D - C_D)$. For curves 2 and 4, Equation 43 was used to estimate $D3$. Note that use of $D3$ provides a more conservative estimate of needed rock size as long as $\Pi4_D > 3.35$. Diamonds show the actual sizes used. Attendant r values indicate the maximum vertical scour found on the side slopes. Observing the values of $(D50/D1) = 0.27$ for $\Pi4_D = 4.0$, it is seen that the maximum scour was $1.4 \times D50$. If the riprap layer had been only $2.0 \times D50$ thick, a bare spot could possibly have resulted. Careful placement of the rock, as opposed to a scraping technique, may have prevented this much scour from occurring. If so, the required rock size calculated by any method may have proven satisfactory for the channel sides. If not, one may surmise that it is desirable to have a slightly thicker rock layer on the side slopes in the region of maximum turbulence.

Even if the rock sizes used could have been placed in such a manner as to prevent any erosion on the side slopes, channel bottom erosion

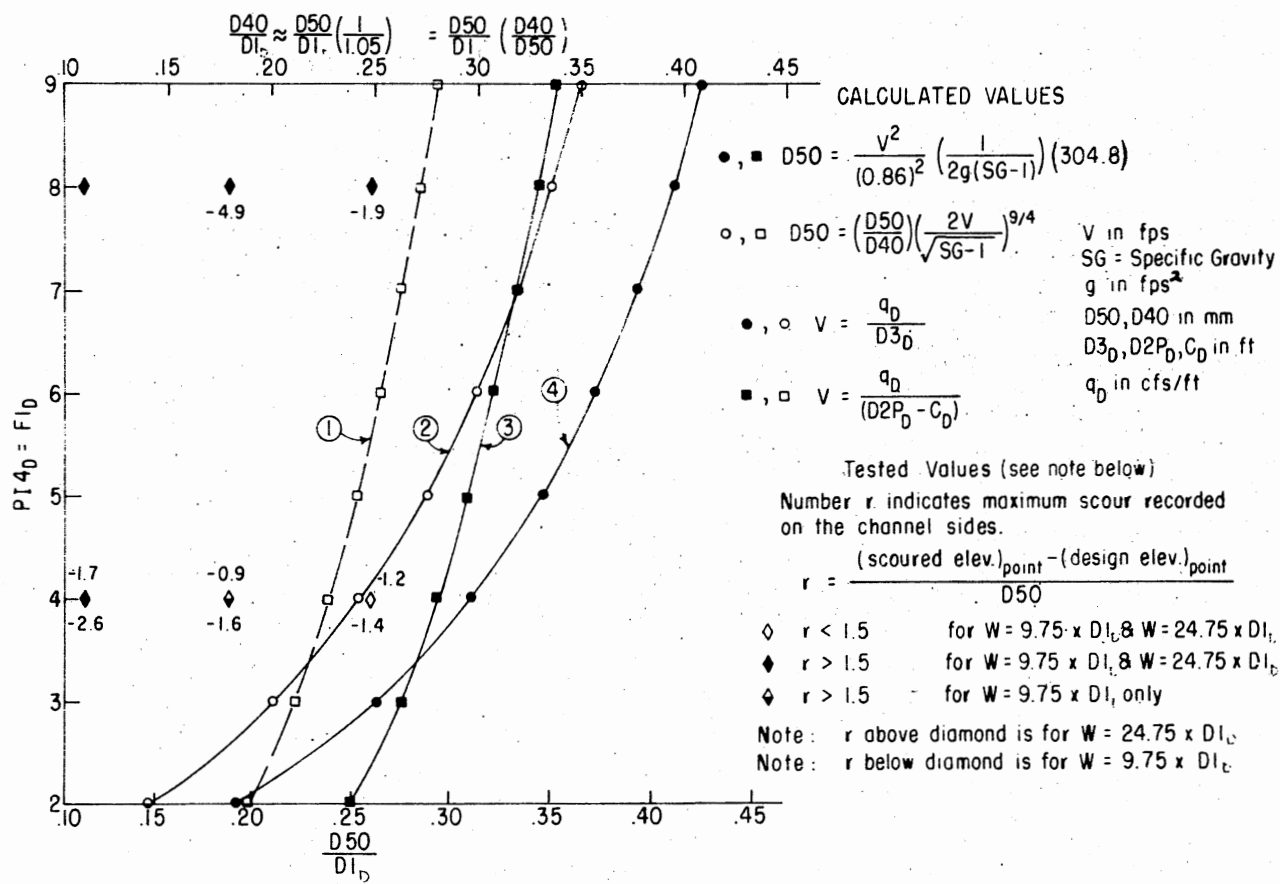


Figure 53. Comparison Between Rock Used in the Tests and Suitable Rock Sizes Calculated by State of the Art Methods as Related to Maximum Vertical Scour on the Channel Side Slopes

could probably not have been eliminated so easily. Figure 54 shows the relation between $D50/D1_D$ and the range of nondimensional scour which occurred for the tests of $F1_D = 4$ and $F1_D = 8$ (shaded regions). It also shows four points which indicate the $D50/D1$ values calculated by the first two of the methods discussed above. In every case, predicted scour exceeds $2 \times D50$. (Recall that riprap layers are generally made $2 \times D50$ thick.) Extrapolation to sizes larger than those used may give some indication of whether methods 3 and 4 would yield scour less than $2 \times D50$. For $F1_D = 4$, it seems likely. For $F1_D = 8$, scour may well always exceed $2 \times D50$ at position 2.

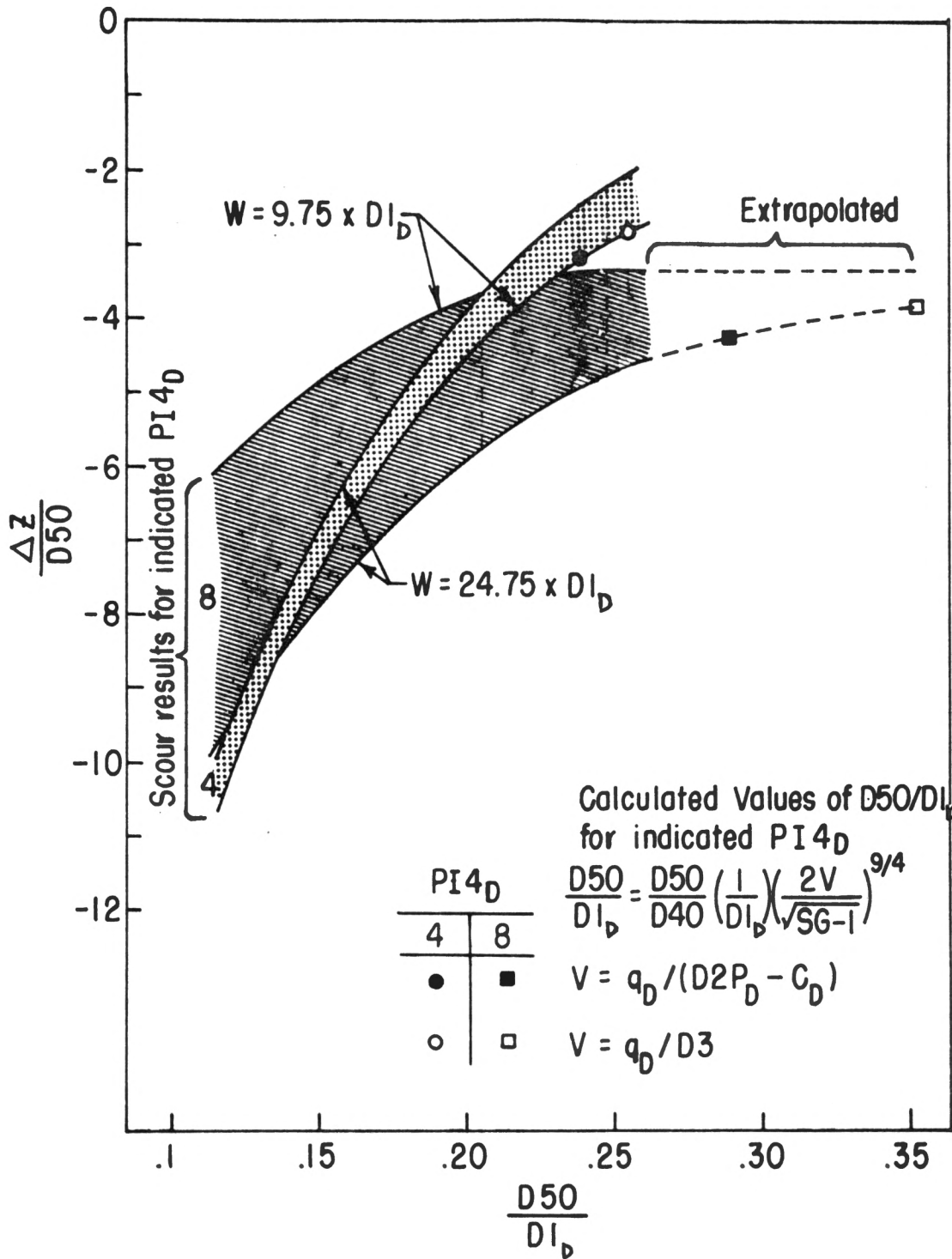


Figure 54. Estimation of the Nondimensional Scour Which Would Occur at Position 2 for Rock Sizes Calculated by Methods 1 and 2

CHAPTER VII

APPLICATION

Pertinent Procedures and Assumptions

The following coordinate system is used: The X, Y, and Z axes intersect at (0, 0, 0) where the top of the downstream edge of the end sill meets the basin centerline. The X axis coincides with the centerline and the Y axis coincides with the downstream edge of the end sill.

Froude modeling criteria were used in this research. The length scale to use when applying the research results is $\lambda = D1_p/D1_m$. $D1_m$ equals 0.0299 m (0.098 ft). This scale may be used for rock size and all dimensions in XYZ space. The time scale will be $\sqrt{\lambda}$. Since the major tests were 24 hours long, they simulated at least a 24-hour prototype occurrence.

Models of $Fl_D = 4$ and 8 were used. At the design flow conditions and minimum acceptable tailwater ($D2P_f$) all SAF basins designed for the same Fl_D value exhibit dynamic similarity. As long as the downstream channels are initially geometrically similar, the scour resulting from the model study will simulate that for any prototype of the same Fl_D . The upper limit of λ is primarily determined by the degree of error which is acceptable for a given situation. It was assumed that: flows in excess of the design rate would cause increased erosion; diminished flows would result in less erosion; erosion would increase with

decreasing tailwater; erosion would not increase with increasing tailwater as long as flow at the crest of the chute was unaffected by tailwater depth; and the location of significant erosion would probably move upstream with a tailwater greater than $D2P_D$.

The chute slope used in this study (3.48:1) was selected because it lies in the range of slopes most commonly used. Reasonable variations in chute slope have no significant effect on scour for tests of constant $F1_D$.

An initial assumption was that scour would decrease as $F1_D$ decreases. This was generally true when comparing tests on models of $F1_D = 4$ with those of $F1_D = 8$. (An exception occurred at position 2 using a rock size which is not recommended for $F1_D = 8$.) The approximately linear relationships between $F1_D$ (Π_4) and Π_1 , Π_2 , and Π_3 (Figure 36) suggest that the assumption is valid anywhere within the range $F1_D = 4$ to 8. One also assumes that the scour for $F1_D = 4$ will be greater than that for $F1_D = 3$. Relying on these two premises, the scour resulting from tests of $F1_D = 8$ may be used in riprap design for prototypes of $4 < F1_D \leq 8$. Tests at $F1_D = 4$ provide guidance for prototypes of $3 < F1_D < 4$. Applicability below an $F1_D$ of 3 is uncertain.

For the major tests, the downstream trapezoidal channel had 1 on 3 side slopes. Its horizontal bottom was as wide as the inside width of the stilling basin and matched the elevation of the end sill. The channel was scraped into shape by the use of a form mounted on a platform which was mobile in the X direction. This process simulated the field procedure of dumping the riprap and then bulldozing it into position. On the channel sides at least, this method will result in more scour than hand placement or tamping rocks into position.

Three different narrowly graded rock groups were used [$SG = 2.81$, $D50 = 3.45, 5.65, 7.85$ mm ($0.0113, 0.0185, 0.0258$ ft)]. Average particle masses for the small, medium, and large sizes are 8.3, 4.0, and 23.1 percent less than spheres of diameter equal to the $D50$ (See Table II). If the particles are compared with spheres of $SG = 2.65$, however, the differences are 2.8, 1.8, and 18.5 percent. In both cases, resultant scour will provide a conservative estimate of what would happen in the field.

Two widths, $9.75 \times D1_D$ and $24.75 \times D1_D$, were used in the testing. The effect of width on scour decreased as rock size increased. Side slope scour increased with increasing width for $Fl_D = 8$. The opposite was true for $Fl_D = 4$. Thus, the width effect was confounded. The scour from the two widths was compared and the worst scour was presented for design purposes. Since in some cases significant scour could occur anywhere between the centerline and the edge (See Figure 65), a two-dimensional approach was used in analyzing scour on the channel bottom. Nondimensional drawings were prepared to allow estimation of maximum scour length and depth at specified positions on the channel bottom (Figures 42, 43, 44 and 45). Nondimensional maximum scour contour maps were prepared by combining points of greatest scour for both sides of each tested channel and for both widths (Figures 51 and 52). During testing, maximum wave height along the channel sides never exceeded $D2P$ above the basin floor.

Design Guidance

Introduction

Downstream of the basin, the riprapped trapezoidal channel should

have 3:1 side slopes. Its bottom should be as wide as the distance between the basin side walls and it should be level with the top of the end sill. Beneath the channel sides and bottom, however, such regular features will probably not exist. Rock placement should be sufficient to insure that a 2 x D50 rock layer exists in all places even if the maximum predicted scour occurs. Therefore, depth of excavation and rock layer thickness must be greatest in areas of anticipated greatest scour.

If a prototype basin has characteristics of width and $F1_D$ similar to one of those tested in the study, the scour shown in the appropriate figure (Figures 63 - 72) may be used directly to determine excavation requirements. If not, the following guidance may be considered for basins of $F1_D = 3$ to 8 and widths = $9.75 \times D1_D$ to $24.75 \times D1_D$. One should include a safety factor in the design calculations.

Guidelines for Erosion on the Channel Bottom

$3 \leq F1_D \leq 4$: To determine the maximum scour profile consider only position numbers 2 and 3 in Figures 8, 42, and 43. Determine the maximum depth of scour at position number 2. Find the maximum length to position number 2. Find the maximum length to position number 3. Prepare a drawing showing these two points. The excavation profile should be at least 2 x D50 below the line connecting these points and should be horizontal between the end sill and position 2. (Basins of $F1_D < 4$ or tailwater $> D2P_D$ may scour closer to the end sill than a basin of $F1_D = 4$ at $D2P_D$.) Downstream of position 3 excavate at least 2.0 x D50 below the elevation of the end sill. Include room for a filter layer.

$4 < Fl_D \leq 8$: Consider only positions 2, 4, and 5 in Figures 8, 44, and 45. Determine the maximum depth at positions 2 and 4. Determine the minimum and maximum distances to positions 2 and 4. Find the maximum distance to position 5. Plot and connect the pertinent points. Draw the excavation profile at least $2 \times D50$ below the maximum scour profile. The riprap layer should be at least $2.0 \times D50$ thick downstream of position 5. Include a filter layer below the riprap layer.

Guidelines for Erosion on Channel Sides

Step Number

B1 -- Determine the length scale ratio between the prototype and the model study.

$$\lambda = \frac{Dl_p}{Dl_m} = \frac{Dl_p}{0.0299 \text{ m}} \quad (44)$$

B2 -- Determine the scaled down size of the rock which is available for the prototype design.

$$D50_m = \frac{D50_p}{\lambda} \quad (45)$$

B3 -- From Figure 51 ($3 \leq Fl_D \leq 4$) or Figure 52 ($4 < Fl_D \leq 8$) trace the scour contours of the size smaller than $D50_m$. You may instead wish to use your judgment and interpolate between 2 contours. Also trace the axes.

B4 -- Prepare new scales for the X and Y directions. The following equations are necessary.

$$\left(\frac{\Delta X}{Dl} \right)_{\text{Fig. 51}} = \frac{(\Delta X_{\text{desired}})}{Dl_p} \quad (46)$$

$$D2P_D = 1.4 D1_D (F1_D)^{0.9} \quad (47)$$

$$C_D = 0.07 [0.5(D1_D) (-1 + \sqrt{8(F1_D)^2 + 1})] \quad (48)$$

$$(D2P_D - C_D)_p = D2P_D - C_D \quad (49)$$

$$\left(\frac{Y2}{(D2P_D - C_D)_p} \right)_{\text{Fig. 51 or 52}} = \frac{(Y2_{\text{desired}})}{(D2P_D - C_D)_p} \quad (50)$$

B5 -- Determine the elevations of the contours from:

$$Z2_p = \left(\frac{Z2}{(D2P_D - C_D)_p} \right)_{\text{Fig. 51 or 52}} \times (D2P_D - C_D)_p \quad (51)$$

B6 -- Since a riprap layer thickness of about $2 \times D50$ is desirable on the channel sides in the region of scour one should subtract at least $2 \times D50_p$ from the contour elevations found above and label the contours accordingly.

$$(Z2_p)_{EX} = Z2_p - 2(D50_p) \quad (52)$$

B7 -- Determine how best to excavate around existing contours. From your working drawing take as many cross sections as are necessary to minimize construction expense. Remember that for a tailwater $> D2P_D$, major scour may occur farther upstream than at $D2P_D$, although it will probably not laterally exceed that shown in the design drawings. A similar situation may exist for basins in which the design entrance Froude number is less than the $F1_D$ of the appropriate design chart. Extend the riprap protection at least as far downstream as it would scour were you to use rock comparable to the smallest tested in this study.

B8 -- Riprap should be used at least $2 \times D50$ above the actual tailwater elevation. Consider using a safety factor to protect against the effect of wind on wave height.

B9 -- Remember to eliminate the discontinuity which probably exists where the excavation cut on the side slope meets the one on the channel bottom. The angle of the interface cut should probably not exceed the submerged angle of repose of the material.

Example

Given: Basin of $F1_D = 3$

$$D50_p = 0.27 \text{ m (0.886 ft)}$$

$$D1_p = 1.22 \text{ m (4 ft)}$$

Tailwater depth above basin floor at design flow conditions
= minimum acceptable tailwater depth ($D2P_D$)

Channel Bottom Design:

-- Determine pertinent position numbers (Figure 8):

Positions 2 and 3 are needed in the design.

-- Determine maximum depth of scour (Figure 43):

$$\frac{D50_p}{D1_p} = \frac{0.27}{1.22} = 0.225$$

$$\text{Maximum } \frac{\Delta Z_{2\text{MAX}}}{D50_p} = 3.6 \text{ at position 2.}$$

$$\begin{aligned} \Delta Z_{2\text{MAX}} &= 3.6 \times D50_p \\ &= .97 \text{ m (3.19 ft)} \end{aligned}$$

-- Determine location of positions 2 and 3 (Figure 42):

Only the most downstream location of position 2 is needed.

For $\frac{D50_p}{D1_p} = 0.225$, Position 2 may occur as far downstream as:

$$\frac{\Delta X_{2\text{MAX}}}{D50_p} = 13.5$$

$$\Delta X_{2MAX} = 3.65 \text{ m (11.96 ft)}$$

Position 3 may occur as far downstream as:

$$\frac{\Delta X_{3MAX}}{D50_p} = 37.5$$

$$\Delta X_{3MAX} = 10.13 \text{ m (33.22 ft)}$$

- Prepare a drawing showing the greatest extent of scour expected on the channel bottom (See Figure 55).
- Decide how thick a riprap layer is desired below the maximum scour profile. Remember to consider the thickness of a filter layer.
- Determine the appropriate excavation profile and show it on the drawing. Downstream of position 3 the riprap layer should be at least $2.0 \times D50$ thick.

Channel Side Design:

Step Number

- B1 -- Determine the length scale ratio between the prototype and the model study presented in this report.

$$\lambda = \frac{D1_p}{D1_m} = \frac{1.22 \text{ m}}{0.0299 \text{ m}} = 40.803$$

- B2 -- Determine the scaled down D50:

$$D50_m = \frac{D50_p}{\lambda} = \frac{0.27}{40.803} = 0.0066 \text{ m (0.022 ft)}$$

- B3 -- The size smaller than this in Figure 51 is 5.65 mm (0.0185 ft). On a clean piece of paper trace the axes and the contours corresponding to $D50 = 5.65 \text{ mm (.0185 ft)}$ found on Figure 51 (See Figure 56).

- B4 -- Prepare new scales for the X and Y directions and mark Figure 56 accordingly.

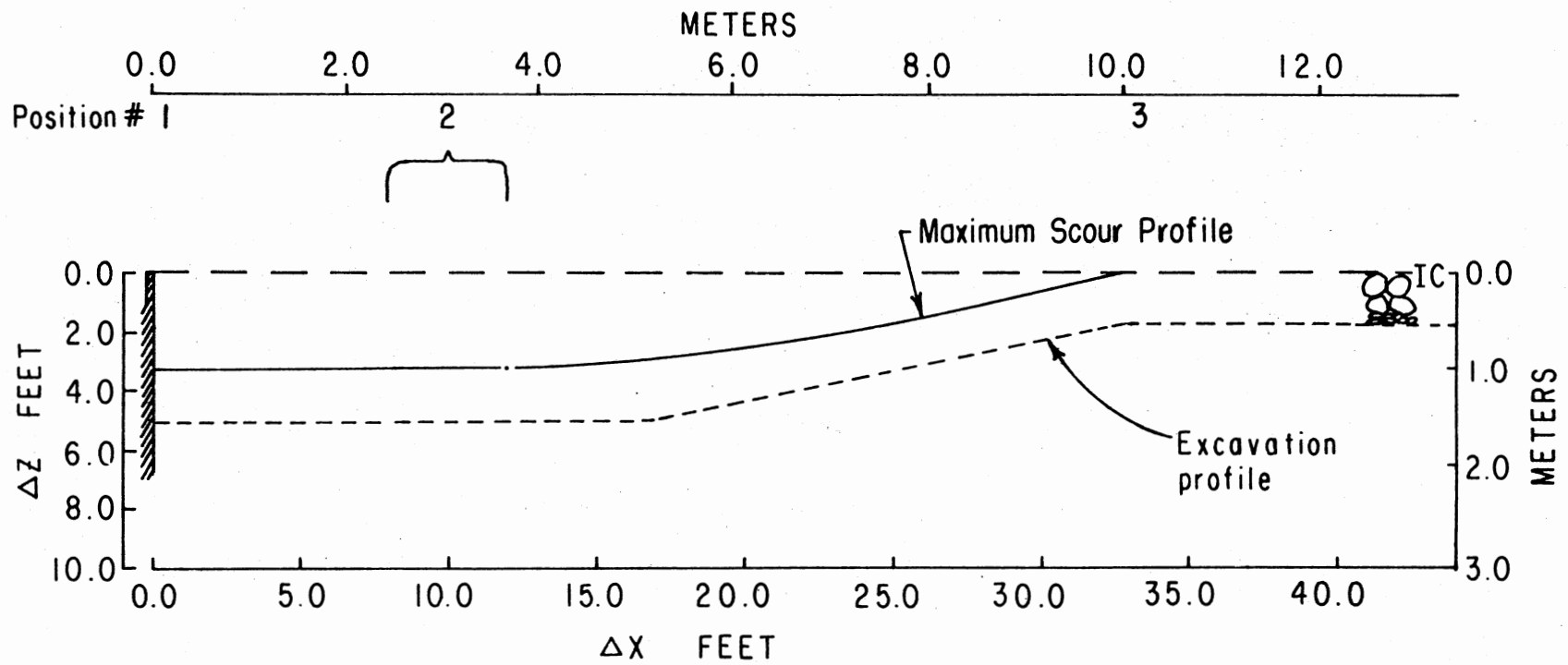


Figure 55. Side View of Channel Bottom Showing the Excavation Profile (Without Safety Factor), the Maximum Scour Profile, and the Finished Channel Bottom Level with the End Sill

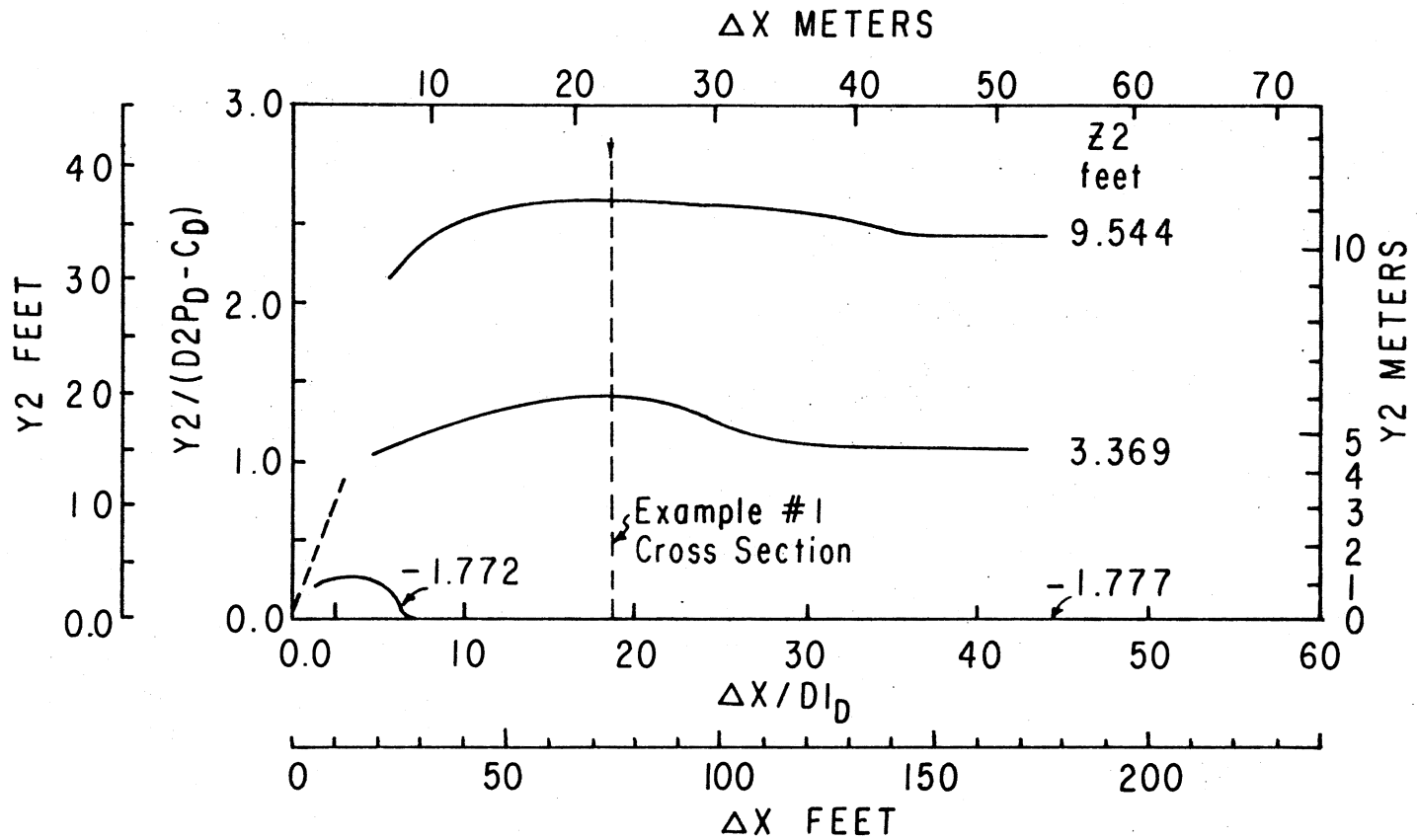


Figure 56. Contour Map of the Channel Side Slope Showing Contours Which Must Be Excavated Around

$$\left(\frac{\Delta X}{D1} \right)_{\text{Figure 51}} = \frac{(\Delta X_{\text{desired}})}{D1_p}$$

$$\begin{aligned} D2P_D &= 1.4 D1_D (F1_D)^{\cdot 9} \\ &= 1.4 (1.22) (3)^{\cdot 9} \\ &= 4.591 \text{ m (15.062 ft)} \end{aligned}$$

$$\begin{aligned} C_D &= 0.07 [.5(D1_D)(-1 + \sqrt{8(F1_D)^2 + 1})] \\ &= 0.07 [.5(1.22)(-1 + \sqrt{8(3)^2 + 1})] \\ &= 0.322 \text{ m (1.057 ft)} \end{aligned}$$

$$(D2P_D - C_D)_p = 4.269 \text{ m (14.006 ft)}$$

$$\left(\frac{Y2}{(D2P_D - C_D)} \right)_{\text{Figure 51}} = \frac{(Y2_{\text{desired}})}{(D2P_D - C_D)_p}$$

$$\left(\frac{Y2}{(D2P_D - C_D)} \right)_{\text{Figure 51}} = \frac{(Y2_{\text{desired}})}{4.269 \text{ m}}$$

B5 -- Determine the elevations of the contours:

$$Z2_p = \left(\frac{Z2}{(D2P_D - C_D)} \right)_{\text{Figure 51}} \times (D2P_D - C_D)_p$$

The elevations found from Equation 51 are 0, 1.567, and 3.449 m (0, 5.140, 11.317 ft).

B6 -- Determine the elevations of the contours which indicate the minimum acceptable amount of excavation by subtracting at least 2 x D50 from the elevations found above:

$$2 \times D50_p = 2(0.27) = 0.54 \text{ m (1.772 ft)}$$

The new contour elevations are:

$$-0.54, 1.027, \text{ and } 2.909 \text{ m (-1.772, 3.369, and 9.544 ft)}$$

B7 -- Determine how best to excavate around existing contours:

In this example, just one cross section is taken, at $\Delta X = 22.56 \text{ m}$ (74 ft) (Figure 57). This cross section could be used between the

wingwall tips and $\Delta X = 40 \times D1_D = 48.8 \text{ m (160.1 ft)}$, except for a region of additional excavation near the wingwalls themselves.

If more cross sections are taken, the volume of riprap required can be reduced.

B8 -- The tailwater depth above the end sill is:

$$D2P_D - C_D = 4.27 \text{ m (14.01 ft)}$$

Riprap should extend at least $2 \times D50$ higher than that (not including a safety factor for wind).

$$\begin{aligned} D2P_D - C_D + 2 \times D50 &= 4.27 \text{ m} + 2 (.27 \text{ m}) \\ &= 4.81 \text{ m (15.78 ft)} \end{aligned}$$

This is shown in Figure 57.

B9 -- An interface cut may be needed to combine the designs for the channel bottom and channel sides. In this case, none is needed downstream of ΔX_{3MAX} at 10.13 m (33.22 ft).

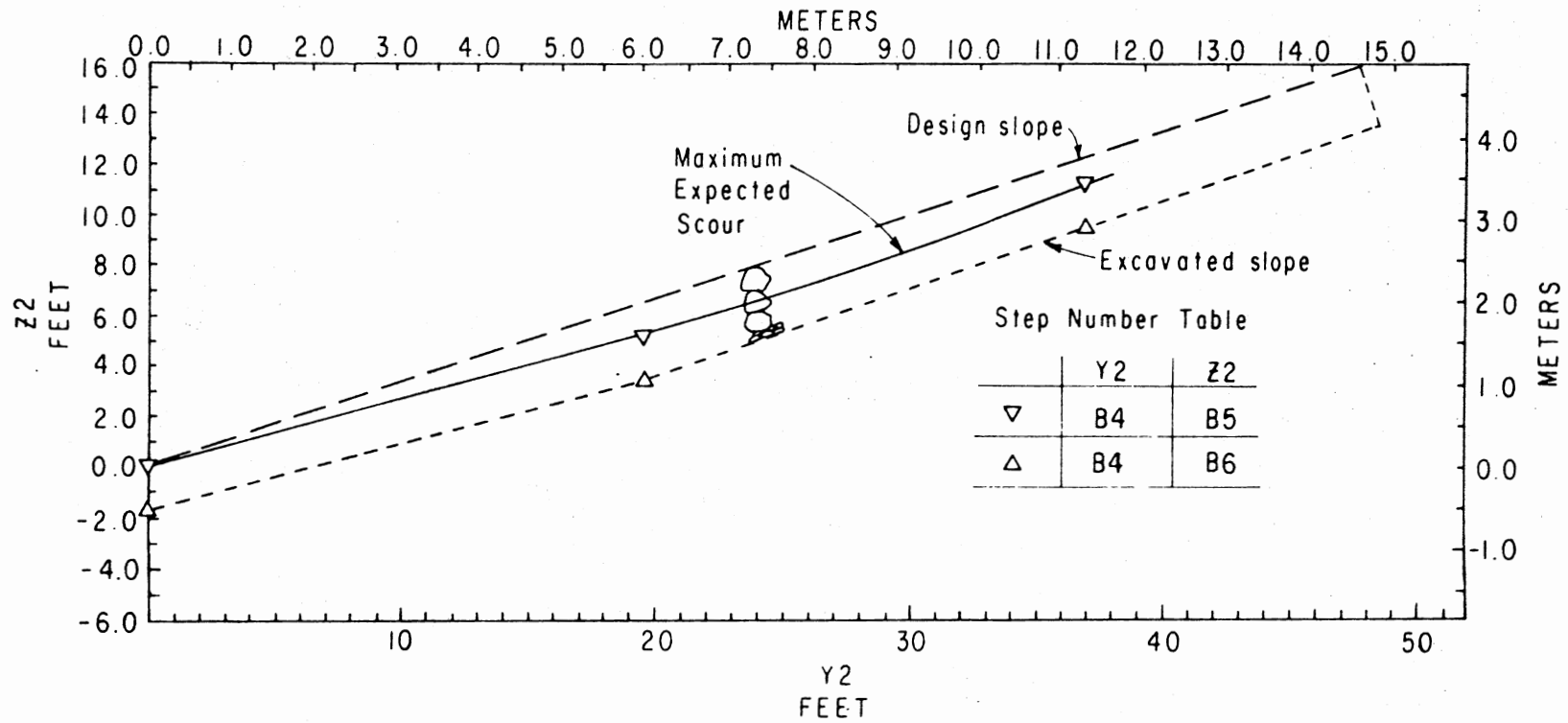


Figure 57. Cross Section of the Channel Side Slope Taken at $\Delta X = 74$ Feet Showing the Intended Finished Surface, the Maximum Expected Scour and the Excavation Slope (Without Safety Factor)

CHAPTER VIII

SUMMARY AND CONCLUSIONS

Froude modeling was used to obtain information for the placement of riprap as erosion protection downstream of Saint Anthony Falls stilling basins. Tests were run for basins of entrance Froude numbers (Fl_D) of 4 and 8, and widths of $9.75 \times D1_D$ and $24.75 \times D1_D$. Rock D50 used in the study ranged from 3.45 to 7.85 mm (0.0113 to 0.0258 ft). The initial conditions of the downstream trapezoidal channel were: 3:1 side slopes; bottom level with the top of the end sill; and bottom width as wide as the inside of the basin. General assumptions were: the minimum acceptable tailwater ($D2P_D$) allows at least as much scour as a higher tailwater; and scour increases as Fl_D increases.

The objectives were:

- show the relative suitability for SAF basins of state of the art techniques for selecting rock sizes below hydraulic jump type stilling basins.
- show whether smaller rock sizes can be used.

Four methods for determining suitable rock size were compared with one another. Those considered to be conservative required the larger rock sizes. These four methods were the possible combinations of: two different equations for determining rock size as a function of average velocity over the end sill; and two methods for determining the average depth and hence velocity over the end sill. The equations were those

of: 1) the U.S. Army Corps of Engineers and 2) the International Institute for Land Reclamation and Improvement. The methods for estimating depth over the end sill were: a) an empirical formula derived from water surface measurements and b) subtraction of the end sill elevation from the tailwater elevation. For Fl_D greater than 3.35, these may be ranked, most conservative first: 1a, 1b, 2a and 2b. For Fl_D below 3.35, the order is: 1b, 1a, 2b, and 2a.

Conclusions are as follow:

- On the channel bottom the less conservative methods definitely require some thickening of riprap layer in locations of high turbulence. The more conservative may or may not require this treatment. Anticipated depths of scour for sizes which scale down to be larger than those tested may be obtained by extrapolation from the design charts presented in the study.
- Thickening is also advised on the side slopes unless the more conservative equations are used.
- Designs using smaller rock sizes, which scale down to within the range tested, may be prepared by following the procedures outlined in Chapter VII.

Some other observations are worthy of repetition:

- As width increased, scour increased for $Fl_D = 8$. The opposite was true for $Fl_D = 4$. Accordingly, the design charts reflect the maximum scour found by comparing both widths. If one were to design for widths greater than those tested or for Fl_D values outside the range of those tested, this information may be important.
- As expected, scour increased as rock size decreased. One result was that the smallest size never formed a "stable" hole for the wide

$Fl_D = 8$ basin. A peculiar result occurred for the narrow width at $Fl_D = 8$. In this case, excessive scour from the channel sides armored the bottom such that bottom scour was less for the smallest rock than for the larger sizes. This rock should not be used for basins of $Fl_D = 8$. Conservatively speaking, one should probably not use the rock for $Fl_D > 4.0$.

- The effect of width on scour decreased as rock size increased.
- After passage of the design flow, rocks in the scour bed were often aligned with their narrow edge parallel to the flow direction.

Some scour will almost always occur. The amount depends on the size of material used. If the material is lighter than that which is "absolutely" stable, a scour hole and deposition mound will occur. The deposition mound must not be removed, except to fill in the scour hole. Removal of the deposition without replacement of scoured material will result in a greatly increased scour hole after passage of the next design flow and the formation of a new deposition mound. In the words of a prominent soil-water engineer (12),

"It's not nice to fool Mother Nature."

A SELECTED BIBLIOGRAPHY

- (1) Abou-Seida, Mohamed Mokhles. "Wave Action Below Spillways." Journal of the Hydraulics Division, ASCE, Vol. 89, No. HY3, May 1963.
- (2) Airy, Wilfred. "Discussion of Paper 'On Rivers Flowing into Tideless Seas, Illustrated by the River Tiber'." Proceedings, Inst. of Civil Engineers, Vol. 82, 1885.
- (3) Alling, Edwin S. Structural Design of SAF Stilling Basins. Washington, D. C.: Soil Conservation Service, SCS-TR No. 54, Oct. 1975.
- (4) Anderson, A. G. and A. S. Paintal. Tentative Design Procedure for Riprap-Lined Channels. Washington, D. C.: Highway Research Board, National Cooperative Highway Research Program Report No. 108, 1970.
- (5) Berry, N. K. "The Start of Bed Load Movement." (Unpub. M.S. Thesis, Univ. of Colorado, 1948.)
- (6) Blaisdell, F. W. The SAF Stilling Basin. Washington, D. C.: U.S. Department of Agriculture, Agricultural Handbook No. 156, 1959.
- (7) Bowers, C. Edward and Frank Y. Tsai. "Fluctuating Pressures in Spillway Stilling Basins." Journal of the Hydraulics Division, ASCE, Vol. 92, No. HY2, March 1966.
- (8) Brater, E. F. and Horace W. King. Handbook of Hydraulics. 6th Ed. New York: McGraw Hill Book Co., Inc., 1976.
- (9) Campbell, F. B. Hydraulic Design of Rock Riprap. Vicksburg, Mississippi: U.S. Army Engineers Waterways Experiment Station, Misc. Paper No. 2-777, Feb. 1966.
- (10) Doubt, Paul D. Chute Spillways. Washington, D. C.: Soil Conservation Service, National Engineering Handbook Section 14, March 1976.
- (11) Fletcher, B. P. and J. L. Grace, Jr. Practical Guidance for Estimating and Controlling Erosion at Culvert Outlets. Vicksburg, Mississippi: U.S. Army Engineers Waterways Experiment Station, Misc. Paper No. H-72-5, May 1972.

- (12) Garton, James E. Personal Communication. Oklahoma State University, Stillwater, OK, 1979.
- (13) Grace, J. L., Jr. Outlet Works for Branched Oak and Cottonwood Springs Dams. Vicksburg, Mississippi: U.S. Army Waterways Experiment Station, 1972.
- (14) Grace, John L. and Glenn A. Pickering. Evaluation of Three Energy Dissipators for Storm Drain Outlets. Vicksburg, Mississippi: U.S. Army Engineers Waterways Experiment Station, Research Report H-71-1, April 1971.
- (15) Hooker, Elon H. "The Suspension of Solids in Flowing Water." Transactions, ASCE, Vol. 36, Dec. 1896.
- (16) Isbash, S. V. "Construction of Dams by Depositing Rock in Running Water." Transactions, Second Congress on Large Dams, Vol. 5, 1936.
- (17) International Institute for Land Reclamation and Improvement/ILRI. Discharge Measurement Structures. Wageningen, The Netherlands: Publication 20, 1976.
- (18) Mavis, F. T. and L. M. Laushey. "A Reappraisal of the Beginnings of Bed Movement - Competent Velocity." Proceedings of the International Association for Hydraulic Structures Research, 1948.
- (19) Murphy, Glenn. Similitude in Engineering. New York: John Wiley and Sons, 1950.
- (20) Peterka, A. J. Hydraulic Design of Stilling Basins and Energy Dissipators. Washington, D. C.: Bureau of Reclamation, Engineering Monograph No. 25, 1974.
- (21) Ree, W. O. Comparison of Chute and Stilling Basin Performance for Three Different Drop Box Inlets. Washington, D. C.: Agricultural Research Service, ARS-S-126, July 1976.
- (22) Ree, W. O. Results of Tests on a Chute with a St. Anthony Falls Stilling Basin. Washington, D. C.: Soil Conservation Service, SCS-TP-107, Sept. 1951.
- (23) Shelford, William. "On Rivers Flowing into Tideless Seas, Illustrated by the River Tiber." Proceedings, Inst. of Civil Engineers, Vol. 82, 1885.
- (24) Simons, D. B. and F. Sentürk. Sediment Transport Technology. Fort Collins, Colorado: Water Resources Publications, 1977.
- (25) U.S. Army Corps of Engineers. Hydraulic Design Criteria. Washington, D. C.: Office of the Chief of Engineers. Jan. 1977.

- (26) U.S. Army Corps of Engineers. Hydraulic Design of Reservoir Outlet Structures. Washington, D. C.: Office of the Chief of Engineers, Engineering Manual EM 1110-2-1602, Aug. 1963.
- (27) U.S. Army Corps of Engineers. McNary Dam - Second Step Cofferdam Closure. U.S. Army Engineer District, Portland: Bonneville Hydraulic Laboratory, Report No. 51-1, 1956.
- (28) Urbonas, B. R. "Forces on a Bed Particle in a Tamped Rock Stilling Basin." (Unpub. M.S. Thesis, Colorado State University, 1968.)
- (29) White, C. M. "The Equilibrium of Grains on the Bed of a Stream." Proc. of the Royal Society of London, Series A, Volume 1974, 1940.
- (30) Yain, M. Selim. Theory of Hydraulic Models. New York: The MacMillan Press Ltd., 1971.

APPENDICES

APPENDIX A

LETTER FROM SCS HEADQUARTERS SHOWING THE NUMBER
OF COMPUTER DESIGNS PREPARED FOR SAF BASINS,
MARCH 1974 THROUGH JUNE 1978

(P. 25)

U.S. Dept. of Agriculture
S.C.S.
Design Unit, Eng. Div.
10,000 Aerospace Rd.
Lanham Maryland
20801

UNITED STATES DEPARTMENT OF AGRICULTURE
SOIL CONSERVATION SERVICE

SUBJECT: ENGINEERING - Froude Numbers for SAF Basin Designs DATE: October 11, 1978

TO: Wendell R. Gwinn
SEA-AR
Stillwater Hydraulic Laboratory
Stillwater, Oklahoma

At the wrap-up of the combined SCS/SEA-AR meeting last week, I promised to send you information on Froude Number distribution in the SAF basin designs we have executed. This information follows. Note that these designs include many performed for study purposes. Thus we cannot separate out those designs selected for either actual work plans or actual construction.

FROUDE NUMBER	NUMBER OF DESIGNS EXECUTED
0 - 10	16
10+ - 20	44
20+ - 30	87
30+ - 40	98
40+ - 50	32
50+ - 60	34
60+ - 70	32
70+ - 80	9
80+ - 90	27
90+ - 100	10
100+ - 200	43
200+ - 300	2
	434

These designs were executed from 3/74 through 6/78. The Froude number definition is

$$F = V^2/gD$$

I hope this information is helpful.

Edwin S. Alling
Edwin S. Alling, Head,
Design Unit, Design Branch
Engineering Division

cc: David C. Ralston, Chief, Design Branch

Figure 58. Correspondence from SCS Indicating Number of Computer Designs Prepared for SAF Basins of Different $(F1_D)^2$, Where $F1_D^2$ Equals the F in the Correspondence



APPENDIX B

AVERAGE CENTERLINE WATER SURFACE
PROFILES AND CENTERLINE
DEPOSITION PROFILE

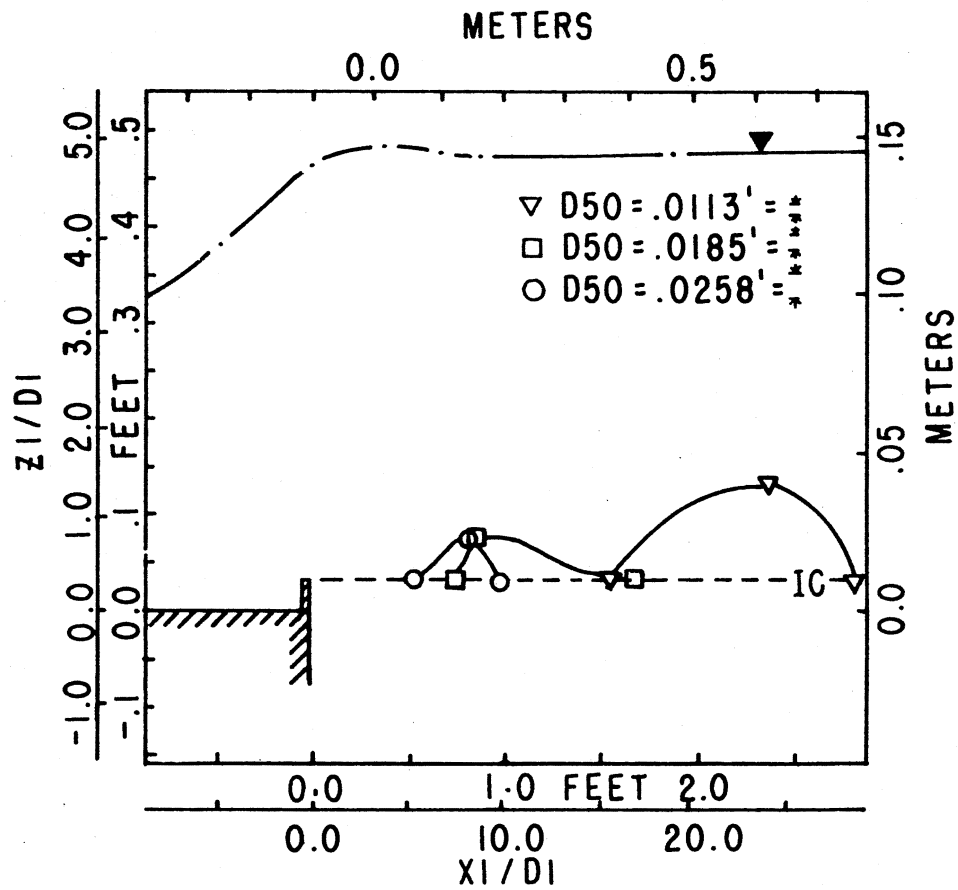


Figure 59. Centerline Water Surface Profile and Deposition Profile for $Fl_D = 4.0$, $W = 24.75 \times D_1$

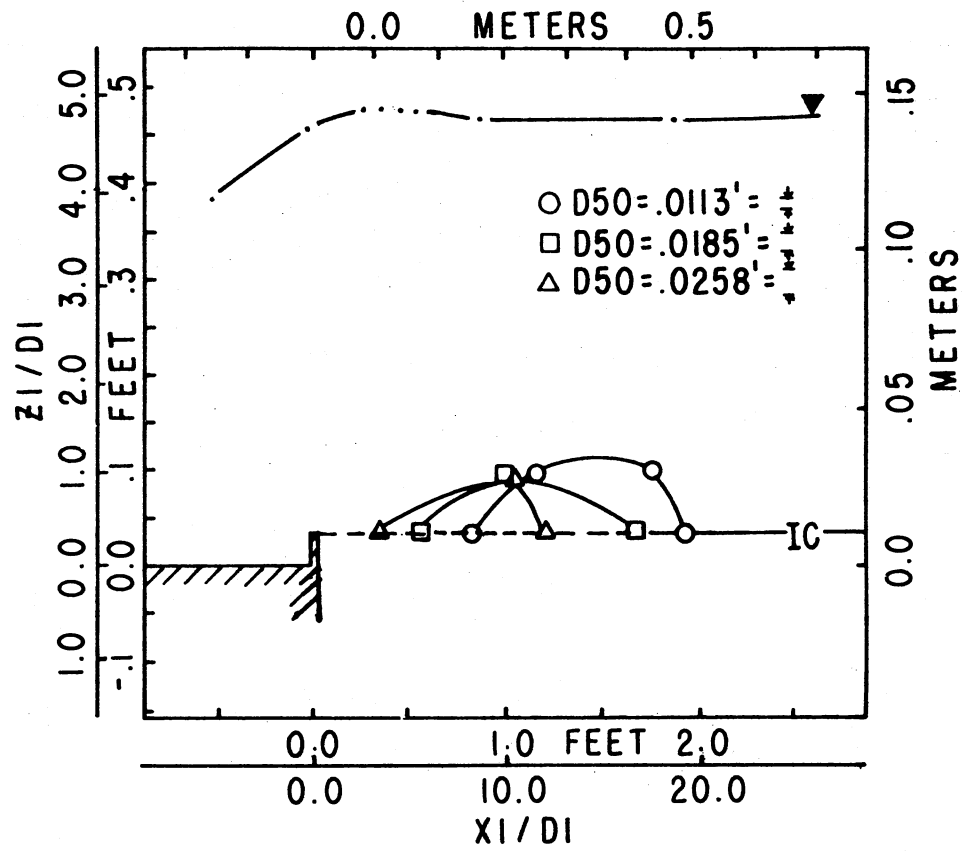


Figure 60. Centerline Water Surface Profile and Deposition Profile for $Fl_D = 4.0$, $W = 9.75 \times D1_D$

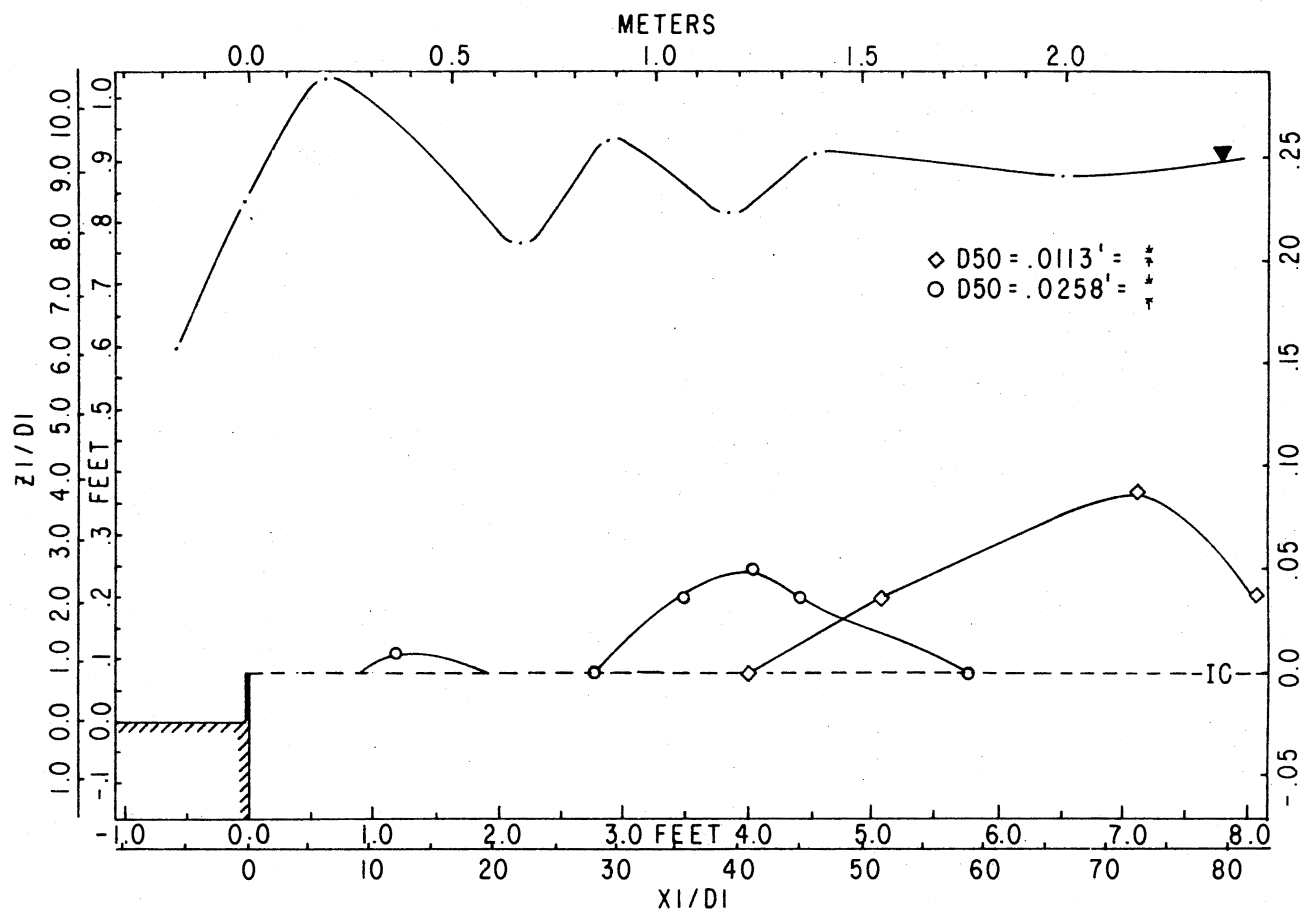


Figure 61. Centerline Water Surface Profile and Deposition Profile for $Fl_D = 8.0, W = 24.75 \times D_1$

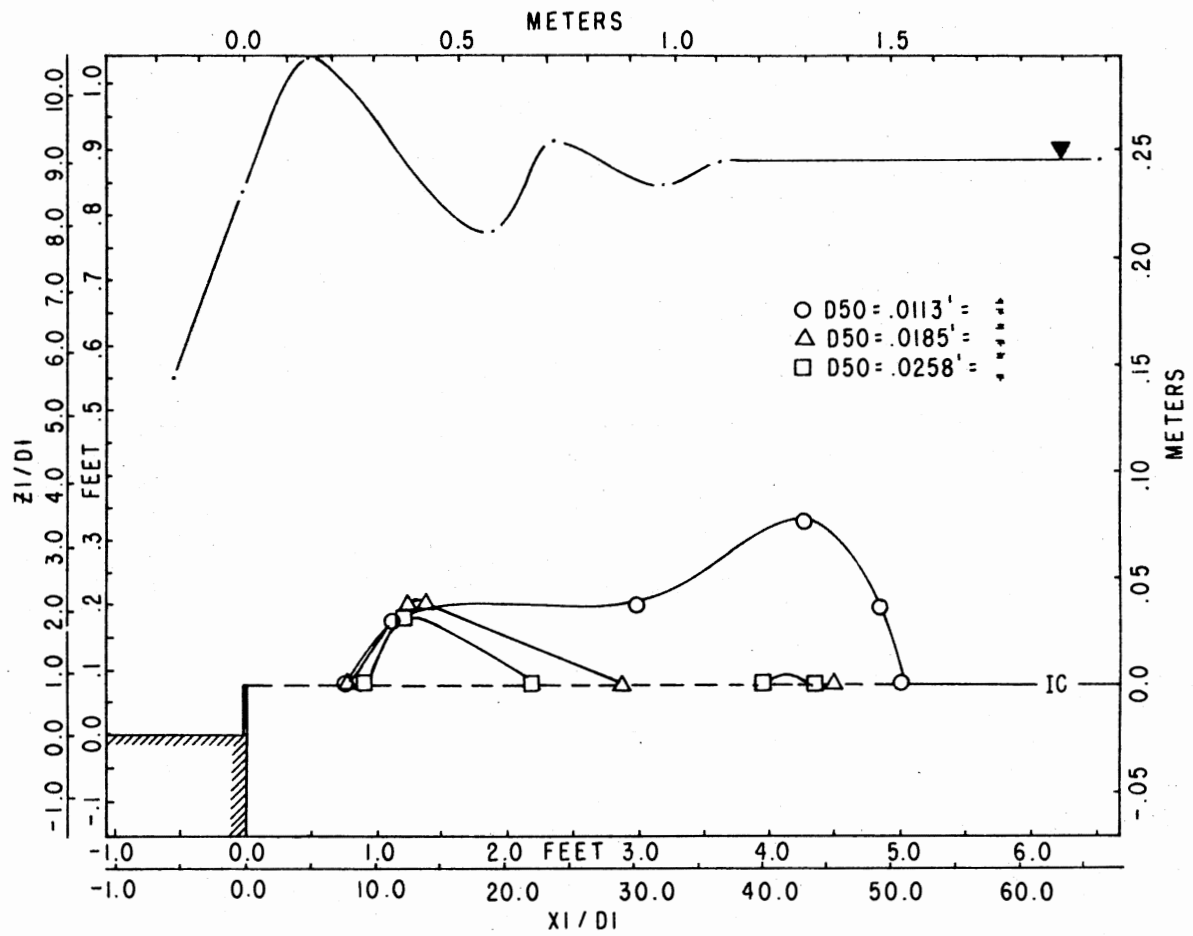


Figure 62. Centerline Water Surface Profile and Deposition Profile
for $Fl_D = 8.0$, $W = 9.75 \times D1_D$

APPENDIX C

MAXIMUM SCOUR CONTOUR MAPS

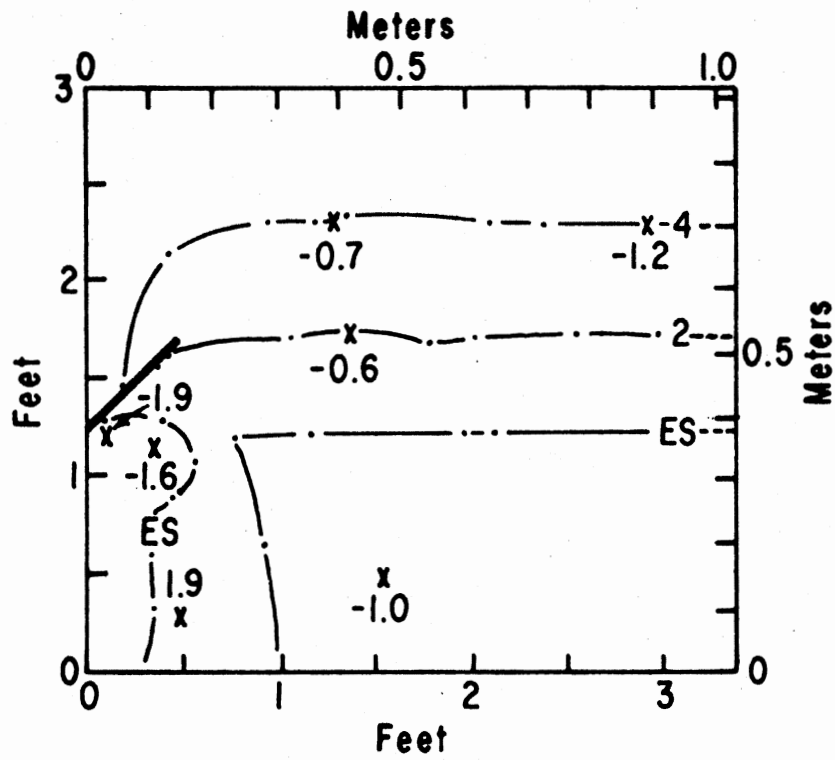


Figure 63. Maximum Scour Contour Map After
 Testing at $F1_D = 4.0$, $W = 24.75 \times$
 $D1_D$, $D50 = 7.85 \text{ mm (0.0258 ft)}$

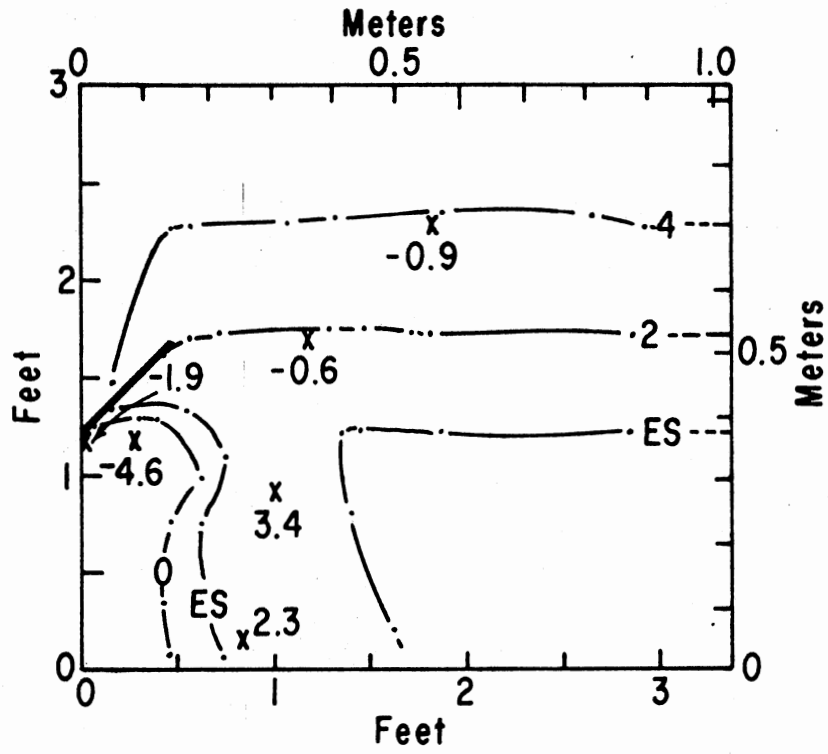


Figure 64. Maximum Scour Contour Map After Testing at $F1_D = 4.0$, $W = 24.75$ x $D1_D$, $D50 = 5.65$ mm (0.0185 ft)

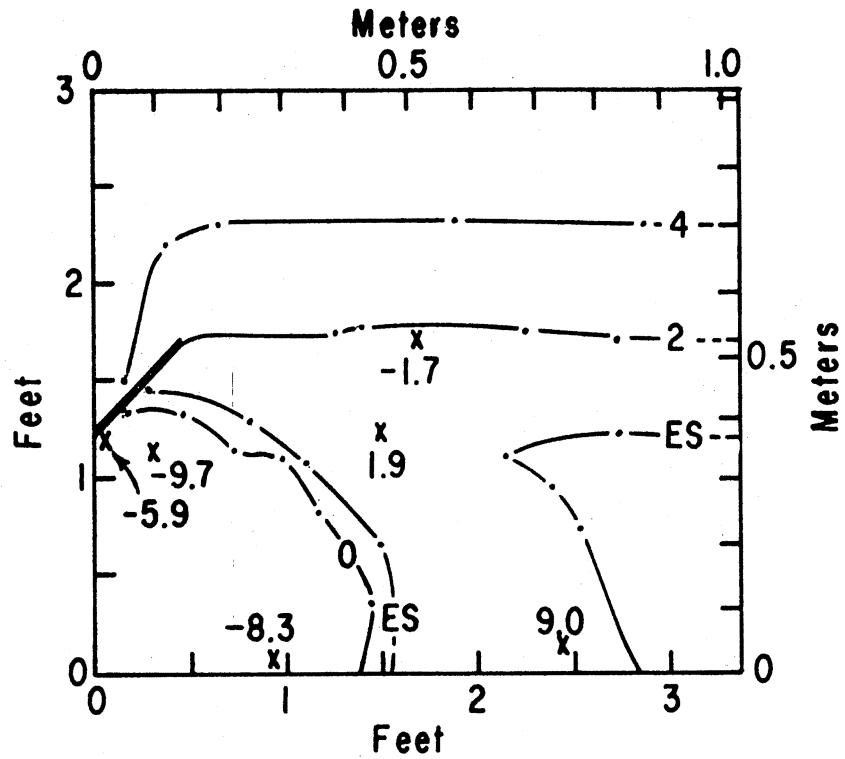


Figure 65. Maximum Scour Contour Map After
 Testing at $F1D = 4.0$, $W = 24.75$
 $\times D1D$, $D50 = 3.45 \text{ mm (0.0113 ft)}$

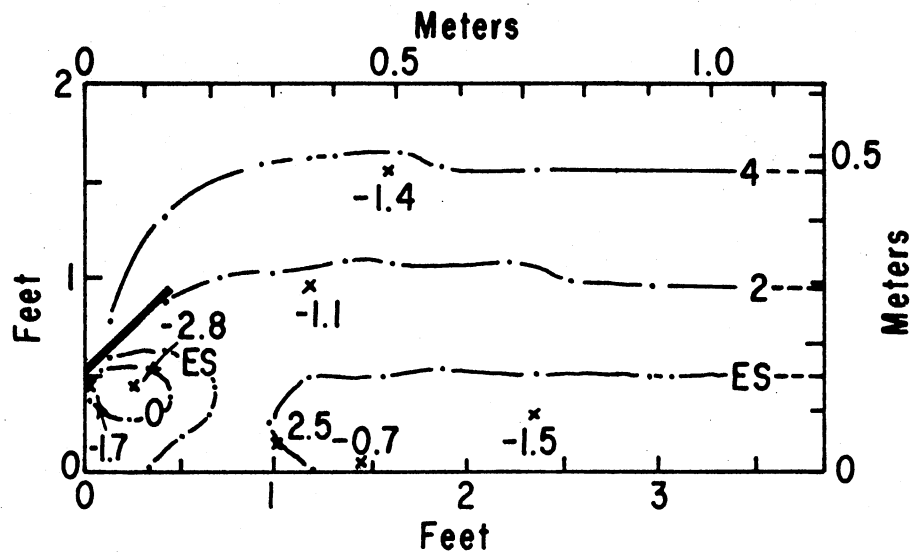


Figure 66. Maximum Scour Contour Map After Testing
 at $F1_D = 4.0$, $W = 9.75 \times D1_D$, $D50 = 7.85$
 mm (0.0258 ft)

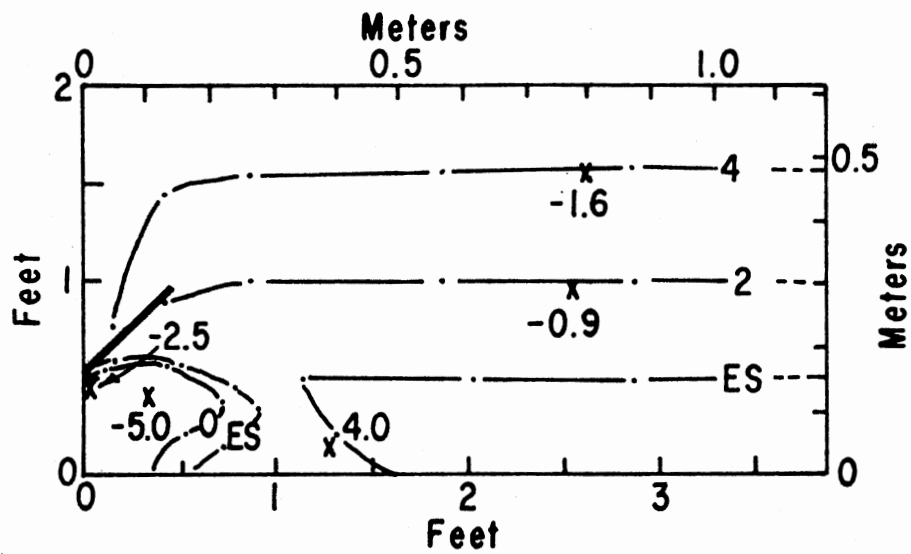


Figure 67. Maximum Scour Contour Map After Testing
 at $F1_D = 4.0$, $W = 9.75 \times D1_D$, $D50 = 5.65 \text{ mm}$ (0.0185 ft)

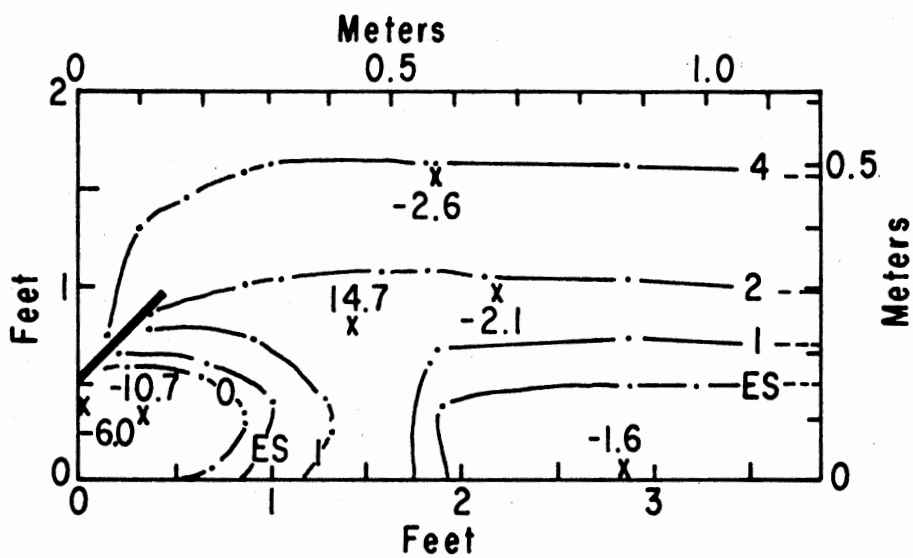


Figure 68. Maximum Scour Contour Map After Testing
 at $F1_D = 4.0$, $W = 9.75 \times D1_D$, $D50 =$
 $3.45 \text{ mm (0.0113 ft)}$

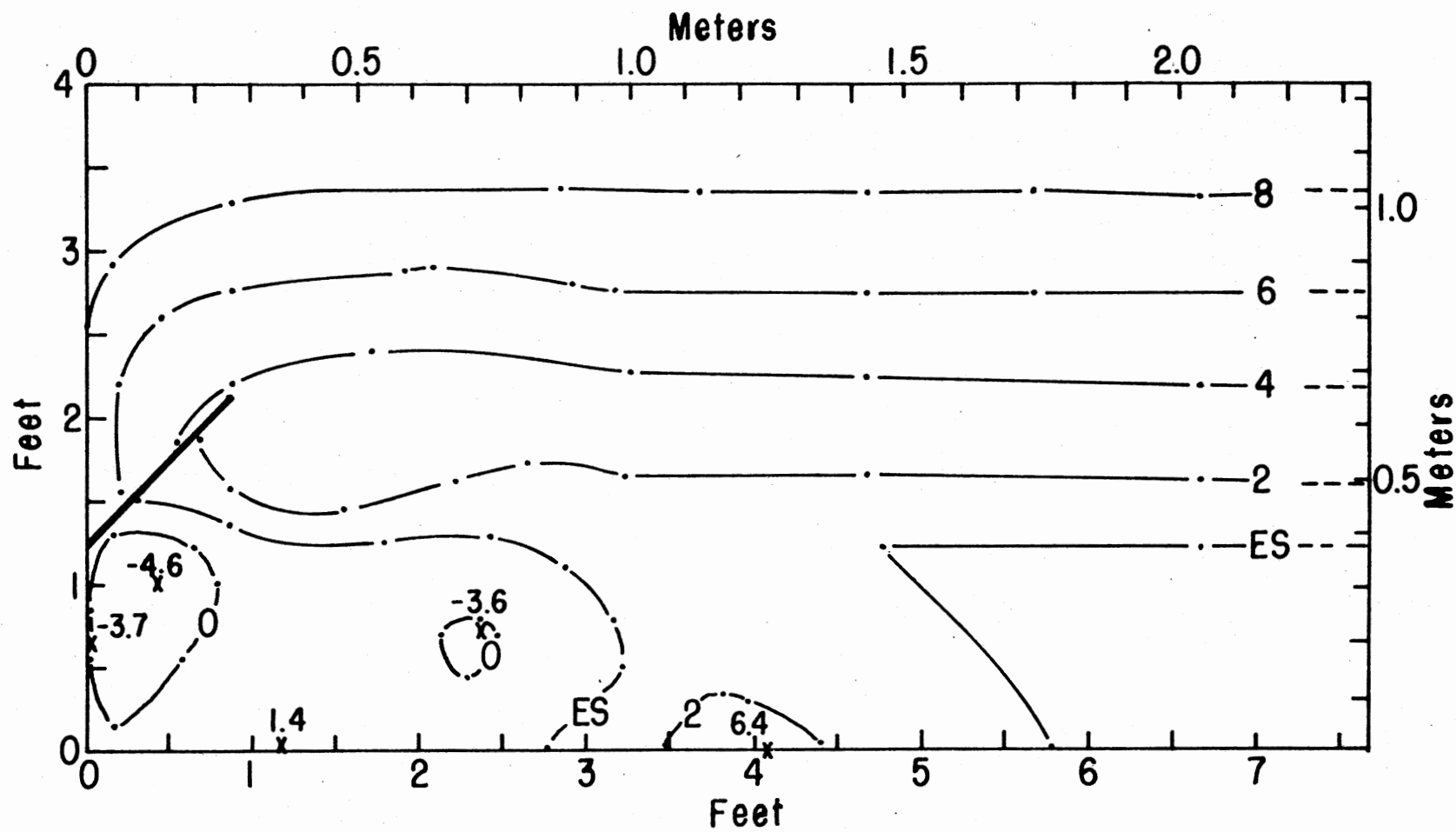


Figure 69. Maximum Scour Contour Map After Testing at $F1_D = 8.0$, $W = 24.75 \times D1_D$, $D50 = 7.85 \text{ mm}$ (0.0258 ft)

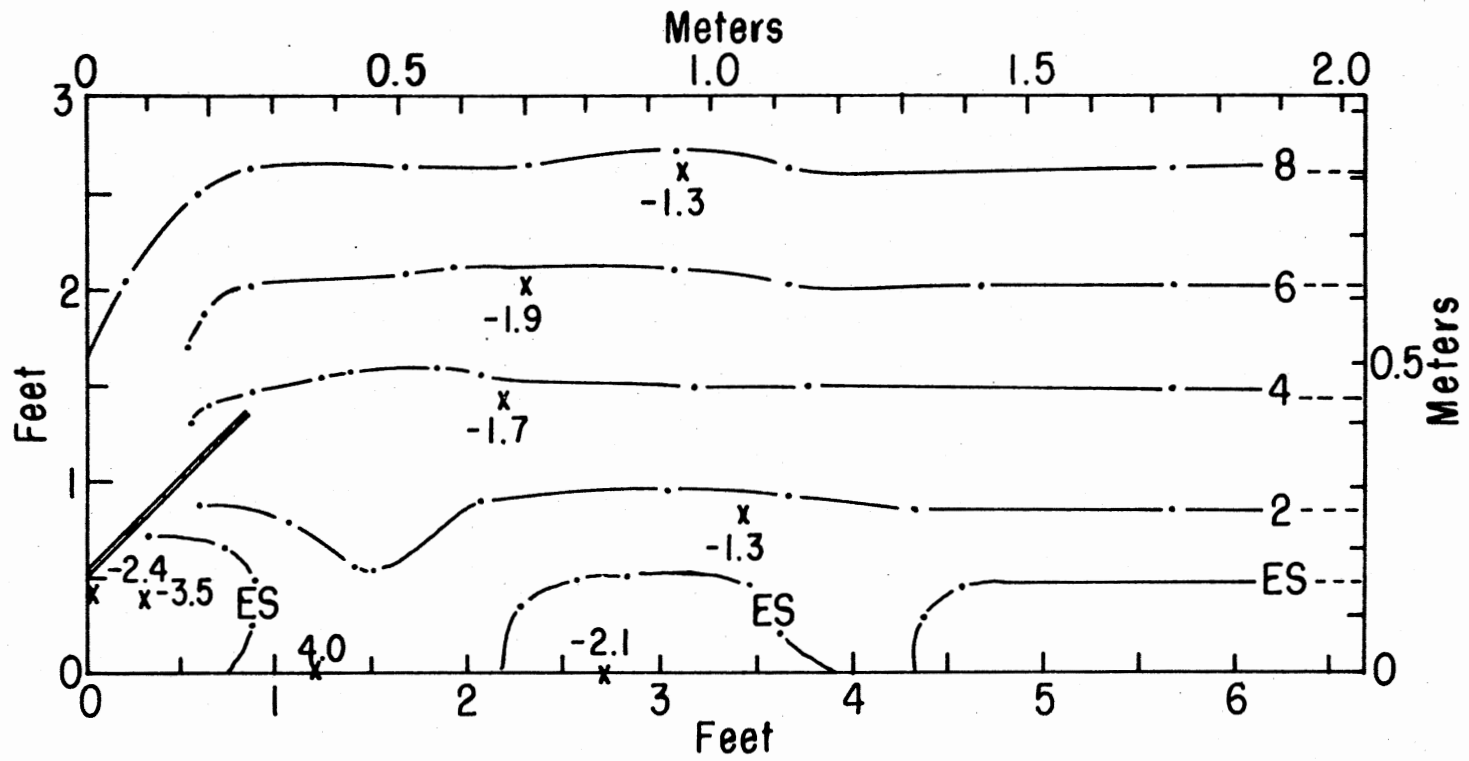


Figure 70. Maximum Scour Contour Map After Testing at $Fl_D = 8.0$, $W = 9.75 \times D1_D$, $D50 = 7.85 \text{ mm (0.0258 ft)}$

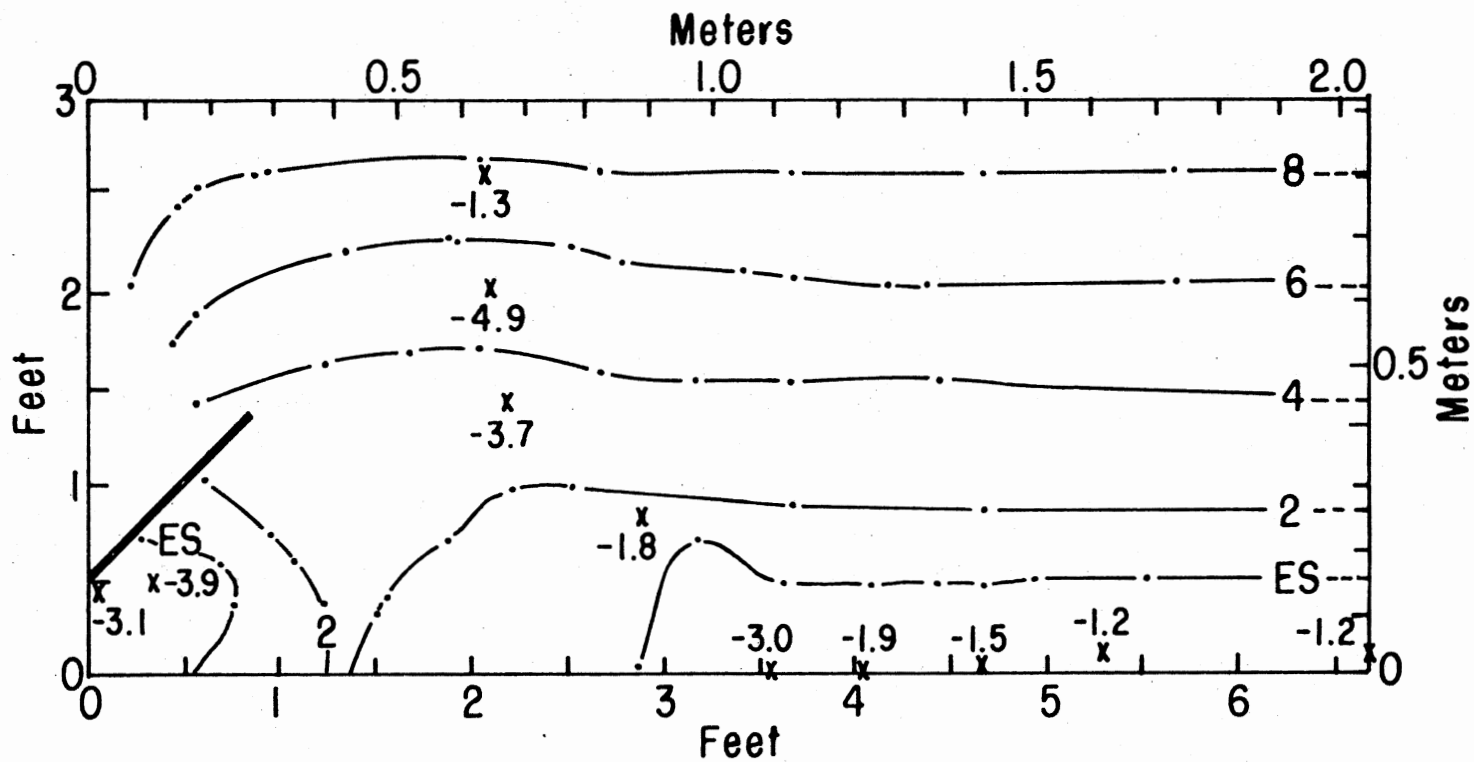


Figure 71. Maximum Scour Contour Map After Testing at $F_{1D} = 8.0$, $W = 9.75 \times D_{1D}$,
 $D_{50} = 5.65 \text{ mm (0.0185 ft)}$

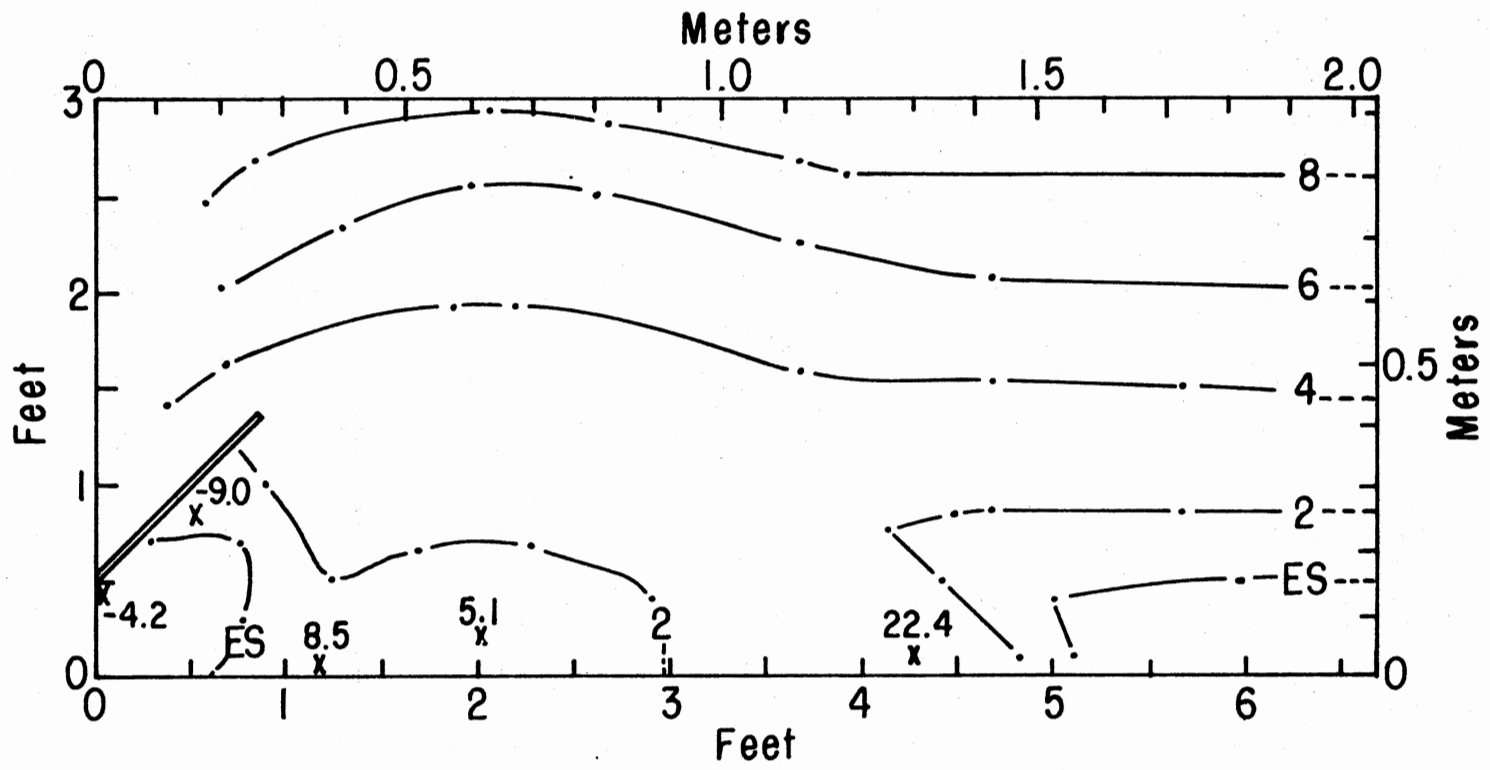


Figure 72. Maximum Scour Contour Map After Testing at $F1_D = 8.0$, $W = 9.75 \times D1_D$, $D50 = 3.45 \text{ mm (0.0113 ft)}$

APPENDIX D

NONDIMENSIONAL LENGTH OR DEPTH OF SCOUR
AS A FUNCTION OF ROCK SIZE FOR
SPECIFIED POSITIONS IN THE
DOWNSTREAM CHANNEL

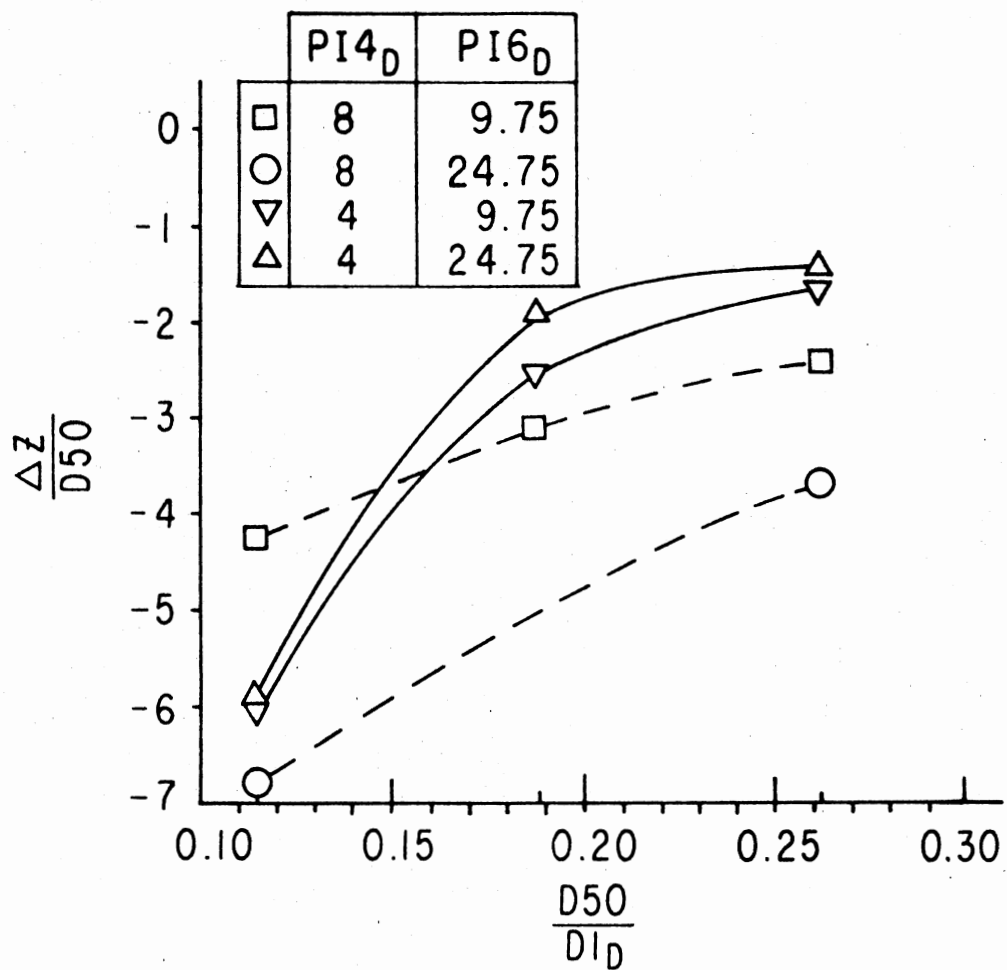


Figure 73. Nondimensional Depth of Scour at Position 1 as a Function of $D50/D1D$

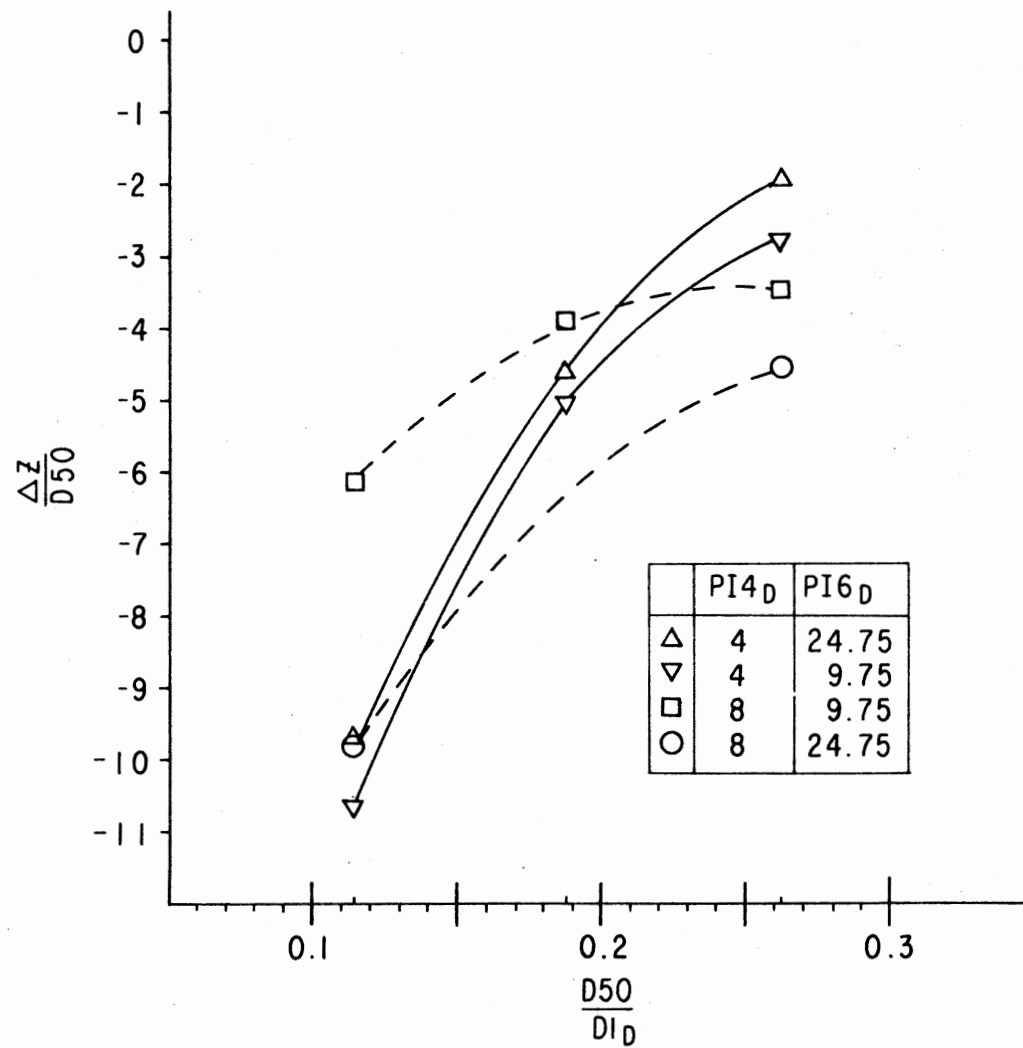


Figure 74. Nondimensional Depth of Scour at Position 2 as a Function of $D50/D1_D$

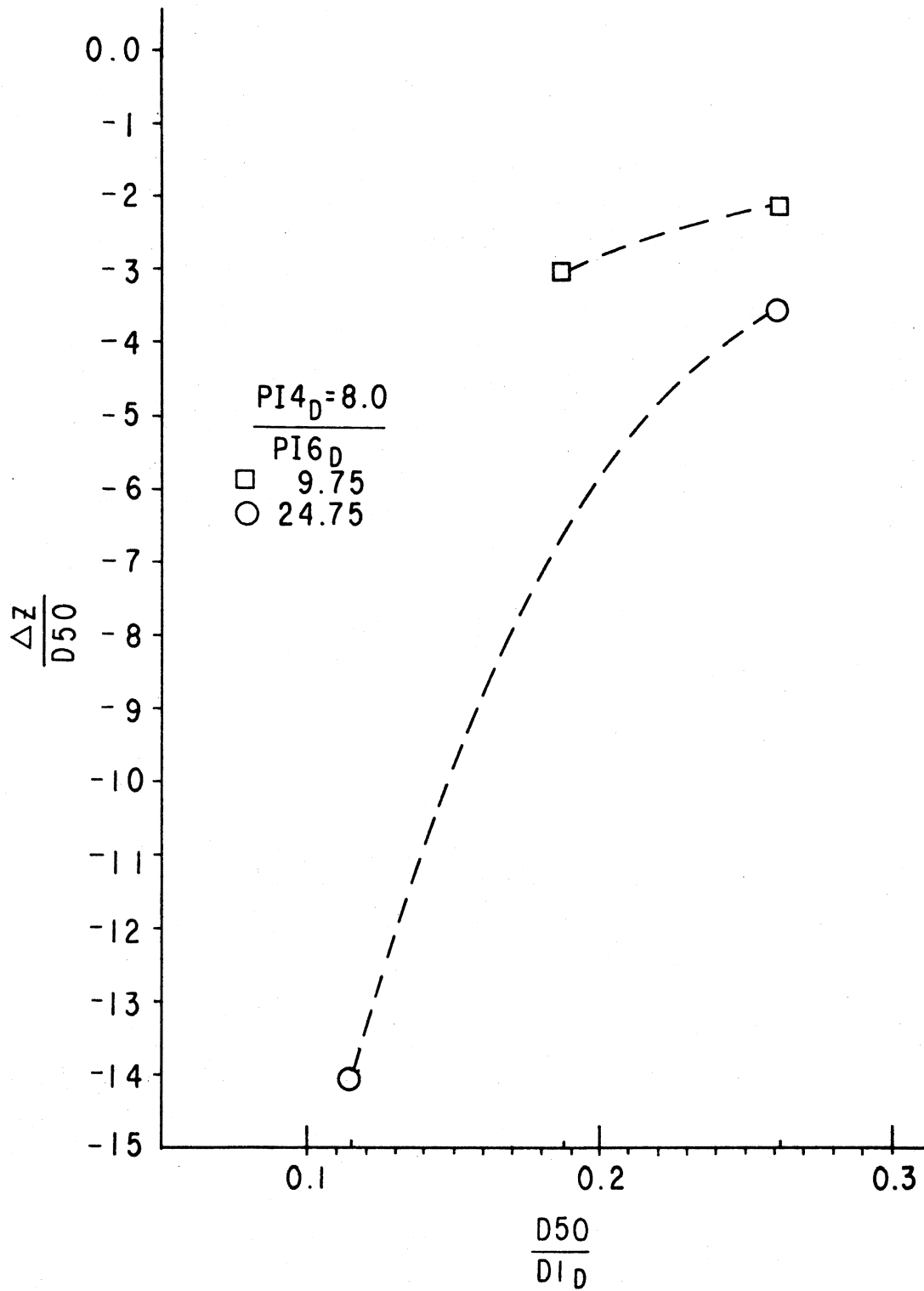


Figure 75. Nondimensional Depth of Scour at Position 4 as a Function of D_{50}/D_{1D}

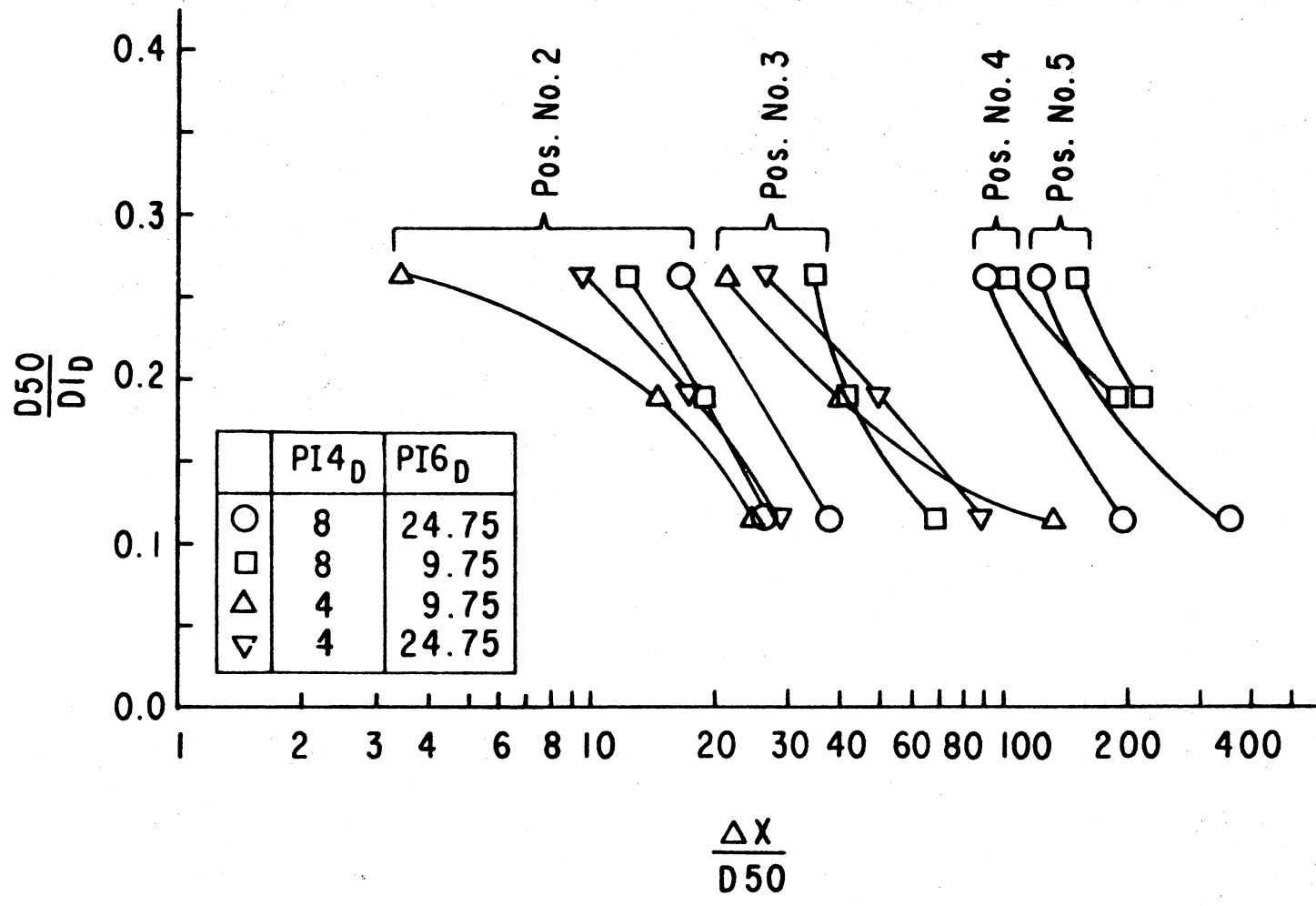


Figure 76. Nondimensional Length to Positions 2, 3, 4, and 5 as Functions of $\frac{D50}{D1D}$

VITA ²

Richard Carl Peralta

Candidate for the Degree of

Doctor of Philosophy

Thesis: RIPRAP DESIGN FOR SAF STILLING BASINS

Major Field: Agricultural Engineering

Biographical:

Personal Data: Born in Enid, Oklahoma, November 8, 1949; the son of Mr. and Mrs. John F. Peralta.

Education: Graduated from A. C. Flora High School, Columbia, South Carolina, in June, 1967; received Bachelor of Science degree, majoring in Chemistry and minoring in Biology, from the University at South Carolina in 1971; attended Texas A & M University and Minot State College, North Dakota, between 1971 and 1974 while in the U.S. Air Force; received Master of Science degree in Agricultural and Irrigation Engineering from Utah State University in 1977; completed requirements for the Doctor of Philosophy degree at Oklahoma State University in December, 1979.

Professional Experience: Environmental Protection Agency Trainee, Agricultural and Irrigation Engineering Department, Utah State University, 1975-1976; Civil Engineering with Environmental and Contract Planning, Tinker AFB, Oklahoma, 1978-1979; Graduate Research Associate, Agricultural Engineering Department, Oklahoma State University, 1977-1979.